INVESTIGATIONS OF ALTERNATIVE DETECTORS FOR THE MEASUREMENT OF PLUTONIUM IN WOUNDS

by

JOHN GRAHAM AUSTIN

Doctor of Philosophy
The University of St Andrews
1992

CONTENTS

LIST OF TABLES

LIST OF FIGURES

ACKNOWLEDGEMENTS AND DEDICATION

I would like to acknowledge the support and guidance of my supervisors Mr Graham Tyler and Dr David Watt, during the course of this project. Additional appreciation is extended to Mr David Smith for answering all my questions about computer programming and Miss Janice Miller and Mrs Lil Bainbridge for their help in the typing of the manuscript. I also wish to thank Health and Safety Division, AEA Technology Dounreay for sponsoring this project.

Finally, I would like to dedicate this work to my parents, Douglas and Rosemary Austin for their patience, love and understanding over the years.

DECLARATION

I, John Graham Austin hereby certify that this thesis has been composed by myself, that it is a record of my own work, and that it has not been accepted in partial or complete fulfilment of any other degree or professional qualification.

Signed Date 15/3/93.....

I was admitted to the Faculty of science of the University of St. Andrews under Ordinance General No. 12 on October 1984 and as a candidate for the degree of Ph.D. on October 1984.

Signed Date 15/3/93.....

I hereby certify that the candidate has fulfilled the conditions of the Resolution and Regulations appropriate to the Degree of Ph.D.

Signature of Supervisor ..... Date .....

ABSTRACT

If a person working in an area in which plutonium is handled sustains a wound, it is necessary to carry out monitoring of the wound for possible plutonium contamination. This monitoring is required to be undertaken rapidly in order to assess (and reduce) the risk of uptake and dispersion of the contaminant within the body and to prevent local tissue receiving a high radiation dose. If plutonium contamination is detected and surgical intervention is decided upon, the monitoring needs to be done repeatedly to assess the progress of wound decontamination. For both these reasons the monitoring equipment needs to be sensitive, robust and easy to use.

Because of the strong absorption of alpha particles by blood and tissues such monitoring is usually carried out by detecting the low energy x-rays from the plutonium. The detectors currently used for this monitoring are usually thin sodium iodide crystals. However, the poor resolution at the x-ray energies of interest of sodium iodide places a limit on the sensitivity that can be obtained because of background interference.

Investigations have been made into the practicability of using cadmium telluride or mercuric iodide detectors, both of which have superior resolution compared with

sodium iodide. Although operational problems prevented a full assessment of the cadmium telluride detector in this study, the results obtained from experimental tests using the mercuric iodide detector indicated that the latter could be used for measurements of plutonium-americium mixtures located in soft tissue up to a depth of not more than 4 cm. The results of these investigations are presented, and suggestions made for future work.

1. INTRODUCTION

1.1 The Objectives and Standards of Radiological Protection

The internal exposure of an individual can result from the accidental intake of radionuclides by inhalation, ingestion, absorption through intact skin or via a contaminated wound. Depending on the radionuclide and the route of exposure involved, such intakes may produce significant internal radiation doses to particular organs and/or the whole body. However, the doses to organs of the body from internally deposited radionuclides are not directly measurable, but must be estimated from knowledge of the intake and of the behaviour of the radionuclide(s) within the body. This particular area of radiological protection is known as internal dosimetry, the objective of which is that of radiological protection as a whole ie to prevent acute radiation effects and to limit the risk of late effects to an acceptable level.

The primary standards currently in force are based on the Recommendations of the International Commission on Radiological Protection (ICRP), an autonomous scientific body established (in 1928) to cover the field of radiation protection. This body develops formal recommendations in the form of publications. Specific legislation is left to the regulatory bodies in each

country; in the United Kingdom this is the Health and Safety Executive (HSE), who also consult scientists and specialist organisations for advice, the most influential of these being the National Radiological Protection Board (NRPB) which was established in 1970.

The primary standards currently in force are based on the recommendations of ICRP Publication 26 (1977) which set out a system of dose limitation. The adoption of such a system relied on secondary limits which were set out in ICRP Publication 30, Parts 1 - 4 (1979a, 1980, 1981b, 1988) in the form of annual limits on intake (ALIs) for individual radionuclides. These ALIs were calculated using models for the principal routes of entry of radionuclides into the body (lung and gastrointestinal tract); also taken into account were the chemical nature of the material and its physical characteristics.

The ICRP issued new radiation protection recommendations in ICRP Publication 60 (1991), which had been developed to take into account new information and to supersede ICRP Publication 26 (1977). Based on these recommendations and the metabolic and biokinetic information contained in ICRP Publication 30 (1979) new values of the ALIs were set out in ICRP Publication 61 (1991). Eventually, a complete revision of Publication 30 will be issued taking into account new biokinetic and respiratory tract model, and a new reference man report.

1.2 The Need for Quantitative Methods for the Measurement of Plutonium Contaminated Wounds.

Plutonium (Pu), atomic number 94, a transuranic element, is a silvery-white reactive metal that melts at 639.5°C and oxidises readily on warming in moist air. In powdered form the metal may be pyrophoric, igniting spontaneously in the range of 300°C to 350°C. Of its fifteen known isotopes (Pu-232 to Pu-246), all of which are radioactive (and ten of which can undergo spontaneous fission), Pu-238 and Pu-239 are the most likely to be encountered in practice.

The most common isotope of plutonium, plutonium-239, has a 24,000 (approximately) year half-life and emits energetic alpha particles (5.11 to 5.16 MeV). It is used as a fissionable material in explosive nuclear devices and as a fuel for nuclear power reactors. Another isotope, plutonium-238, is used as a heat source in thermoelectric power devices, such as have been employed on lunar missions, in communications satellites, in heart pacemakers, and for powering artificial hearts. Plutonium-238 is also an alpha-emitter and has a half-life of 86.4 years. The heavier isotopes of plutonium will become more abundant as they are produced in breeder reactors. Of these, Pu-240 and Pu-242 are long-lived alpha emitters and should not differ in any essential biological respect from Pu-239. Plutonium-241 is a

relatively short-lived (13.2 year half-life) beta emitter and is of primary interest as the parent of americium-241, an alpha-emitter that accumulates in tissues and constitutes a hazard comparable to plutonium (Bair and Thompson, 1974).

From a biological standpoint the variability which toxicologists like to blame for their lack of precision is often complicated by "chemical variability" in studies with plutonium (Bair and Thompson, 1974). Plutonium can exhibit five oxidation states from a valence of +3 to +7 (Taylor, 1973; ICRP, 1986) and has a marked tendency to hydrolyse and form complex ions under physiological conditions. The compounds formed may be monomeric, in which state any particulates are less than about 0.01μm in diameter, or polymeric with particle diameters ranging from about 0.01μm to over 1μm. In the body, monomeric compounds become converted to at least minimally polymeric forms. Hydrolytic reactions can also change the chemical form after intake. Biological ligands to which plutonium may bind in the body include proteins, apoferritin, amino acids, phosopholipids, hydroxy acids, and other metabolites (Taylor, 1973). Polymers and particulates formed by hydrolysis lead to binding on cell surfaces and phagocytic uptake of plutonium (Taylor, 1973).

Because of the unique history of plutonium as a man-made

element, it was possible to consider its potential biological hazards and to impose controls for personnel protection from the time (late in 1943) when milligram quantities were first produced at the Oak Ridge reactor. In February 1944, 11 milligrams of plutonium were allocated for biomedical studies; these studies involved the administration to laboratory animals of several chemical forms of plutonium by various routes. It was found that plutonium injected into the blood was deposited principally in bone and liver, that plutonium was not appreciably absorbed from the gastrointestinal tract when given orally, that it was not quickly cleared from the lung when introduced into the trachea, and that it was not quickly lost from the body.

Since this first study, radiobiological research on the effects of plutonium has been extensive, the motivation for this research being concern for the health and safety of occupationally-exposed workers and for the general population exposed to plutonium in the environment. As a result of this research much has been learned about the toxicity of plutonium - possibly more than is known about most other hazardous elements. The results of such research have been reviewed on many occasions (for example, Bair and Thompson, 1974; Vaughan et al, 1973; Bair et al, 1973; ICRP, 1986) and used as the basis for the setting of secondary standards (ALIs) by the ICRP in Publication 61 (1991).

For occupationally-exposed workers who may work with MBq of plutonium the principal routes of entry to the body are through inhalation and contaminated wounds; ingestion in the adult human and contaminated intact skin result in little absorption and are not considered to be important modes of exposure (ICRP, 1972; ICRP, 1986). (The ALIs for plutonium-239 are 300 Bq and 40000 Bq for exposure by inhalation and ingestion respectively. No "official" ALIs exist for entry into the body via a contaminated wound or intact skin.)

After plutonium has entered into the body via a contaminated wound some or all of the material will be solubilised by the body fluids (including blood), and redistributed within the body. The rate and amount of plutonium translocation will be markedly influenced by the deposition site, the physical and chemical form of the deposited compound, and the specific activity of the material. Hence, even under the most favourable conditions the fraction of plutonium absorbed into the blood stream will not be known very accurately (Leggett, 1985).

Although inhalation is a particularly important route of intake of plutonium as it accounts for about 75 per cent of industrial exposures (Ross, 1968; ICRP, 1986), cases of exposure through wounds are still significant; the problem in these cases is that the delay in reaching the

bloodstream and the amount that reaches the bloodstream depend strongly on the conditions of the given case and still may not be characterised meaningfully in a general setting (Leggett, 1985).

Three types of skin wounds are of interest in the present study - abrasions, puncture wounds and lacerations (Austin, 1991; Austin, 1992). A contaminated abrasion presents a potential for absorption since the surface is often raw and bleeding and the epidermal barrier is no longer intact. (After a reasonable effort, there is probably no need to attempt to remove all of the contamination since any residue that remains on the surface will probably be incorporated in the scab which will then slough).

Puncture wounds may result from contaminated metal or glass slivers and small tools. In explosions a small missile may be driven through the skin and leave only a small entry wound. Its exact position may be difficult to locate and thus considerable surgical extension of the wound may be required.

Lacerations can be the simplest type of wound (in terms of detection of the contaminant and subsequent decontamination) if they are made superficially by a contaminated sharp object as much of the contamination is deposited on the lips of the wound. Conversely, when

lacerations are ragged and deep, the contamination may be deposited in fascial planes with subsequent migration that makes difficult the detection of the contamination and subsequent decontamination. There is also the possibility of direct entry of contamination into a blood vessel or major lymph channel (NCRP, 1980).

At AEA Technology Dounreay where there is a potential risk of wound contamination a set of 'house rules' have been drawn up to reduce this risk. These rules advise against the use of glass apparatus or sharp pointed tools in fumehoods and gloveboxes. In cases where scissors (which must be round ended), screwdrivers, etc must be used, then they must be clearly marked with red tape and stored in a special container, likewise clearly marked (Fischer, 1985).

In experiments on beagles, particles of high-fired PuO_2 (geometric diameter, 0.7μm) that had been implanted as a simulated wound, were detected in the regional lymph nodes within a few minutes to one or two hours after exposure with concentrations reaching a maximum of about 60 per cent of the implanted dose after 30-40 days (Bistline et al, 1972). Translocation of air-oxidised plutonium was slower, being 3 per cent at 14 days and 17 per cent at one year (Watters and Lebel, 1972). This slower movement may have been due to larger particle size. Plutonium nitrate implanted in the dog's paw built

up rapidly in the superficial lymph node, concentrations reaching a maximum in ten days. Those dog experiments indicated that insoluble PuO_2 in the form of small particles can be readily translocated along lymph to the regional lymph nodes. The regional node, however, is often only a partial and temporary block in which case the contaminant moves on to the thoracic duct and enters the general circulation (Gomez et al, 1972).

Contamination, on the other hand, may not be removed from the wound site; plutonium allowed to remain subcutaneously for several years has been reported to result in a fibrous nodule not unlike a foreign body reaction (Lushbaugh et al, 1967). In one case the alpha radiation dose to the surrounding cells from a 185 Bq subcutaneous deposit of plutonium was estimated to be over 0.75 MGy and the resultant nodule showed severe cellular changes in the basal area of the epidermis cytologically similar to precancerous changes (Lushbaugh and Langham, 1962). In a long-term follow-up study of workers exposed to plutonium, one individual with a deposit of about 185 Bq in a finger for 27 years showed no clinical evidence of skin changes or subcutaneous nodule formation (Hempelmann et al, 1973). It has been suggested that the depth of deposition in relationship to the basal epithelial layer of the skin may be related to nodule formation (Voelz, 1975).

It can be seen, therefore, that when a person is suspected to have suffered an accidental intake of plutonium via a contaminated wound, it is imperative to determine within a short time not only the amount of the isotope but also its depth within the wound so that the physician in charge can determine a source of action, eg excision of the wound or chelation therapy. Once this has been done other studies, eg whole body monitoring, faecal and urine analysis can be performed so that a clearer picture of the extent of the contamination can be obtained.

1.3 Physical Considerations of Plutonium Measurements.

Plutonium is formed by neutron irradiation of U-238, and the most important and commonly formed isotope is Pu-239 which is produced in the following manner;

$$\text{U-238}(n,\gamma) \longrightarrow \text{U-239}(\beta^-) \xrightarrow[23.5\ \text{min}]{} \text{Np-239}(\beta^-) \xrightarrow[2.3\ \text{days}]{} \text{Pu-239}$$

Pu-239 is an alpha emitter with a half-life of 2.4×10^4 years. Other plutonium isotopes are formed by neutron irradiation of Pu-239 as follows;

Pu-239 (n, 2n) Pu-238 (half-life = 86 years)
Pu-239 (n, γ) Pu-240 (half-life = 6.5×10^3 years)
Pu-240 (n, γ) Pu-241 (half-life = 13.3 years)
Pu-241 (n, γ) Pu-242 (half-life = 3.8×10^5 years)
Pu-242 (n, γ) Pu-243 (half-life = 5.0 hours)

Thus, upon separation of uranium and fission products, plutonium (Pu) will consist of an isotopic mixture of several Pu isotopes. The ratios of these isotopes will, in turn depend upon irradiation time, neutron flux in the reactor, and the reactor and fuel type. (Dawson, et al, 1965).

Figure 1 (page 19) shows the nuclear reactions that occur within Prototype Fast Reactor (PFR) fuel and Table 1

(page 16) shows the plutonium isotopic composition after irradiation of a PFR sub-assembly (inner core) (Judd, 1981; Fischer, 1985).

A PFR fuel sub-assembly can be assumed to contain 46 kg of heavy metal in the core zone, with a plutonium concentration of 25%. The plutonium is taken to be of MAGNOX grade, containing 21% of Pu-240 and 3.7% of Pu-241 and is assumed to have been separated at Sellafield one year prior to the beginning of the irradiation. The sub-assembly is assumed to generate a constant power of 7.5 MW during each of four periods of 90 days operation, separated by shutdowns lasting 55 days. A post-irradiation cooling time of 180 days is assumed (Judd, 1981; Powell, 1985). Although the isotopic mixture is predominantly Pu-239, it can be seen that a certain percentage is actually Pu-241. As americium-241 is formed by the beta decay of Pu-241, then even in chemically purified PFR plutonium solution there is an increasing percentage of Am-241.

Plutonium from the Dounreay fuel reprocessing plant is eventually used in the manufacture of new fuel elements which are, in turn, recycled through the reactor. With each period of irradiation in the reactor, the isotopic composition of the plutonium changes and Table 1 (page 16) lists the expected percentages after each cycle (Fischer, 1985).

It is convenient to consider mainly Pu-238, Pu-239, Pu-240 and Pu-241 since any other isotopes produced do not contribute significantly to the radioactivity of the Pu mixture. Pu-243 has a half-life of only five hours and, if produced, will decay even before chemical separation. Pu-242 has a half-life of 3.8×10^5 years and is produced in such small amounts that its contribution to the total activity of the isotopic mixture can be neglected. It should also be noted that the spectrum and abundance of electromagnetic radiation from Pu-242 is very similar to that of Pu-240 (Lister, 1964). Pu-241 decays with a half-life of 13.3 years into Am-241. Table 2 (page 17) shows the decay characteristics of plutonium isotopes and Am-241.

Plutonium-239 decays by the emission of alpha particles followed by gamma emission or internal conversion. (In the latter process the excited nucleus, instead of emitting a gamma-ray of energy $h\upsilon$, imparts the energy directly to one of its own atomic electrons, which then escapes the atom with a net kinetic energy of $h\upsilon - E_b$, where E_b is the binding energy of the electron's original shell. The resulting vacancy is promptly filled by another electron falling from a less tightly-bound shell; for K- and L-shell vacancies the transition is sometimes accompanied by the emission of a characteristic x-ray.) In the case of plutonium internal conversion predominates (>99%) resulting in the emission of characteristic

uranium-235 L x-rays, with energies lying principally in the range 13 keV to 21 keV. For americium, the same process (internal conversion) follows the emission of alpha particles but in this case the x-rays are characteristic L x-rays of neptunium.

Thus, in practical cases we must consider the contributions of Am-241 in addition to that of the three plutonium isotopes. The amount of Am-241 present will depend upon the time elapsed since chemical separation and the amount of Pu-241 at the time of separation.

The activity (and in particular the electromagnetic emission) of Am-241 in the mixture becomes significant a short time after chemical separation. If a Pu mixture contained initially only 1% of Pu-241, then at 100 days post-separation, about 10% of L x-rays emitted (13-20 keV) will be equal to those from Pu-239.

In addition, Am-241 emits gamma-rays of 59.6 keV at approximately the same abundance as L x-rays. This makes the detection of a Pu/Am mixture in wounds much easier when the Pu/Am ratio is known; when the Pu-Am ratio is unknown, however, Am-241 can present a major interference with accurate measurements of plutonium content because its abundant x-rays are of approximately the same energies as those of Pu-239 (Jones and Saxby, 1968)and hence are not easily resolvable.

From the preceding discussion, it can be seen that in order to determine the Pu-239 content *in vivo* by the external measurements of electromagnetic emissions, it is necessary first to determine the ratios of different plutonium isotopes and Am-241. It is not always possible, however, to obtain a sample of the material that caused the contamination and to determine the Pu/Am ratio by alpha spectroscopy. It is also possible that samples taken in the environment will not correspond to the contamination (Brodsky, 1967).

Although many investigators have worked on the measurement of radioactive contaminants in the whole body only a small number of investigators have developed techniques to measure the contamination of wounds; much of this work has been limited to wounds of shallow depths and also has depended on an *a priori* knowledge of the Pu-Am ratio. Reviews of the instrumentation and techniques used are given in Sections 1.5 and 1.6, respectively.

Table 1: Plutonium Isotopic Composition of PFR Sub-Assembly (Inner Core) After Irradiation

Cycle	Pu-238	Pu-239	Pu-240	Pu-241	Pu-242	Bq/g Pu[1]
1	0.14	70.09	24.96	3.86	0.96	4.7E9
2	0.18	66.62	27.86	4.07	1.27	5.1E9
3	0.23	63.81	29.98	4.35	1.57	5.6E9
4	0.27	61.73	31.53	4.62	1.86	5.9E9
5	0.31	60.03	32.67	4.86	2.14	6.2E9
6	0.34	58.61	33.52	5.05	2.40	6.4E9
10	0.40	55.59	35.16	5.60	3.25	6.9E9

Data taken from Judd (1981) and Fischer (1985)

NOTE: (1) The specific activity

Table 2: Decay Characteristics of Plutonium Isotopes and Americium-241

Isotope	Half-Life (Years)	Radiation	Energy	Abundance
Pu-238	86	Alpha	5.495 MeV	72%
		Alpha	5.452 MeV	28%
		L x-ray	11.62 keV	0.26E-2/α decay
		Lα x-ray	13.62 keV	4.15E-2/α decay
		Lβ x-ray	17.22 keV	5.61E-2/α decay
		L x-ray	20.22 keV	13.60E-2/α decay
		Gamma	44.00 keV	3.40E-4/α decay
Pu-239	24.400	Alpha	5.147 MeV	72.5%
		Alpha	5.134 MeV	16.8%
		Alpha	5.096 MeV	10.7%
		L x-ray	11.62 keV	0.11E-2/α decay
		Lα x-ray	13.62 keV	1.82E-2/α decay
		Lβ x-ray	17.22 keV	2.16E-2/α decay
		L x-ray	20.17 keV	0.53E-2/α decay
		Gamma	39.00 keV	2.00E-5/α decay
		Gamma	53.00 keV	7.00E-5/α decay
Pu-240	6,600	Alpha	5.162 MeV	76%
		Alpha	5.118 MeV	24%
		L x-ray	17.00 keV(av)	1.00E-1/α decay
		Gamma	44.00 keV	1.00E-4/α decay

Table 2 (contd)

Pu-241	13.2	Beta (-)	21.00 keV(max)	99.9%
		Alpha	4.9 MeV	4.00E-3%
Pu-242	3.8 E5	Alpha	4.898 MeV	76%
		Alpha	4.858 MeV	24%
		L x-ray	17.00 keV(av)	1.00E-1/α decay
		Gamma	44.00 keV	1.00E-4/α decay
Am-241	464	Alpha	5.477 MeV	85%
		Alpha	5.435 MeV	12.6%
		Alpha	5.378 MeV	1.7%
		Alpha	Other	<1.0%
		L x-ray	11.89 keV	0.86E-2/α decay
		L x-ray	13.94 keV	13.20E-2/α decay
		L x-ray	17.75 keV	19.25E-2/α decay
		L x-ray	20.79 keV	4.85E-2/α decay
		Gamma	26.4 keV	2.50E-2/α decay
		Gamma	43.00 keV	6.0 E-2/α decay
		Gamma	59.6 keV	35.9 E-2/α decay

Figure 1: Nuclear Reactions Within PFR Fuel

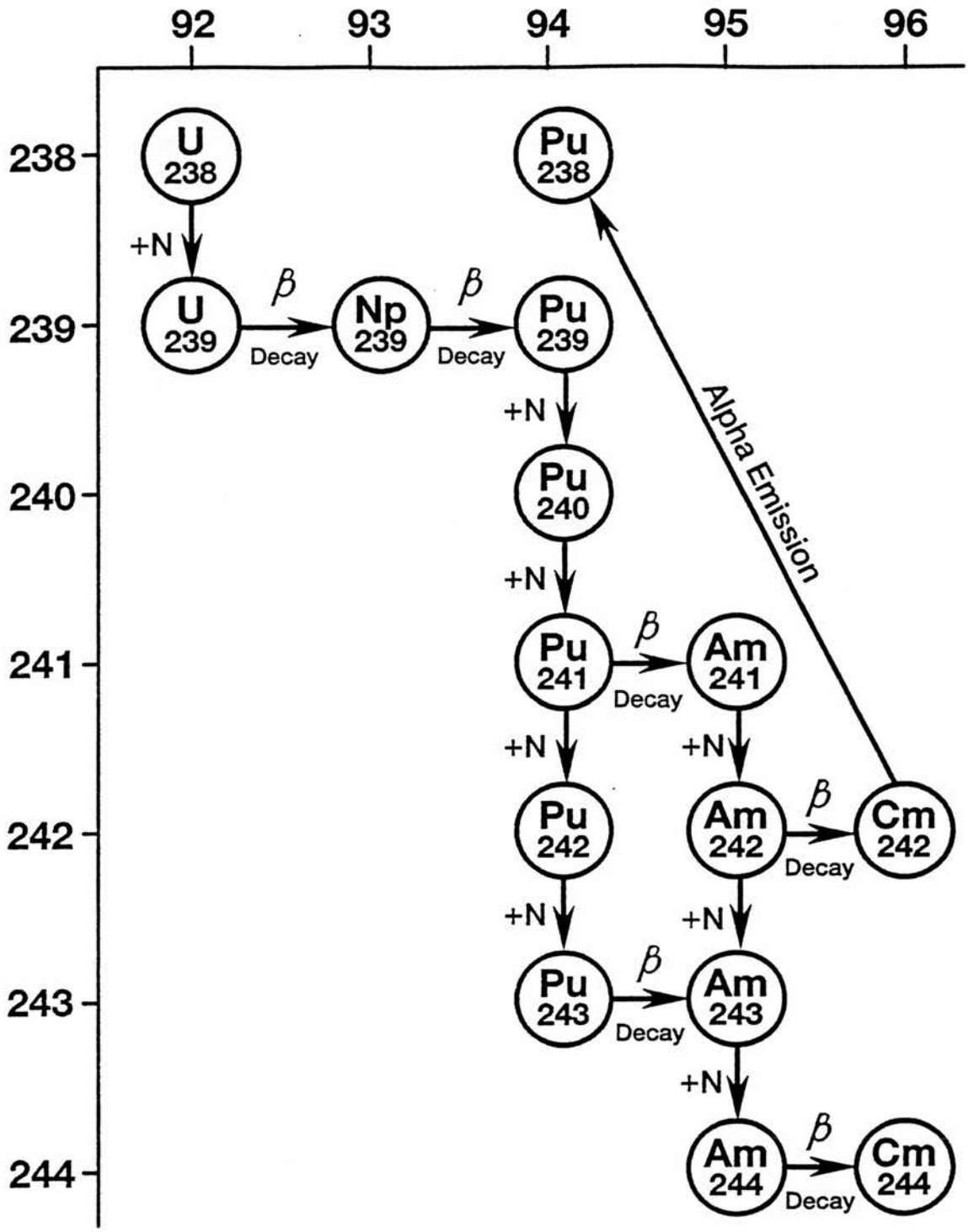

1.4 Model Concerning the Radiological Assessment of a Contaminated Wound

1.4.1 Quantity of Activity Deposited in a Wound

Four basic factors can be considered to be involved in the deposition of activity in a wound:

(a) The degree of penetration of the wounding object. This has a strong bearing on the size and depth of the wound and the quantity of contamination which can potentially be deposited in the wound.

(b) The degree of mobility of the contamination on the wounding object, ie what proportion of the contamination is fixed on the wounding object.

(c) The proportion of mobile contamination which is deposited on any protective clothing worn and thereby not able to enter the wound.

(d) The contamination level on the wounding object.

These factors can be quantified as shown below;

(a) An intramuscular wound could be assumed to be

caused by an 0.5 mm diameter object (eg a strand of wire) puncturing human tissue to a depth of 5 mm. For example the area of contact between the object and the wound in this case would be;

$$\text{contact area} = \pi \times d \times l$$
$$= \pi \times 0.05 \times 0.5 \text{ cm}^2$$
$$= 7.9\text{E-}2 \text{ cm}^2 (\sim 0.1 \text{ cm}^2)$$

Two wound sizes can be considered for subcutaneous wounds, "nominal" and "large";

A "large" wound could be assumed to be caused by a 1 cm wide sharp edge penetrating to a depth of 0.2 cm giving an area of contact between the object and the wound of 0.4 cm^2.

A "nominal" wound could be assumed to be caused by a 0.1 cm wide sharp edge penetrating to a depth of 0.2 cm giving an area of contact between the object and the wound of 0.04 cm^2.

(b) Monitoring by swab of a contaminated object typically returns a value of around 10% for loose activity on a lightly contaminated

surface. Therefore it could be assumed that 10% of the activity on a wounding object is loose.

(c) The injured operator would be afforded some protection by any gloves worn, which could be assumed to remove half the loose contamination from the portion of the wounding object which passes through it.

Hence, for the calculation of the activity deposited at a wound site, factors (a), (b) and (c) above (ie the wound/object contact area, the proportion of loose contamination, and the proportion deposited on the protective clothing) can be combined into a single factor, the Transfer Factor given by:

wound/object contact area x loose contamination factor x clothing protection factor

Hence, typical values of this Transfer Factor for intramuscular, nominal- and large-size subcutaneous wounds are 5E-3, 2E-3 and 2E-2 respectively.

1.4.2 Description of a Metabolic Model Applicable to Contaminated Wounds

It is often difficult to evaluate the systemic burden

resulting from a contaminated wound. Although a generic assessment can be made of the activity deposited in a wound using the methodology outlined in Section 1.4.1 above the final systemic burden will result from the rapid transfer taking place from the wound to the blood at the time of the incident and then, for a longer period, from possible chronic transfer from the contaminated tissue. As for the post-surgery residual activity, it is important to be able to distinguish the fraction which remains located in situ without being metabolised, from that which, on the contrary, slowly passes into the blood.

As previously stated any contaminated wound may present a large number of different characteristics; these characteristics will depend upon the nature of the wound eg abrasion, cut or puncture wound and the physical and chemical form of the contaminant. Thus, a detailed description of the kinetics of a radionuclide cannot be proposed. Hence, in order to embrace a very large number of different situations, the schema of transfers has been intentionally reduced to a minimum.

The proposed model, as shown in Figure 2 (page 30), contains three possible routes of movement of the contaminant. Thus, the activity Q, deposited in a wound can be divided into three fractions:

(a) Q_1, metabolically inert, stays localised in the place where it is deposited.

(b) Q_2, which rapidly penetrates into the circulation through vascular injuries.

(c) Q_3, which diffuses into soft tissues ie connective tissues, muscle from whence it is finally transferred into the blood, either directly or indirectly via the lymphatic system.

If clearance from the wound site is considered to be similar to (the ICRP assessment of) clearance of activity from lymph nodes (ICRP, 1986) then Q_1 can be considered to be 10% of the activity, and (Q_2 and Q_3) considered to be 90% with an overall clearance half period of 500 days.

Different types of measurement ie local measurements and the analysis of excreta (mainly urine) generally allow sufficient information to be gathered for the assessment of these activities. In practice, the interpretation of results can be complicated when;

(a) the urinary excretion of any plutonium is increased in a variable manner by the administration of DTPA.

(b) surgery is used to remove the activity present in the wound.

(c) any activity remaining in the wound being

incorporated into the scab which is formed, rises to the surface of the skin and is then lost.

1.4.3 LOCAL MEASUREMENTS

These measurements give the values for the sum $Q_1 + Q_3$. In cases of excision of the contaminated tissue the local measurement will drop suddenly from $Q_{1,i} + Q_{3,i}$ (i = initial) to $Q_{1,r} + Q_{3,r}$ (r = residual), the difference being theoretically present in the excised tissue and any swabs, bandages etc used in the process of decontamination (Figure 3, page 31).

In reality the value of $Q_{1,i} + Q_{3,i}$ can be over-estimated because of the presence of any skin contamination not removed by normal cleaning processes. Conversely, the value of $Q_{1,r} + Q_{3,r}$ may be under-estimated because any residual activity will be low and buried deep within the tissue. Therefore, the activity present in the excised tissues and the swabs etc would be lower than $(Q_{1,i} + Q_{3,i}) - (Q_{1,r} + Q_{3,r})$.

1.4.4 URINARY MEASUREMENTS

Initial excretion: The initial excretion over (approximately) the first ten days following the incident, is essentially attributable to the activity

that has passed rapidly into the blood. Measurements performed during this period can therefore be used to determine Q_2.

Excretion over long and medium periods is more difficult to interpret. Measurements performed beyond the first month allow a theoretical determination of the residual activity, $Q_{3,r}$ transferred very slowly to the blood. The results of these measurements have to be corrected beforehand by subtracting the activity excreted due to the fraction Q_2. Any uncertainties in estimating the latter (due to the variability of action of any DTPA administered) will also have to be taken into account. (It can be considered that DTPA will affect the excretion of plutonium by a factor of 25 at least and 100 at most). Table 3 (page 32) gives a general review on the interpretation of results concerning contaminated wounds.

1.4.5 Calculation of Dose

1.4.5.1 Internal Dose

Although each case of a contaminated wound must be treated as a unique situation it can be seen that from measurements performed locally and on urine samples collected it is possible to make a reasonable assessment of the systemic burden resulting from a wound contaminated with plutonium.

For the purposes of assessment of the resulting internal exposure, the systemic uptake of the radionuclide can be compared with an Annual Limit of Intake. Although there is no "official" Annual Limit of Intake (ALI) for intakes via a contaminated wound, one can be calculated by making an approximation to the short-term systemic uptake from the ICRP 30 lung model (Austin, 1991; Austin, 1992). Using this protocol the ALI (wound) can be taken to be 12% of the ALI (inhalation). Hence, for each radionuclide the systemic uptake can be compared to the appropriate modified ICRP 30 ALI to obtain an estimate of committed effective dose equivalent.

Similarly, estimates of committed dose equivalent can be made for specific organs or tissues for those cases where the ICRP 30 limiting ALI is based on non-stochastic effects. For plutonium, the bone surface is the organ which dominates the ALI.

1.4.5.2 Dose to the Wound Site

Currently, for the purposes of radiological protection, the dose to the local tissue surrounding the wound site may not be considered to be of primary importance but may be recorded for illustrative purposes(for example Foster, 1986). However, for contamination by beta/gamma and alpha-emitting radionuclides varying methods can be used for the calculation of dose to the local tissue

surrounding the wound site as follows;

For beta/gamma emitting radionuclides the method of Loevinger (1950) can be used to calculate the initial dose rate and the absorbed dose expected in calender year periods to both the cells in the basal layer of the epidermis and the one gram of tissue surrounding the wound site. (For the calculation of integrated dose the pessimistic assumption can be made that the amount of activity in the wound declines by radioactive decay only.)

For an alpha-emitting radionuclide a simplistic calculation of absorbed dose to the most exposed gram of tissue would be; Activity (Bq) x Energy of particles (MeV) x 1.6E-13 x 3.6E3 x 24 Joules/g/year = Bq x MeV x 1.38E-5 J/kg/year (Gy/year). (It should be noted, however, that on biological grounds the relevant parameter would appear to be the energy actually deposited in a cell or critical group of cells. Hence, an absorbed dose calculated in this manner is only a statistical concept which does not measure the energy concentration actually deposited in single cells. In fact, for alpha radiation, the concept of absorbed dose loses all significance at the dimensions of single cells and must be replaced by the concept "specific energy" which is defined as the energy imparted to a microscopic region divided by its mass (Rossi, 1967; ICRU, 1971). A

12 μm-diameter cell traversed by a single plutonium-239 alpha particle receives a specific energy of about 0.20 Gy and a nucleus of 5 to 6 μm-diameter receives a specific energy of about 1 Gy, such energies being sufficient to kill a cell. When activity is deposited in a wound such that the distance between the contaminant and the basal layer of the skin is approximately 40 μm (the range in tissue of a plutonium-239 alpha particle) then these considerations should be noted.)

Figure 2: Schema of Transfers from a Contaminated Wound

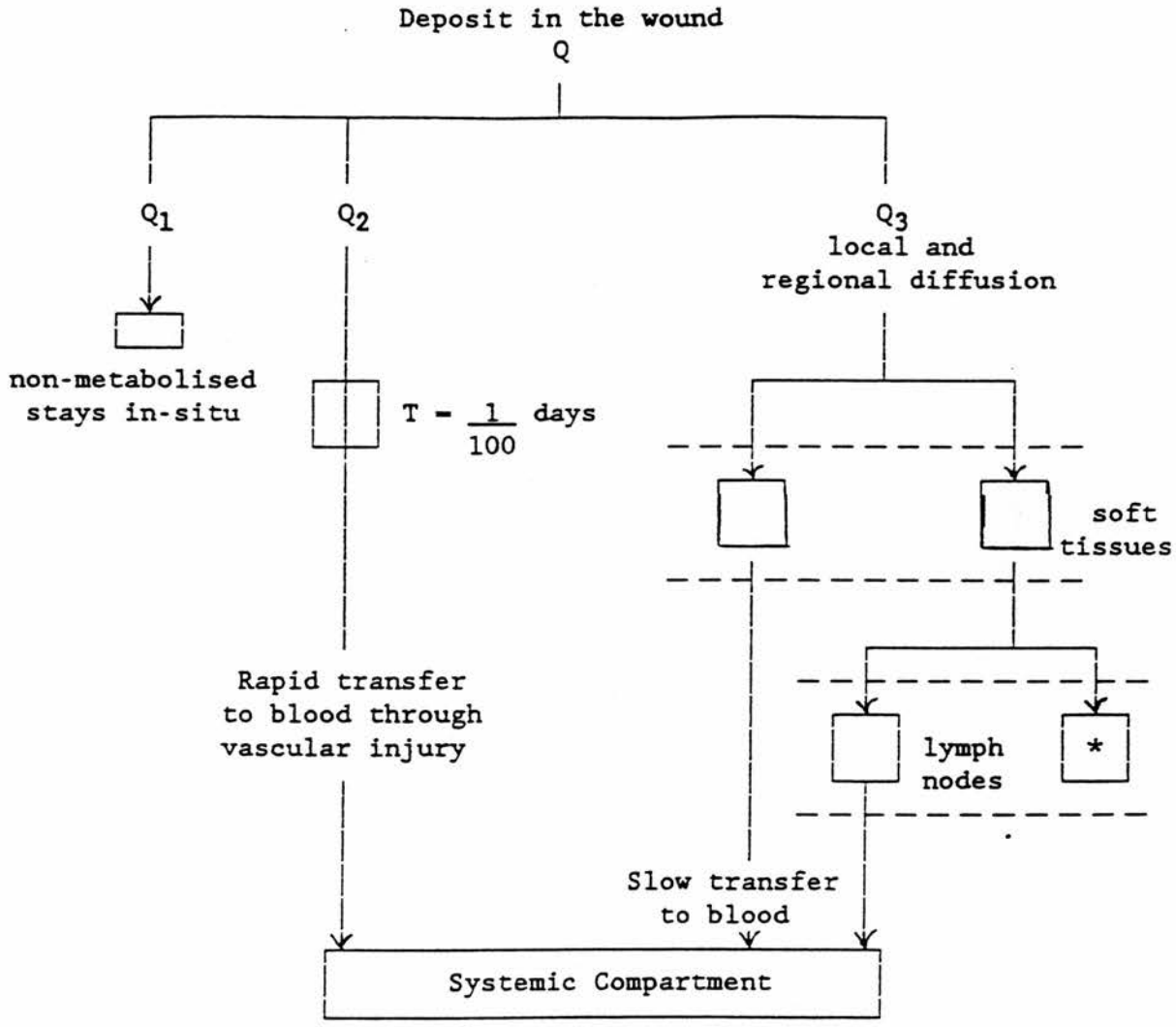

*A part of the activity can be permanently retained in the lymph nodes

Figure 3: Evolution of Local Measurements

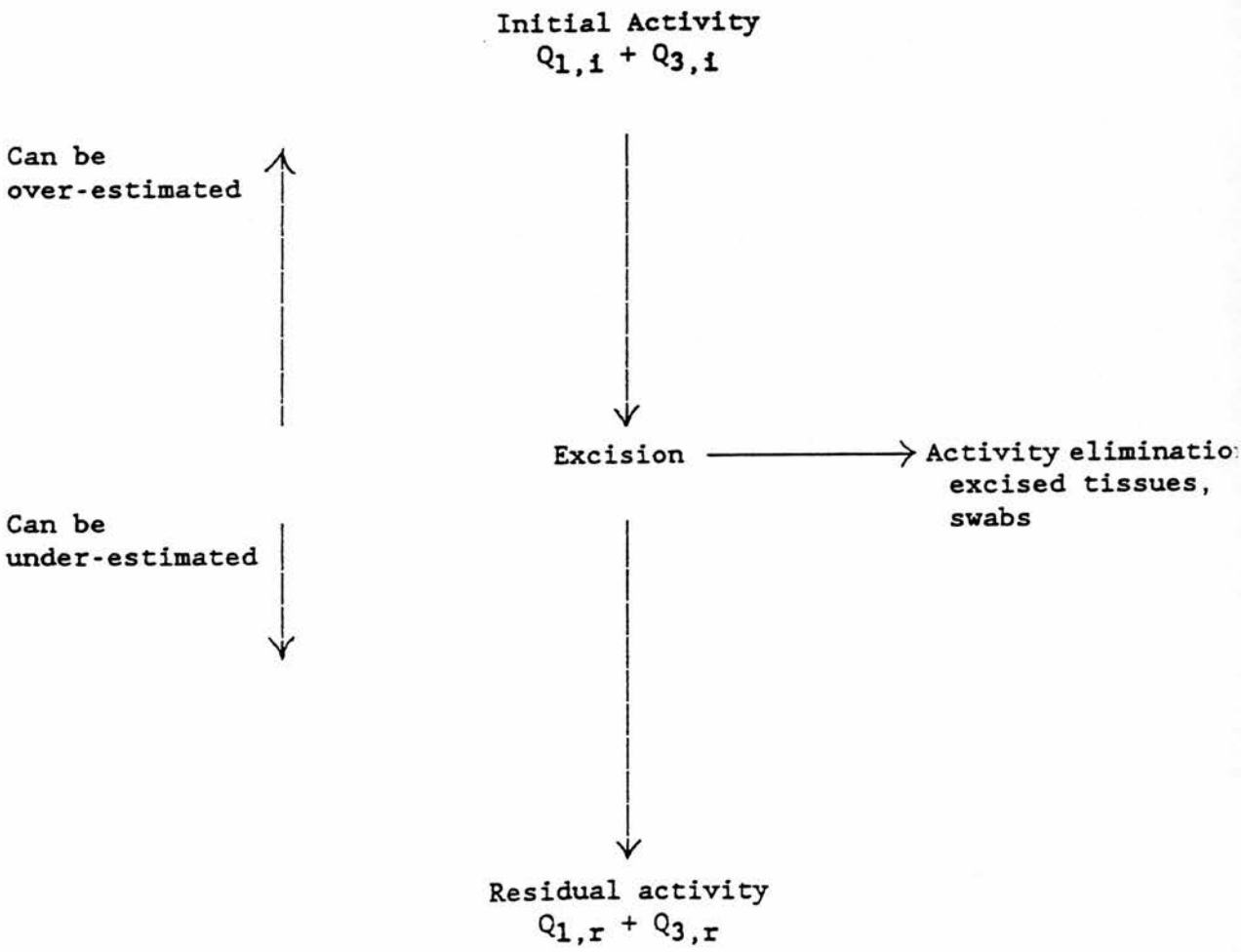

Table 3: Quantities Estimated From Results Of Measurements

Local Measurements

Initial activity	Residual activity after excision
$Q_{1,i} + Q_{3,i}$	$Q_{1,r} + Q_{3,r}$

Urinary Measurements

Measurement during the first ten days	Measurements beyond the first month
Q_2	$Q_{3,r}$

Q_1 = non-metabolised component

Q_2 = rapidly transferred component

Q_3 = slowly transferred component

1.5 Survey of Instrumentation used for the Measurement of Plutonium in Contaminated Wounds

1.5.1 Introduction

In Table 4 (page 34), the photons emitted by plutonium isotopes which have previously been used for detection of these isotopes in vivo have been summarised. Most investigators have used proportional counters or scintillation detectors for detection and measurement of these photons. Since the 1960s lithium-drifted-silicon (Si(Li)) and lithium-drifted-germanium (Ge(Li)) detectors have also been utilised for the detection of plutonium in wounds. Although high-purity germanium (HPGe) detectors have been available since the early 1980s any application of these to the purpose of monitoring plutonium in wounds does not (to date) appear to have been reported. Two recently developed room temperature semi-conductor detectors, namely cadmium telluride (CdTe) and mercuric iodide (HgI_2), have already been marketed for the purpose of detection of low-energy x-ray emitters although some investigators feel they are, at the moment, best used as academic research tools, rather than as instruments for practical radiological protection (Totterdell, 1984; Manson, 1985; Cooke, 1986; Manson and Austin, 1985).

Table 4: Photon Energies Useful for Identification of Plutonium and Americium Isotopes (Lister, 1964; Putzier, 1966; Swinth, 1967)

ISOTOPE	ENERGY (keV)	PHOTONS/ALPHA
Pu-238	17 (average) L x-ray	1.30×10^{-1}
Pu-239	13.2*	1.40×10^{-2}
	17.0	2.10×10^{-2}
	20.4	0.40×10^{-3}
Pu-240	17 (average) L x-ray	1.00×10^{-1}
Am-241	14.0**	1.35×10^{-1}
	17.8	1.84×10^{-1}
	20.8	5.00×10^{-2}
	26.4	2.50×10^{-2}
	59.6	3.59×10^{-1}

* keV average total L x-ray 3.9×10^{-2} photon/alpha.

** keV average total L x-ray 3.7×10^{-1} photon/alpha.

1.5.2 Scintillation Detectors

For the measurement of radioactive contaminants in wounds, the type of detector that appears to have been used most frequently is a sodium iodide crystal activated with thallium (NaI(Tl)), that is optically coupled to a photomultiplier tube. The high density of the crystal, together with its high effective atomic number, results in a high detection efficiency. This can be seen in Figure 4 (page 38), from Tait (1980), which shows the mass attenuation coefficient as a function of photon energy for NaI(Tl) crystals. For low-energy measurements, however,a very thin crystal should be chosen in order to reduce the background count due to Compton scattered photons (Compton continuum). The ratio of the square of the net signal (per unit activity being detected) to the background count rate ie S^2/B can be used as a figure of merit (Laurer and Eisenbud, 1967) for the determination of the optimum crystal thickness as a function of the photon energy being detected. Laurer and Eisenbud (1967) also state that a crystal thickness of 1 mm is a good choice for the detection of plutonium and americium.

Thin sodium iodide crystals have been used from 1958 to the present day to detect localised sources of plutonium in wounds. Roesch and Baum (1958) used a two-inch diameter, 1.0 mm thick NaI (Tl) crystal placed close to

the surface of the tissue; quantities the order of 37 Bq could be detected but in order to achieve this sensitivity the plutonium source had to be localised and close to the surface of the tissue. Putzier et al (1958), Gale et al (1960), Epstein and Johanson (1966) and Splichal Jnr (1966) described equipment and procedures similar to Roesch and Baum (1958) with variations in sensitivity being achieved by refinements in shielding, electronics, crystal size, area and thickness. Jones and Saxby (1968) described a number of wound monitors (all using NaI(Tl) crystals) then commercially available; for all of these instruments the technique used was that of single-channel spectrometry around the 17 keV x-ray region of the L x-rays produced by plutonium-239. In general all detected radiation was attributed to the presence of plutonium-239, which lead to the over-estimation of the plutonium content in a wound in certain cases. The methods and sensitivities described were adequate for monitoring plutonium contamination in small wounds within about 1 cm of the skin surface.

Other investigators utilised more complex analytical techniques; Heath (1966), Yamoaka et al (1968), Sharma and Somasundaram (1971), Norwood (1972), Vasilik et al (1968), Waechter et al (1983) and Erkilla (1984) have all developed methods which either involved spectral analysis and/or comparison of the relative transmission of the

different X-ray energies in order to determine the depth of the contaminant. Fromhein et al (1975) used three detectors to obtain the position of a plutonium source in a wound; the detectors were manipulated until the maximum response of the pulses produced was obtained.

Unfortunately, the scintillation crystals normally used (sodium iodide, caesium iodide) do not provide good resolution of the different L x-rays or good separation of the 26 keV gamma peak of Am-241 from its L x-rays (for example, Roesch and Palmer, 1962). Moreover, the iodine escape peak that always accompanies the 60 keV Am-241 gamma-ray peak (Swinth, 1967; Axiel, 1954) is not readily resolved from the L x-ray peak. Figure 5 (page 39) shows a Pu-Am spectrum obtained with the 0.5 inch diameter, 1 mm thick NaI(Tl) crystal used in the Dounreay Occupational Health Department, and indicates the typical minimum resolution of about 30% (or more) that is attainable in the Pu or Am L x-ray region.

Figure 4: Mass Attenuation Coefficient as a Function of Photon Energy for Sodium Iodide (Tait, 1980)

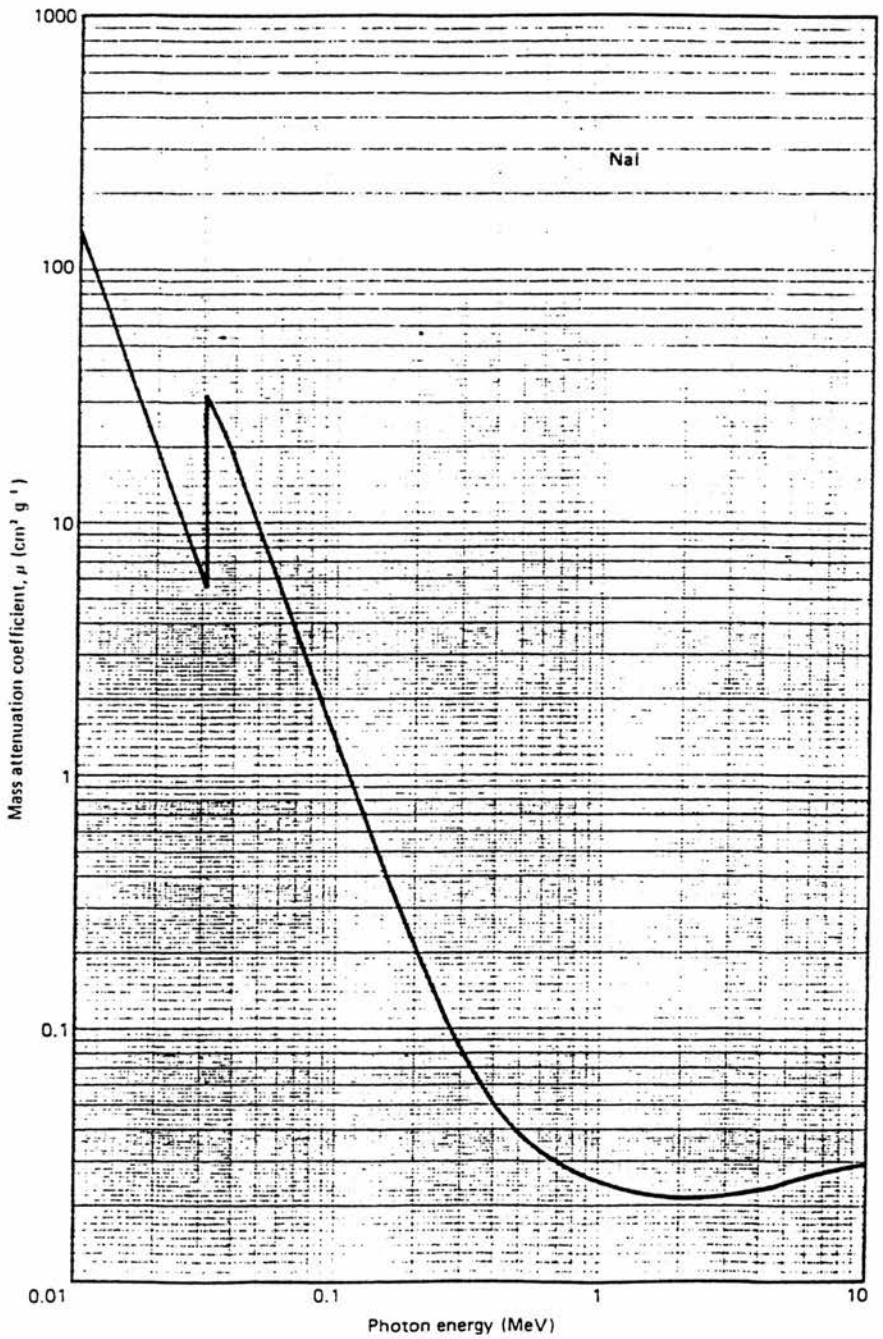

Figure 5: Spectra of Pu-Am Samples; 0.5 inch x 1 mm NaI crystal

Curve 'a' - 100 KBq Pu-Am source 9% Am-241 by alpha activity, 10 minute count

Curve 'b' - 5.6 KBq Pu-Am source 70% Am-241 by alpha activity, 10 minute count

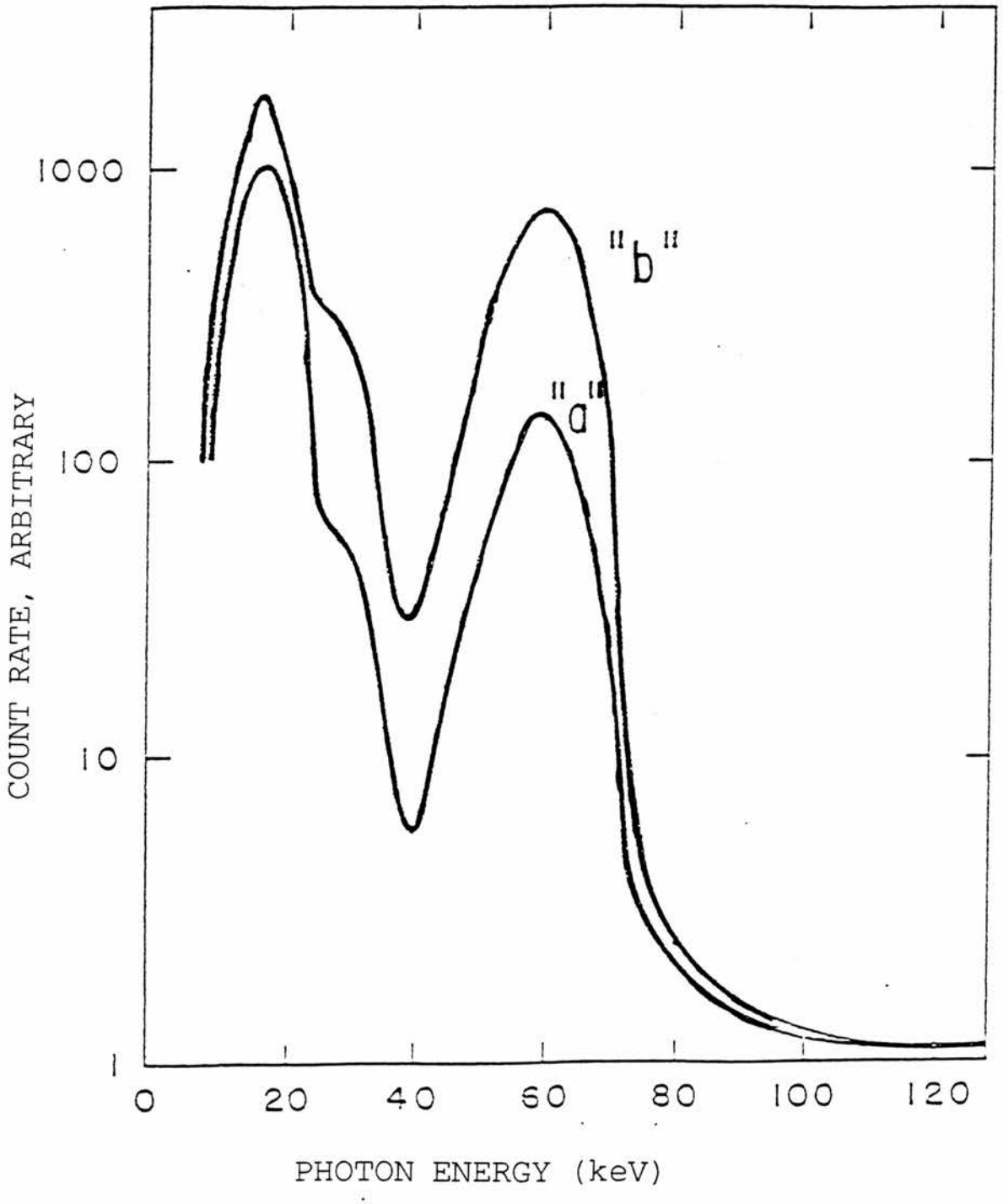

1.5.3 Proportional Counters

Proportional counters can be used for the detection and spectroscopy of soft x- and gamma-rays whose energy is low enough to interact with reasonable efficiency in the counter gas. The main advantages in the use of these counters for the detection of plutonium in vivo are their good resolution, low background and the possibility of being produced in large dimensions (for example, Fessler et al, 1961; Kiefer and Maushart, 1962, 1964, 1968; Lansiart and Morucci, 1964; Ehret et al, 1964; Ramsden, 1969). For localised scanning, however, they are not as sensitive as scintillation detectors such as NaI(Tl) and hence have been used for whole body counting, rather than measurements of radionuclides at wound sites. The resolution obtained with proportional counters for whole body counting is 13% to 16% at 13 keV (Kiefer and Maushart, 1968) and about 11% at 17 keV (Ramsden, 1969), the gas mixtures used being either argon and methane or xenon and methane.

A low background can be achieved by standard techniques using clean, heavy, graded shielding and by the careful choice of the constructional materials. Anticoincidence detectors are incorporated into the main counting chamber using the multiwire technique (for example,Ramsden and Speight, 1967). The gating detectors operate in the proportional mode with a common gas filling and share a

common gridded cathode with the main counters. Using anticoincidence techniques, the background in the 10-25 keV region can be reduced to 1.0 counts per minute (Ramsden and Speight, 1967).

The efficiency of proportional counters depends upon the gas used, its pressure and "thickness", and, of course, the energy of the incoming photon. Figure 6 (page 43) shows the interaction probability of gas counters in 5.08cm each of argon, krypton and xenon at STP (Knoll, 1989). Figure 7 (page 44) shows Pu-239 point source spectra obtained with a xenon-methane filled counter (Lansiart and Morucci, 1964). Figure 8 (page 45) shows the spectral comparison of Pu-239 and Am-241 (Boss and Mann, 1967); the spectra (except for the 60 keV Am-241 gamma) were obtained using an argon-methane filled counter. Figure 9 (page 46) shows spectra of Pu-239 with 0 to 30 mm thicknesses of plexiglass interposed between the source and detector (Lansiart and Morucci, 1964).

It should be possible to construct a proportional counter that will have an absorption of close to 100% for uranium L x-rays, using the proper gas, pressure and thickness. The response function of these counters for low-energy x-rays can be complicated, however, by several effects related to characteristic x-rays generated by interaction of the primary radiation within the counter. The most

significant involves the characteristic K x-rays which usually follow the photoelectric absorption of the primary radiation in the fill gas. Because the corresponding energy can be relatively large (K_α x-ray energies are 2.97, 12.6 and 29.7 keV in argon, krypton and xenon, respectively), this x-ray may escape from the gas without further interaction, leading to the appearance of a corresponding "escape peak" in the response function. Other peaks in the response function may also arise from the absorption of characteristic x-rays generated by interaction of the primary radiation in the entrance window or walls of the counter. A low-Z window material such as beryllium is often chosen to minimise this contribution.

Utilising the ratios between the L x-ray peaks it is possible to estimate the depth of a point source of plutonium in tissue. Methods have been developed by various investigators (for example, Lansiart and Morucci, 1964; Yamoaka et al, 1968; Johanson and Lawrence, 1974; Toohey et al, 1983) which are quite satisfactory providing the contamination can be regarded as a point source within the body, and the only absorber is soft tissue. Thus, in many cases of contamination with plutonium, it is possible to determine not only the amount of plutonium but also the effective depth of the contaminant providing the plutonium to americium ratio is known.

Figure 6: Fraction of Incident Photons Absorbed in a 5.08 cm Thick Layer of Several Proportional Gases at 1 Atmosphere Pressure (Knoll, 1989)

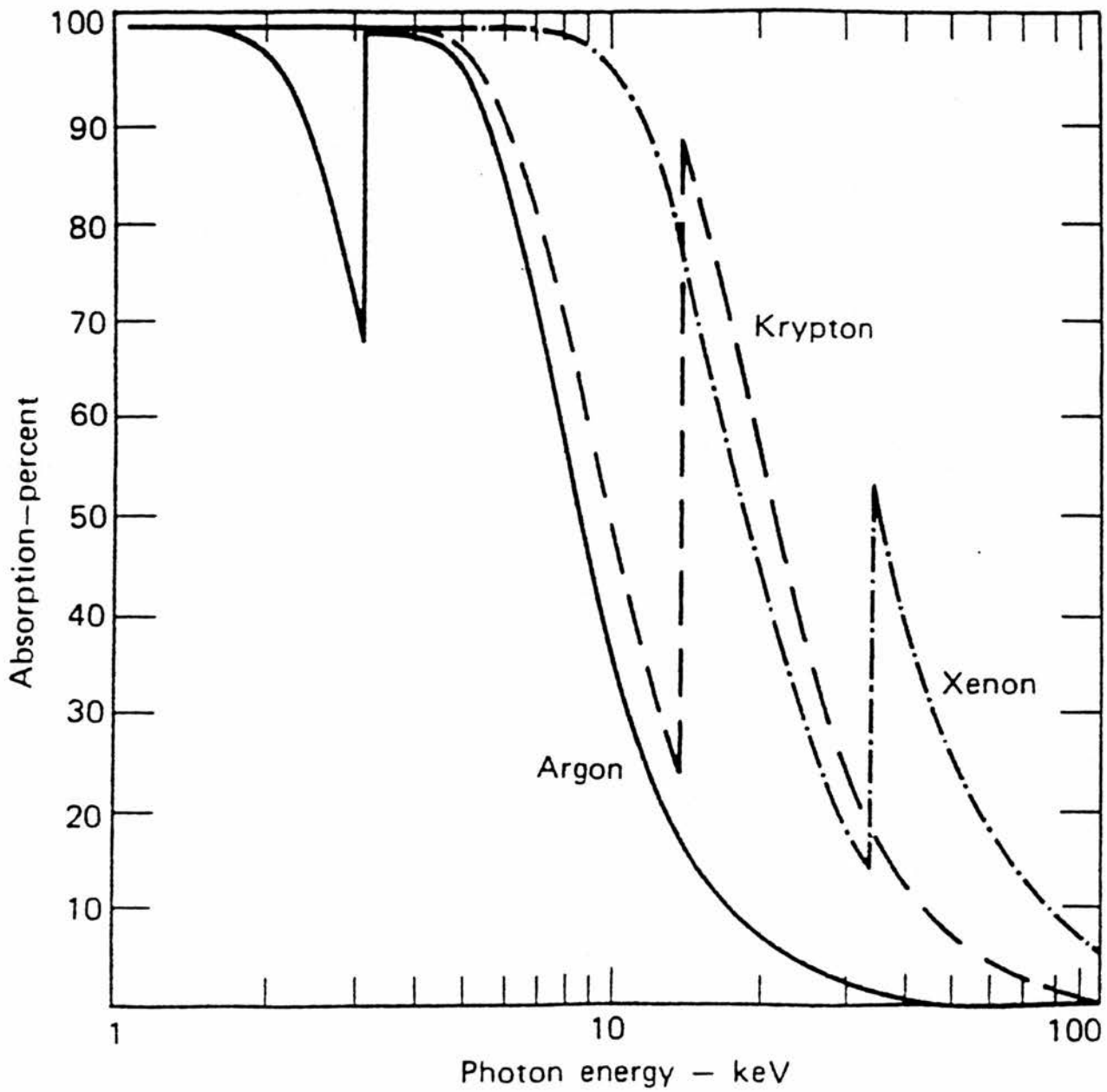

Figure 7: Spectra of Pu-239 L X-Rays Obtained Using a Xenon Proportional Counter (Lansiart &

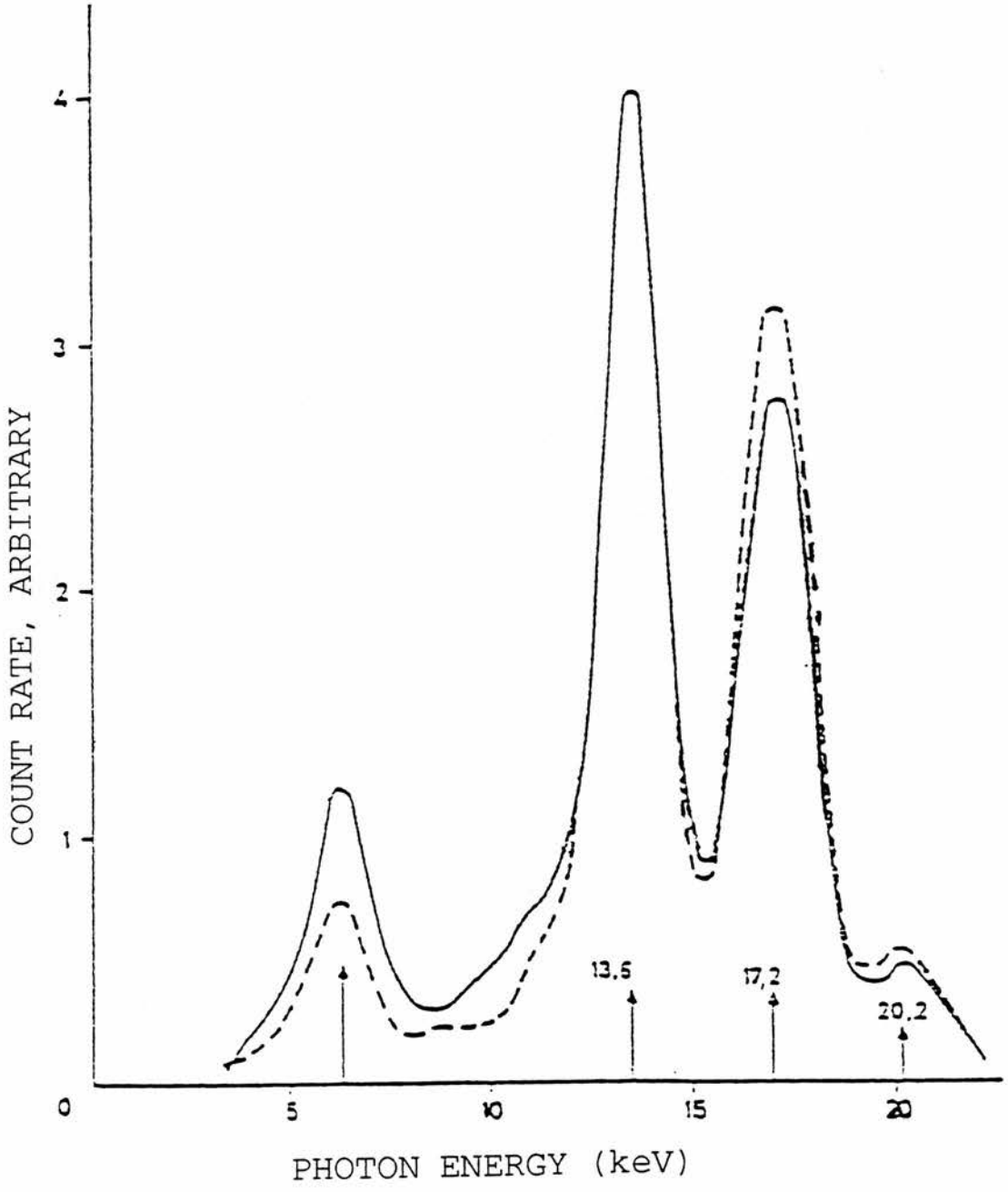

_____ SOURCE AT 10 cm FROM THE DETECTOR

---- SOURCE IN CONTACT WITH THE DETECTOR

Figure 8: Spectral Comparison of Pu-239 and Am-241 Using a Proportional Counter (Boss & Mann, 1967)

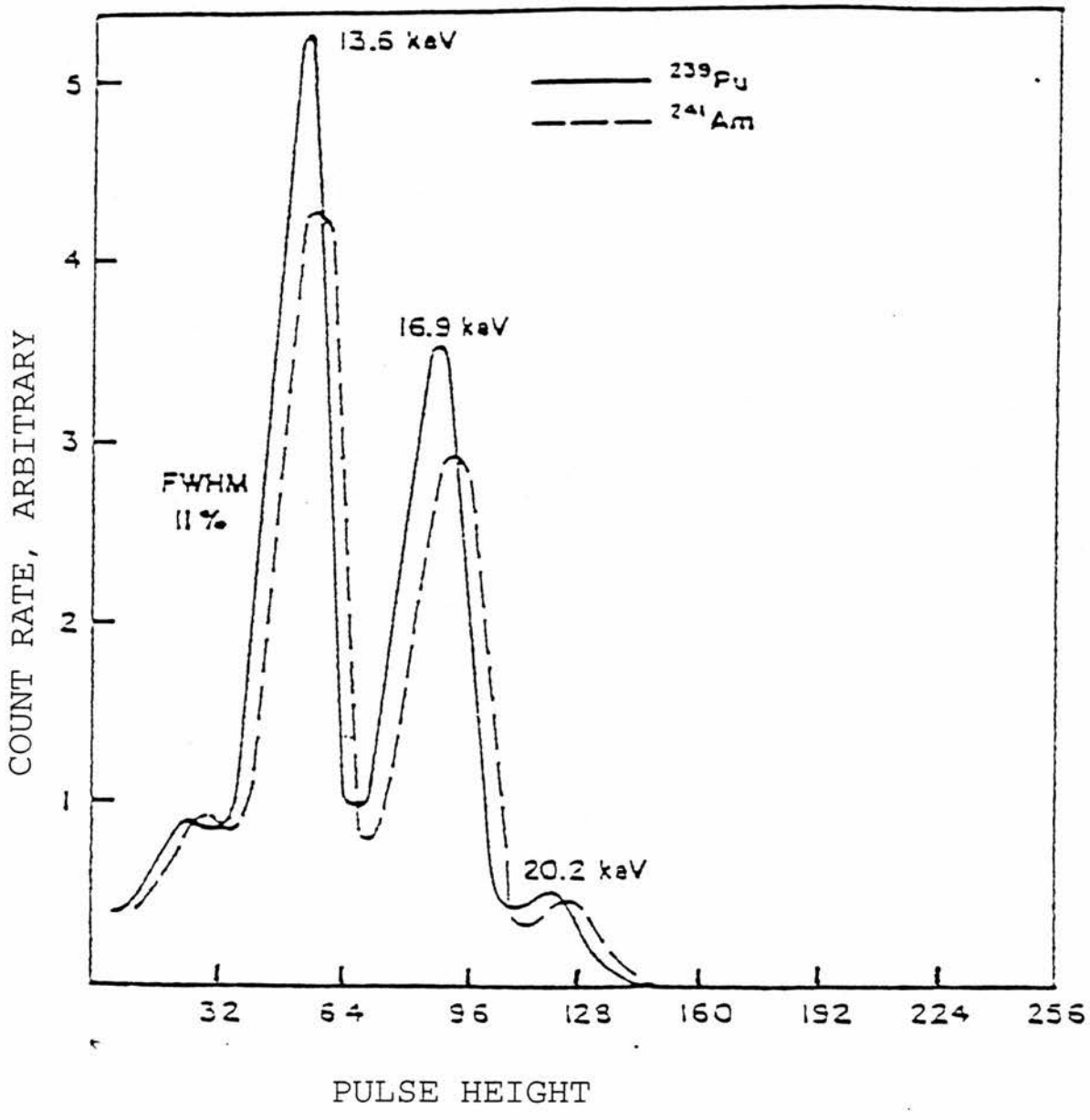

Figure 9: Absorption of Pu L X-Rays in Plexiglass

(Lansiart & Morucci, 1964)

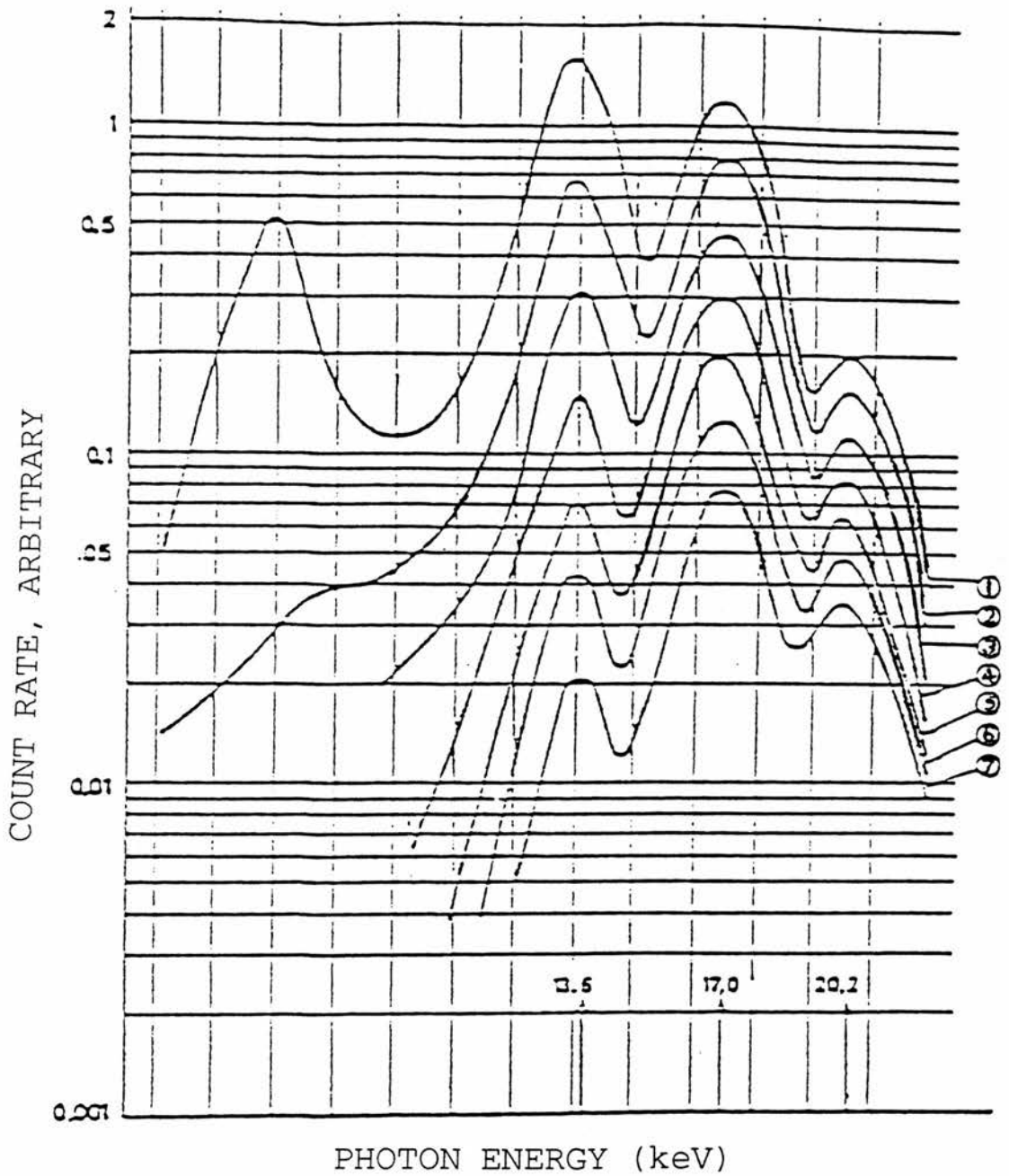

(1) WITHOUT ABSORBER (2) 5 mm ABSORBER

(3) 10 mm ABSORBER (4) 15 mm ABSORBER

(5) 20 mm ABSORBER (6) 25 mm ABSORBER

(7) 30 mm ABSORBER

1.5.4 Semiconductor Detectors

1.5.4.1 Lithium and Germanium Detectors

Lithium-drifted silicon (Si(Li)) detectors have several physical properties that make then ideal for low-energy photon spectrometry eg excellent resolution as shown in Figure 10 (Beck, 1969; page 51). Also, the intrinsic detection efficiency for uranium L_α, L_β, and L_γ x-rays in a 3 mm thick detector is 100%, 100% and 93% respectively (Palmer et al, 1967) and there are no resolvable escape peaks to interfere with spectrometry (the K-electron binding energy for silicon is 1.838 keV). Silicon detectors can be made with less than 0.05mg/cm^2 dead layer on the entrance window, which allows the detection of photons with energies less than 6 keV. As a result of the low atomic number (Z=14) and density of silicon, the detector efficiency is limiting at energies above 50 keV (compared with germanium (Z=32) the photoelectric cross-section is lower by about a factor of 50 for typical gamma-ray energies (Knoll, 1989)); hence, silicon detectors are not widely used in general gamma-ray spectrometry. However, one of the areas of application in which the lower atomic number of silicon is not a hindrance but a help is that of the detection of low-energy x- and gamma-rays, where the probability of photoelectric absorption can be reasonably high. Silicon detectors have therefore been used since the mid-1960s

for the detection and determination of plutonium in wounds, as given in the following examples.

Swinth (1967), Bistline and Tyree (1967), Palmer et al (1968) developed techniques for use with Si(Li) detectors that involved using the distinct absorption in tissue of the plutonium L x-rays. Palmer and Rieksts (1980) went on to study shallow depositions using the M x-rays from Pu-238/239 and Am-241; they showed that the M x-rays can be used to estimate shallow contamination at depths when the count rates from the L x-rays are not significantly altered by tissue thickness.

Lithium-drifted germanium (Ge(Li)) detectors have been found to have several advantages over Si(Li) detectors eg by Drexler and Perzl (1967); a higher atomic number (Z=32) increases the efficiency for photon detection. The greater mobility of electrons and holes in germanium enhances charge collection and hence greater count rates are obtainable than in silicon. Also, the lower energy required for the creation of electron-hole pairs in germanium causes less statistical fluctuation and hence less energy broadening than in silicon (eg Beck, 1969). However, because of the greater transparency of the detector to secondary gamma-rays, escape peaks play a much more important role than in NaI(Tl) scintillators. The escape of the characteristic x-rays from germanium following photoelectric absorption can be significant,

especially for small detectors with a large surface-to-volume ratio. A small peak will then be found in the spectrum at 11 keV below the photopeak, with the energy difference corresponding to the characteristic K x-ray energy for germanium. These x-ray escape peaks will be most prominent for incident low-energy gamma-rays, because photoelectric absorption is then most probable, and interactions will tend to occur near the detector surface. This is one of the reasons why silicon detectors, rather than germanium, have become the most common choice for low-energy photon spectrometry (LEPS) systems.

Neither Si(Li) nor Ge(Li) detectors are ideal from certain standpoints. Ge(Li) detectors must always be operated at low temperatures to reduce thermally generated leakage current. In low-noise applications, such as x-ray spectroscopy, Si(Li) detectors must always be cooled for the same reason. Since the early 1980s, however, the widespread availability of high-purity germanium has provided an alternative to lithium-drifting of germanium, and most manufacturers have now discontinued production of Ge(Li) detectors in favour of the high-purity germanium (HPGe) type. A major reason for this evolution is the much greater operational convenience afforded by HPGe detectors, in that they can be allowed to warm to room temperature between uses. In general, the most important performance characteristics

such as detection efficiency and energy resolution are nearly identical for HPGe and Ge(Li) detectors of the same size. In silicon, however, large depletion thicknesses can only be achieved by lithium drifting because of the present limit on available purity, one reason being that the higher melting point for silicon (1410 °C versus 959 °C for germanium) makes the exclusion of purities in the refining process more difficult.

In principle, a different semiconductor material with a wider band gap (eg greater than 1.5 eV) could reduce the bulk-generated leakage current so that use at room temperature would be possible. In many applications, this convenience would likely outweigh the disadvantages of a wider band gap, such as the greater energy required to create an electron-hole pair.

In gamma-ray spectroscopy, detectors with a high Z-value are at a premium. In this respect, (remembering that the photoelectric cross-section varies as Z^5 where Z is the atomic number), germanium (Z=32) is a great improvement over silicon (Z=14), but many other elements would obviously be even better. A great deal of attention has therefore been focused on seeking other suitable semiconductor materials which incorporate at least one element with a high atomic number, and this is discussed in the next section.

Figure 10: X-Ray Spectrum of Am-241 Obtained Using a Si[Li] Detector (Beck, 1969)

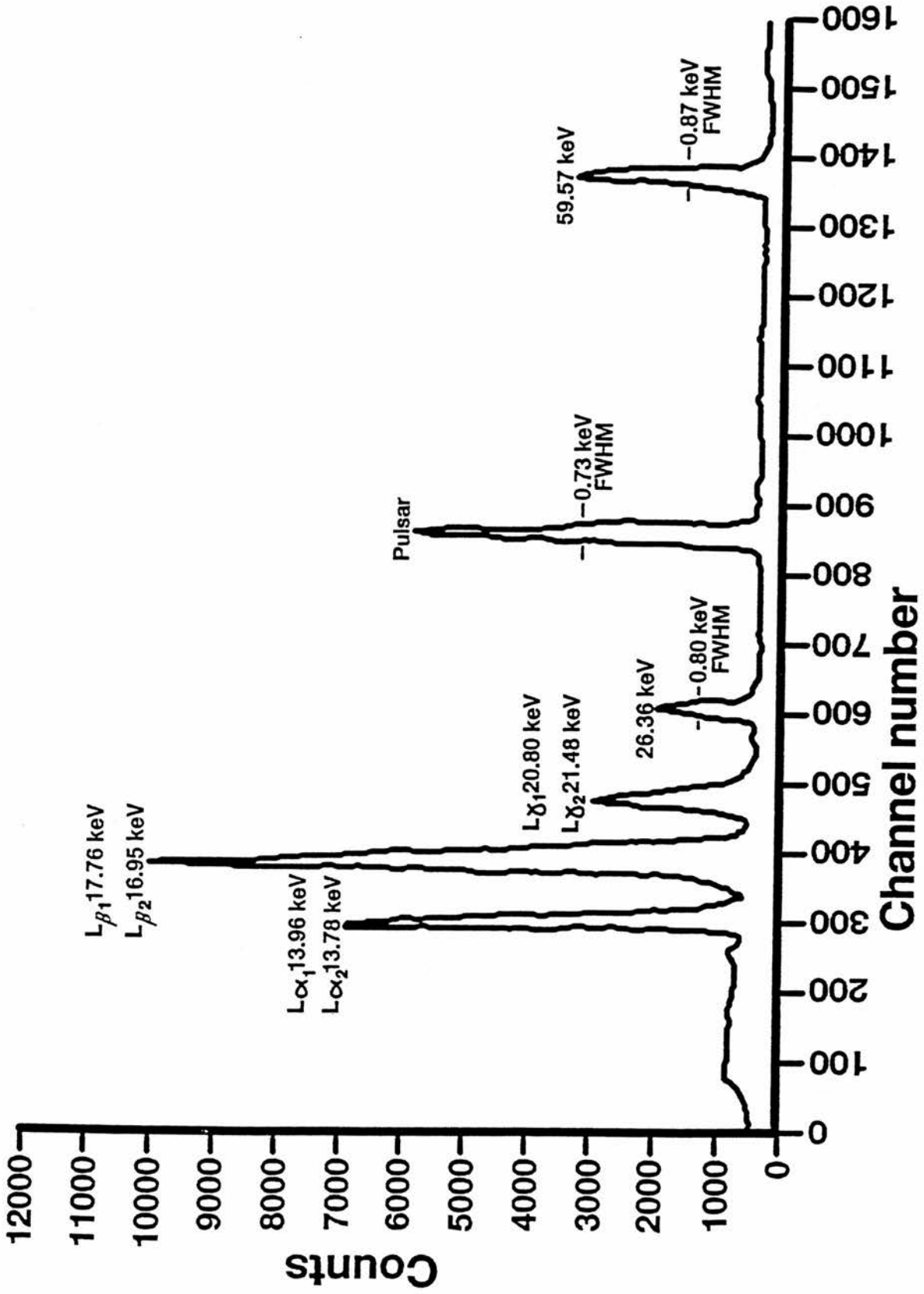

1.5.4.1 Other Semiconductor Detectors

To date, three specific compound semiconductors have received the most attention as potentially operable at room temperature: cadmium telluride (CdTe; Z_{max}=52), mercuric iodide (HgI_2; Z_{max}=80) and gallium arsenide (GaAs; Z_{max}=33). Some properties of these materials are compared with those of silicon and germanium in Table 5 (page 60).

In order for useful detectors to be fabricated from these semiconductors some practical requirements must also be met. Foremost is the ability to grow crystals of sufficient size to be interesting as detectors, while maintaining adequate purity. The density of trapping impurities determines the main charge carrier lifetime, which sets a practical limit on the distance over which charges may be collected with good efficiency. A low net impurity concentration is also required if large depletion depths are to be created within the material. Compound semiconductors are also sensitive to stoichiometric imbalance which can upset their theoretical behaviour.

Most high-Z semiconductor materials with wide band gaps, which are suitable for operation at room temperature, unfortunately tend to have low mobility (particularly for holes) and short carrier life times compared with silicon

or germanium. As a result, the effects of trapping and recombination are enhanced and charge collection is often incomplete over distances greater than 1 mm. The signal pulse shapes and pulse height spectra then become strong functions of detector geometry and/or irradiation conditions and are not easy to predict in advance. Furthermore, the small dimensions of these detectors lead to enhanced escape probabilities for secondary electrons and fluorescent x-rays. Swierkowski (1976) has reported some results from a Monte Carlo computational model which takes into account these effects for both mercuric iodide and cadmium telluride detectors.

Gallium arsenide has a photo-efficiency similar to germanium but with its higher band-gap does not require cooling. X-ray detectors using liquid phase epitaxial layers have been constructed by Gibbon and Howes (1972); the depleted layer in GaAs, However, is only of the order of 100 μm thus making it insufficient for use at 0.5 MeV (or above). After a series of investigations in the 1970s (eg Kobayushi and Sugita, 1972; Kobayushi et al, 1976) active development of GaAs as a detector material does not appear to have continued into the 1980s. The problems with this material include the limitation of available high-purity crystals to less than 1 mm thickness and experimental problems with abnormal leakage current and intermittent burst noise. However, the recent intense development of GaAs for fast

microelectronic components could stimulate new interest in detector development with this material.

Cadmium telluride (CdTe) combines a relatively high Z-value (48 and 52) with a large enough band gap energy (1.47 eV) to permit room temperature operation. The probability of photoelectric absorption per unit path length is roughly a factor of 4-5 higher in cadmium telluride than in germanium, and 100-200 times as large as in silicon for typical gamma-ray energies. Applications of this material therefore often involve situations in which a compact gamma-ray detector capable of operating at room temperature is required; its application as such has been reported by Entine (1976) and Howes and Totterdell (1978).

Crystals of relatively high purity can be grown for CdTe in which either chlorine or indium doping is used to make the material p-type. Although less common, the use of high-purity n-type CdTe has also been reported in practical detectors by Dabrowski et al (1976). The detectors are then operated as surface barrier junctions with metallic or carbon contacts. Presently available chlorine-doped material has a typical mobility-lifetime product of 1 or 2 x 10^{-3} cm^2/V and a corresponding value for holes of 3 to 8 x 10^{-5} cm^2/V, as reported by Bell et al (1975). The low value for holes is traceable to a residual acceptor impurity of about $10^{15}/cm^3$ and currently

limits the size of detectors in which reasonable energy resolution can be achieved, and if higher applied voltages can be supported by the detector before breakdown. Currently produced detectors can be operated only up to 100 volts reverse bias but improvements should be expected over the next few years, if the problem of copper impurity in the start material can be overcome.

Because of the rather poor collection efficiency for holes, the energy resolution achievable in CdTe detectors is generally not comparable with that obtainable in silicon or germanium. Reported energy resolutions range from about 3% at 122 keV to about 1% at 661 keV (Bell, 1975).

A persistent problem in the use of cadmium telluride is the phenomenon of polarisation which, under certain conditions of operation, leads to a time-dependent decrease in the counting rate and charge collection efficiency. This phenomenon has been reported by Bell et al (1974), Malm and Martini (1974) and Siffert et al (1976). This polarisation is apparently related to the capture of electrons by deep acceptors within the material. The resulting build-up of space charge interferes not only with carrier collection, but also leads to a gradual decrease in the thickness of the depletion region. Various remedies are currently being considered, as reported by Siffert et al (1976) and the

most promising appear to be connected with the manner in which electrodes are attached at the surface of the crystal. (The poor charge collection results in serious limitations on energy resolution at gamma ray energies in excess of 200 keV.) Calculations of the expected pulse height spectra from gamma-ray irradiation have been reported by Siffert et al (1974), together with data on the full-energy peak efficiency as a function of applied bias voltage, position of the interaction and energy of the incident radiation.

Despite the low manufacturing yield of useable material, CdTe detectors are commercially available in sizes ranging from 1 mm to over a centimetre in diameter. The commercial literature describes then as relatively rugged and stable in field use, with routine operation at temperature up to 30^{0}C without excessive thermal noise. Several investigators (Totterdell, 1984; Manson,1985; Manson and Austin, 1985; Cooke, 1987; Farnsworth, 1987) have reported otherwise.

Since about 1973, mercuric iodide (HgI_2) has been extensively investigated as a potential detector material combining a high-Z constituent and a wide band gap (2.1 eV). Due to the high photoelectric cross section for Hg (Z=80), low-energy gamma-ray interaction probabilities are as much as a factor of 50 larger than those for germanium. Because 85% of 100 keV photons are absorbed

within a 1 mm thickness, the material holds substantial promise for compact detectors of low-energy gamma and X-radiation. The unusually large band gap energy of 2.10 eV permits room temperature operation without excessive thermally generated noise.

Although detectors made from mercuric iodide are commercially available, some investigators still regard them as being in the research stage (Totterdell, 1984). Manufactured detectors are still limited to thicknesses less than 1 mm and active volumes of 20 or 30 mm^3. Furthermore, the material seems to be characterised by an inherently low mobility-lifetime product for holes (2 x 10^{-6} cm^2/V, compared with $10^{-1}cm^2/V$ for electrons) as reported by Randtke et al (1976). Thus, even if larger detectors could be fabricated, complete charge collection is likely to be very difficult. The poor hole migration properties can be overcome to some extent if the application involves relatively soft (30 keV) x-rays. It has been shown by Slapa et al (1976) and Schieber (1977) that useful detectors can be made from HgI_2, provided the incident radiation does not penetrate deeply into the detector volume. Then, the distance over which holes must be collected can be kept small, and charge collection will therefore be reasonably complete.

Further applications of mercuric iodide await the development of larger crystals with good charge

collection properties, and the solution to some of the polarization problems which have tended to plague these crystals in the past. Of all semiconductor materials investigated to this time, however, HgI_2 has the highest effective Z-value. This factor can be critically important in those applications where compact detectors of minimum thickness are required for gamma ray or x-ray detection.

The most recent developments in compound semiconductor detector research are those of cadmium selenide (CdSe; Z_{max}=31), bismuth sulphide (Bi_2S_3; Z_{max}=83), lead iodide (PbI_2; Z_{max}=82), gallium selenide (GaSe; Z_{max}=34) and aluminium antimonide (AlSb; Z_{max}=51). All of these materials have wide band gaps (ranging from 1.3 eV for Bi_2S_3 to 2.6 eV for PbI_2)and although several show promise for further development, none of them appear to have reached the point of commercial utilisation (Knoll, 1989). Most are limited to very small sizes, and there are often persistent problems with efficient charge collection. Development work continues on these materials, however, in the hope of producing an alternative to silicon or germanium that is capable of room temperature operation.

A promising development is that of an avalanche silicon photodiode used with scintillators; here, it has been possible to achieve charge multiplication in a solid-

state detector and hence this device is an analogue of a proportional counter. To date, small detectors have been developed by workers which have been used in place of a photomultiplier with a NaI(Tl) scintillation crystal. Typical avalanche detectors have an active diameter of 24 mm and an overall length of 30 mm, achieving 9.5% resolution at 662 keV. Systems can apparently be scaled down to 10 mm diameter leading to possible improvements in resolution but a loss in photon efficiency (Webb and Jones, 1974; Webb and McIntyre, 1976). The principal advantage of this is the compactness and ruggedness of the detector as compared to a photomultiplier assembly.

Avalanche detectors offer some attractive properties both from the viewpoint of signal-to-noise ratio and in speed of response. This combination of properties permits use of avalanche detectors for the detection of very soft radiation or under conditions in which the detector temperature is elevated. For example, Huth (1969) reported that 1.5 keV x-rays could be detected with a 30-40% intrinsic efficiency at temperatures between 85 and 100 °C while maintaining very low background levels.

Avalanche detectors appear to have been used in the biomedical field for the <u>in vivo</u> measurement of plutonium and other low-energy x-ray emitters, as detailed by Moldofsky and Swinth (1972).

Table 5: Properties of Semiconductor Materials

MATERIAL (OPERATING TEMPERATURE)	Z	BAND GAP (eV)[a]	ENERGY PER e-h PAIR (eV)[a]	BEST X-RAY ENERGY RESOLUTION (FWHM)[b]
Si (77 K)	14	1.12	3.61	
Ge (77 K)	32	0.74	2.98	420 eV @ 100 keV 920 eV @ 660 keV 1300 eV @ 1330 keV
CdTe (300 K)	48-52	1.47	4.43	3500 eV @ 122 keV 8000 eV @ 661 keV
HgI_2 (300 K)	80-53	2.13	6.5	650 eV @ 6 keV 2500 eV @ 122 keV
GaAs (300 K)	31-33	1.43	4.2	650 eV @ 60 keV 2600 eV @ 122 keV

a - data from Cuzin (1987).

b - representative resolution figures as tabulated by Siffert et al (1975).

1.6 Methods and Procedures Previously Used for the Measurement of Plutonium in Contaminated Wounds

From the discussion on instrumentation, it can be seen that it is possible to construct detection systems with low background and high sensitivity. The main problem is the translation of observed counts into the actual activity of any contamination.

Jones and Saxby (1968), and Yamoaka et al (1968) list the following sources of error in the determination of plutonium in a contaminated wound:

1) Assumption that the contamination is a point source;
2) Self-absorption of the x-rays within the active material lying in the wound;
3) Absorption of x-rays in overlying tissue;
4) Presence of Am-241 (or other isotopes) in the wound;
5) Positioning of the detector relative to the wound;
6) Calibration errors in the detector calibration source;
7) Counting statistics.

Some of these errors are reducible if a thin reference source is made from the same contaminating material and if both the wound and the reference source are to be examined using a low energy gamma spectrometer. Tyler

(1966) considered the possible error produced by self-absorption of the x-rays within a source which can occur when the plutonium is in particulate form. The conclusions drawn indicated that the measurement of plutonium contamination in wounds using an x-ray detector will be in error due to self-absorption if the contaminating material has a thickness greater than that of the standard source used for calibration of the detector. At the same time, the energy deposition in the tissue surrounding the contamination will be reduced by self-absorption of the alpha particles. Hence, for a single particle fixed within a wound, self-absorption will not cause monitoring with an x-ray detector to seriously underestimate the local hazard.

Yamoaka et al (1968) made the point that it is not really practical to consider that the contaminants are distributed in several points of the wound, in the case of insoluble contaminants, and distributed continuously in the case of soluble contaminants. In such cases the estimated value of the depth of the 'point source' will become the effective depth of the whole of the contaminant.

At AEA Technology Dounreay, all potentially contaminated wounds are measured using a thin NaI(Tl) detector and the method used is that of single-channel spectrometry around the 17 keV region of the L x-rays produced by plutonium-

239 (Austin, 1991; Austin, 1992). The decision on whether the wound is contaminated or not is done using the criterion proposed by Hartwell (1972); there is deemed to be no contamination if the net wound count is less than 2.33 times the standard deviation of the background count.

Should it be decided that activity is present in the wound then action will be taken to decontaminate the wound with further checks being made on the wound using the detector. Further monitoring, such as urine and faecal analyses and whole body monitoring, may be undertaken at the discretion of the Radiation Protection Advisor for the area concerned in consultation with the Dounreay Approved Dosimetry Service.

For assessment of the results from any biological sampling carried out at Dounreay as part of further monitoring, the metabolic models currently used for converting bioassay results to resulting dose are (Austin, 1991; Austin, 1992);

(a) Fission products: those given in ICRP 54. (1988)

(b) Plutonium: that given by Jones (1985) in conjunction with the lung model of ICRP 30 (ICRP,1979);

(c) Americium: that given by Griffith (1983);

(d) Uranium: that given by ICRP 54 (1988);

The medical centre at Sellafield also uses a thin NaI(Tl) detector for the measurement of contaminated wounds. At this establishment, however the detector is located in a shielded room in order to minimise the background count (Hadwin, 1986). At BNF Springfields an end-window G-M tube (and associated mini-monitor) is used with further checks being carried out using the whole body counter there (Cooke, 1987).

At all these establishments any contamination detected in the wound is presumed to be Pu-239 (the most pessimistic assumption) thus ignoring the presence of any other isotopes.

1.7 The Advantages of Plutonium Measurement by Means of the Am-241 60 keV Gamma Rays

The ability to measure deposited contamination is related to the number of photons reaching the sensitive volume of the detector. This, in turn, is related to the number of photons emitted and the absorption of the photons in the material between the source and the detector.

Figure 11 (page 67) shows the mass energy absorption coefficients for bone and muscle in the energy range 100-1000 keV. The half-value layer of Pu L x-rays is of the order of 0.6 cm in tissue and 0.02 cm in bone (eg Roesch and Palmer 1962). It can be seen that when Pu is deposited in bone there is little chance to detect it by measuring the L x-rays. It is possible, however, to detect the 60 keV gamma rays from Am-241 as they have a much greater half-value layer in tissue and bone (Hubbell, 1982). From the above, we can see that if Pu is deposited at a depth of a few cm in the body, more 60 keV photons will escape the body than L x-rays (assuming at least 100 ppm Am-241).

In the measurement of Pu in humans, one has to consider cases where the material is not solubilised, but is deposited as particles.

Figure 12 (from Cloutier and Watson, 1967; page 68) shows

the effect of self-absorption on the 13.2, 17.0 and 59.6 keV photons for spherical plutonium particles. As expected, the error introduced by self-absorption, even in small particles, will be much smaller if measurements are based on the 60 keV photon. Therefore, it appears advantageous to base a system for quantitative estimation of plutonium and americium contamination in wound sites on the 60 keV gamma measurements, provided the plutonium-to-americium ratio is known.

Figure 11: Mass Energy Absorption Coefficient of Muscle and Bone as a Function of Photon Energy (from Hubbell, 1982)

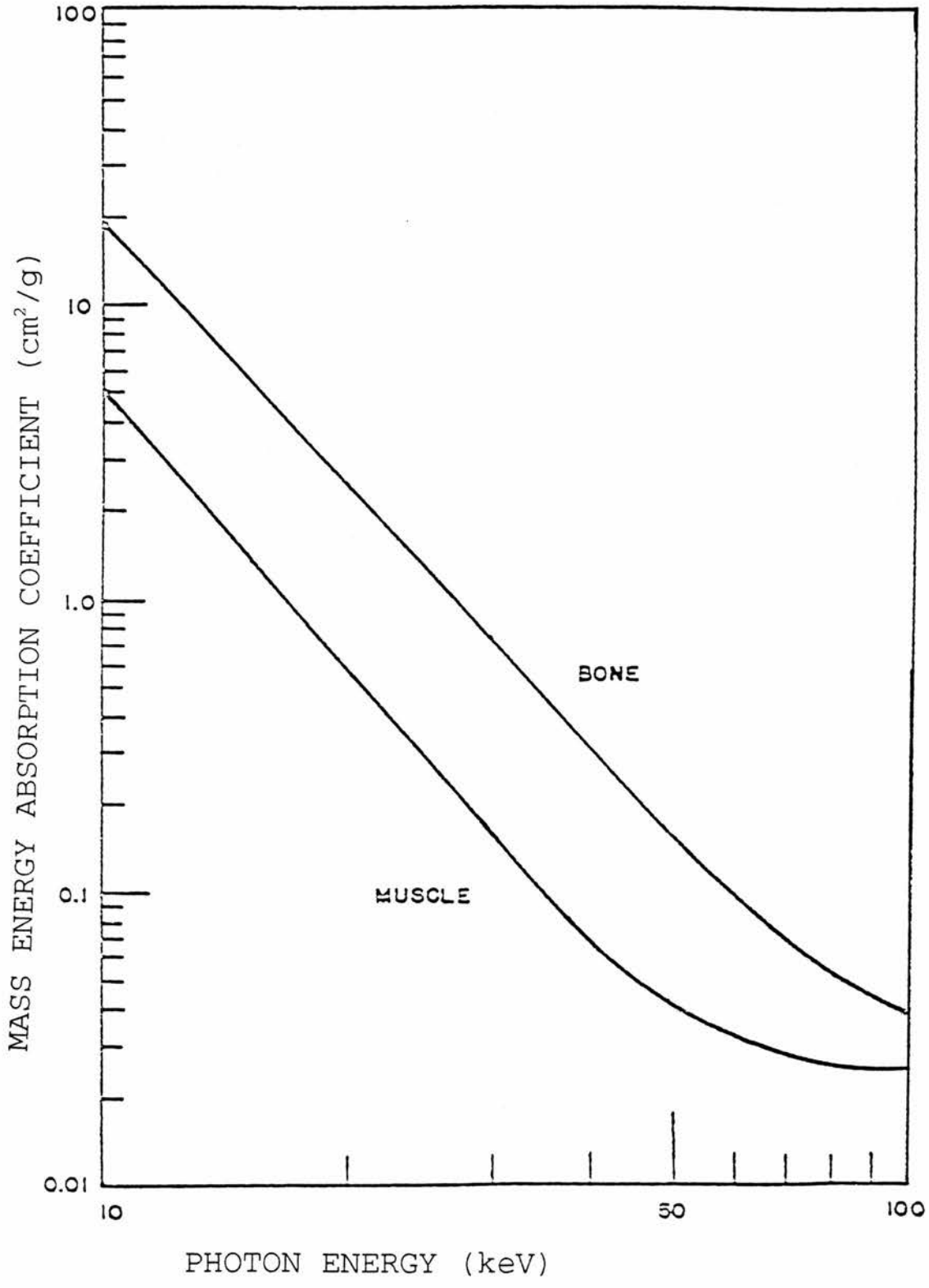

Figure 12: Effect of Self-Absorption on Relative Intensity as Related to Particle Mass (from Cloutier and Watson, 1967)

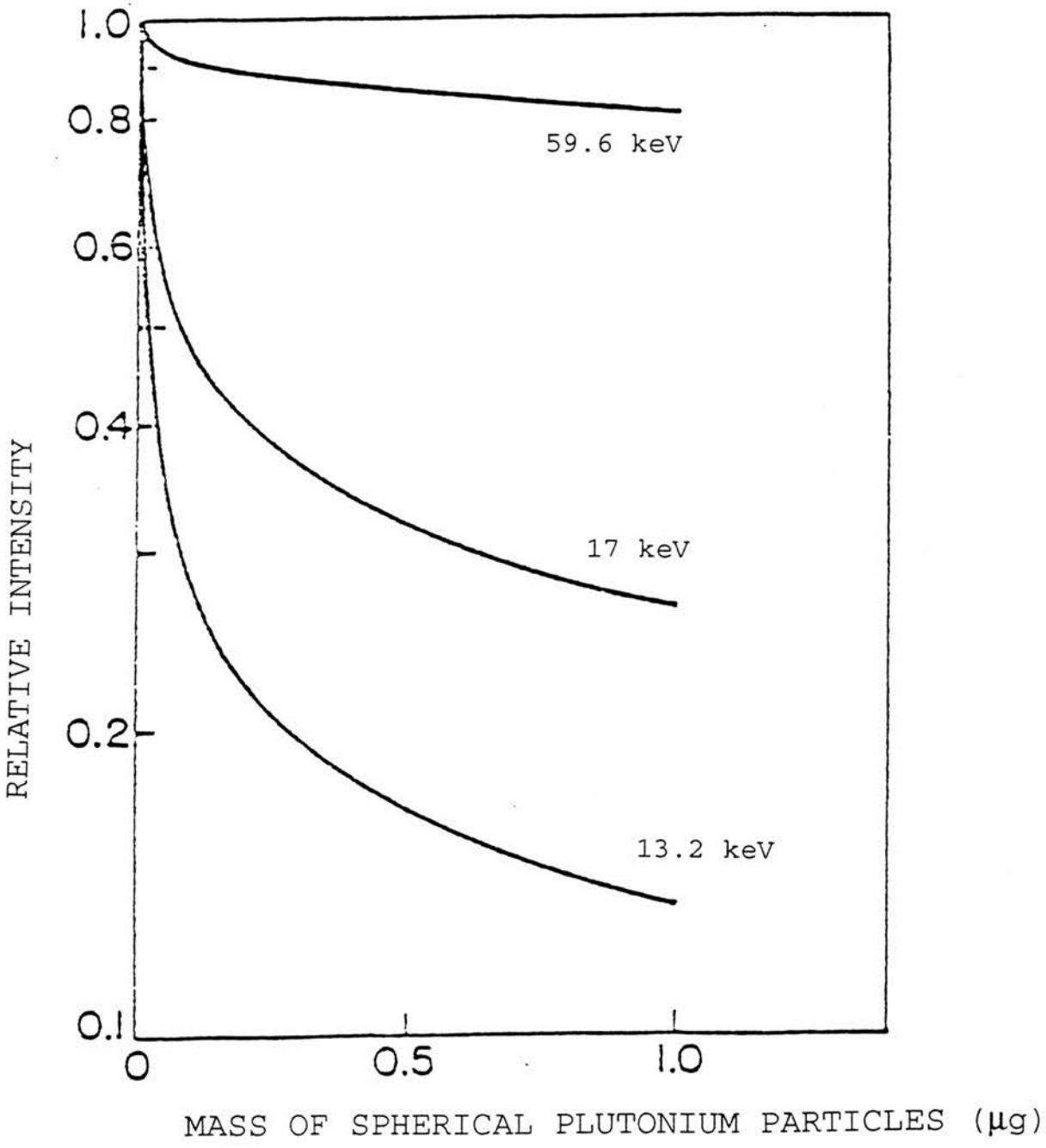

2. OBJECTIVES AND SCOPE OF INVESTIGATION

The objectives of this study were to assess two of the new types of semiconductor detectors that have been, or are in the process of being, developed for use as practical x- and gamma-ray detectors and which are now commercially available and, if possible, to develop a method for determining the depth and activity of plutonium isotopes and americium-241 within a contaminated wound, using those types of detectors (mercuric iodide and cadmium telluride) that were obtained for use in this study. Furthermore, the method to be developed was to be based only on the electromagnetic radiation emitted from the wound site, without reliance on the availability of standards having a known composition related to that of the contaminating material.

The hypothesis was that the x and gamma-ray spectra emanating from a wound site carry sufficient information to permit the estimation (within limits) of the attenuation of the 60 keV gamma rays from americium and of the different L x-rays. It was also supposed that it would be possible to separate the L x-rays emitted by plutonium from those emitted by americium, by calculating the contribution from the americium L x-rays using measurements of the 60 keV photons that are emitted only by americium, and to determine the plutonium-americium

ratio. Once this ratio is known, quantitive assessments can be obtained of both the Pu and Am deposits within a wound site.

The objectives of this study have now been partially achieved, and the results will be presented here to demonstrate, using plutonium and americium as an example, that it is possible to estimate the wound contents of low-energy (less than 100 keV) x- and gamma-ray emitters using a mercuric iodide detector. It was not possible, however, to assess the performance of the cadmium telluride detector obtained for use in this study because of its poor performance under operational conditions.

The present work has been limited to "point source" distributions in order to obtain an understanding of the relationships between observed spectral changes and changes in absorption paths and scattering geometries for various materials that simulate human tissue.

A "point source" can be defined as a source distributed within tissue in such a manner that distances from any two points within the source to the surface of the detector do not differ by more than one relaxation length ($1/\mu$ where μ is the linear attenuation coefficient). Thus, the size of the "point source" is a function of;

(a) the photon energy under consideration;

(b) the distance between the source and the detector;

(c) the size of the detector;

(d) the equivalent atomic number of the absorber.

The scope of the present work is also limited to cases in which there is no significant contamination by radioisotopes other than those of plutonium and americium, and the americium contributes at least 2% of the total alpha activity. In cases of wound contamination by essentially pure plutonium the problem is simpler, since there are no Am-241 L x-rays nor are there problems associated with the escape of the characteristic x-rays. The investigations were carried out for sources containing more than 2% Am by alpha activity since the contribution of the americium L x-rays to the observed count rates can be neglected for smaller percentages of americium.

3. THEORETICAL BASIS FOR A METHOD OF PLUTONIUM AND AMERICIUM MEASUREMENTS

3.1 Measurements of the L X-Ray Photons from Plutonium and Americium

The absorption of low-energy x-rays from plutonium and americium is strongly dependent on their energy and on the atomic number of the absorber (Hubbell, 1969; Hubbell,1982). Since the human body is not homogeneous in its chemical composition and density, it would be impractical to try to determine an "universal" attenuation coefficient for all types of tissue for these low energy x-rays.

At very low quantum energies, the absorption of photons is due mainly to the photoelectric process; in oxygen, for example, the Compton scattering cross-sections, with and without coherent scattering, for a 15 keV photon are 8.00 barns/atom and 5.03 barns/atom, respectively, whereas the photoelectric cross-section is 38.1 barns/atom (Hubbell, 1969). (The total scattering cross-sections, with and without coherent scattering are 46.1 barns/atom and 43.1 barns/atom, respectively.)

There is also an appreciable Rayleigh (coherent) scatter. The small amount of Compton scatter present is virtually coherent since the effectiveness of Compton scatter for

transfer of energy in biological tissues is not great until the incident photon energy is in excess of 100 keV or so. The change in wavelength due to Compton scatter as a function of the angle of scattering is given by the Compton formula (eg Johns and Laughlin, 1956):

$$\lambda' - \lambda = \Delta\lambda = h/m_o c\ (1-\cos\phi) = 0.0241(1-\cos\phi) \quad (3.1)$$

where;

λ = wavelength of incident photon in Angstroms;

λ' = wavelength of scattered photon in Angstroms;

m_o = electron mass;

c = velocity of light;

ϕ = angle of scattered photon with respect to its initial direction;

As seen from equation (3.1), $\Delta\lambda$ assumes its maximum value at $\phi = 180^0$, $\Delta\lambda max = 0.0482$ Å.

For a 15 keV photon, the maximum possible energy loss in a single collision is therefore 0.8 keV. As a result of this, it can be assumed that there are only two types of photon interactions that matter at these low energies; these are photoelectric absorption and "coherent" (true elastic plus Compton) scatter (no matter what the absorber).

The above facts suggest that for a monoenergetic x-ray beam of low-energy photons, there would be simple exponential attenuation of a broad beam over many mean free paths. Thus, for the specified beam an universal absorption curve, independent of atomic number, can be utilised to express transmission versus the product of absorber thickness times the energy absorption coefficient of the respective absorber.

The reason for this is as follows; since the scatter is all essentially elastic, the photons at any depth have practically the same energy as the original photons and the fluence is the same except for those photons that have been absorbed. Then a single value of μx (the number of 'mean free paths') uniquely describes the actual absorption. The effect of Rayleigh scattering can now be considered.

The differential cross-section per unit solid angle $d_e\sigma/d\Omega$ in cm^2/electron per steradian gives the probability that a photon will be scattered by an electron into a unit of differential solid angle, $d\Omega$, at angle ϕ. The value of $d_e\sigma/d\Omega$ for Rayleigh scattering is given by (eg Johns & Laughlin, 1956);

$$d_e\sigma/d\Omega = (e^4/2m_o^2c^4)(1 + \cos^2\phi) \qquad (3.2)$$

Where;

e = electronic charge

m_o = electron mass

c = velocity of light

It can be seen that there will be the same number of photons scattered at angle ϕ as at angle $(\phi + 180^0)$ because $\cos \phi = -\cos [\phi + 180^0]$. Furthermore, the total fluence of photons is emitted omnidirectionally, and in the case of the point source of photons, is the same in all directions. Thus, due to the symmetry of coherent scatter, the photon flux density (in terms of the net number of photons passing out through one cm^2) will not be appreciably affected by scattering.

Any distributed source can be considered to be composed of an infinite number of point sources and so it can be concluded that the Rayleigh scattering will not appreciably change the number of photons per unit solid angle escaping from an absorber (in the range of tissue thicknesses to be encountered in <u>in vivo</u> counting). The attenuation in the absorber can also be described by a simple exponential function, since the energy spectrum, and consequently the effective absorption coefficient, changes only slowly through many mean free paths of the material.

Another useful fact is that the ratio of the mass-energy absorption coefficients for the photon energies under

consideration is nearly a constant over the range of Z for elements encountered in the human body as shown in Figure 13 (Hubbell, 1982; page 78). Thus, in the case of a point source of americium-plutonium, the following four equations can be written for the low energy x-rays, when the detector is located at the surface of the absorber;

$$N_1 = N_{1,0}\, e^{-\mu_1 x}\, f_1.g(x) \qquad (3.3)$$

$$N_2 = N_{2,0}\, e^{-\mu_2 x}\, f_2.g(x) \qquad (3.4)$$

$$\mu_1 x/\mu_2 x = r, \text{ a constant} \qquad (3.5)$$

$$N_{1,0}/N_{2,0} = a \qquad (3.6)$$

where;

N_1 = the total number of counts minus the background counts measured by the detector in the 13-14 keV region;

N_2 = the total number of counts minus the background counts measured by the detector in the 17-18 keV region;

$N_{1,0}$ = total number of photons in the 13-14 keV region emitted by the contaminant;

$N_{2,0}$ = total number of photons in the 17-18 keV region emitted by the contaminant;

$e^{-\mu_1 x}$ = describes the effective attenuation of the 13-14 keV photons in the body;

$e^{-\mu_2 x}$ = describes the effective attenuation of the 17-18 keV photons in the body;

f_1 = efficiency factor of the detector for 13 - 14 keV photons;

f_2 = efficiency factor of the detector for 17-18 keV photons;

$g(x)$ = geometry correction factor.

A similar set of equations can also be written using the 20-21 keV L x-rays in place of either the L_α or L_β x-rays.

Equations 3.3 through 3.6 can be solved for plutonium alone or for americium alone. For a mixture, however, the plutonium-americium ratio must be known. Otherwise $N_{1,0}/N_{2,0}$, (which can vary from 0.667 (for plutonium) to 0.734 (for americium) as seen in Table 1, page 16) will not be known.

This small difference in ratios of L x-rays between Am-241 and Pu-239 will obviously limit the ultimate precision in discriminating between Am and Pu compositions. The geometry correction factor, in "good" (narrow beam) geometry, is independent of photon energy and atomic number of absorbing material. "Good" geometry can be assured at all energies by counting only those photons that do not undergo energy degradation, and hence by selecting, for each energy, a narrow band of the spectrum for analysis. (In this case, however, it is more probable that we have nearly ideal broad beam geometry, rather than one of true narrow beam geometry.

Figure 13: Mass Energy Absorption Coefficients of Low Z Elements as Function of Photon Energy (from Hubbell,1982)

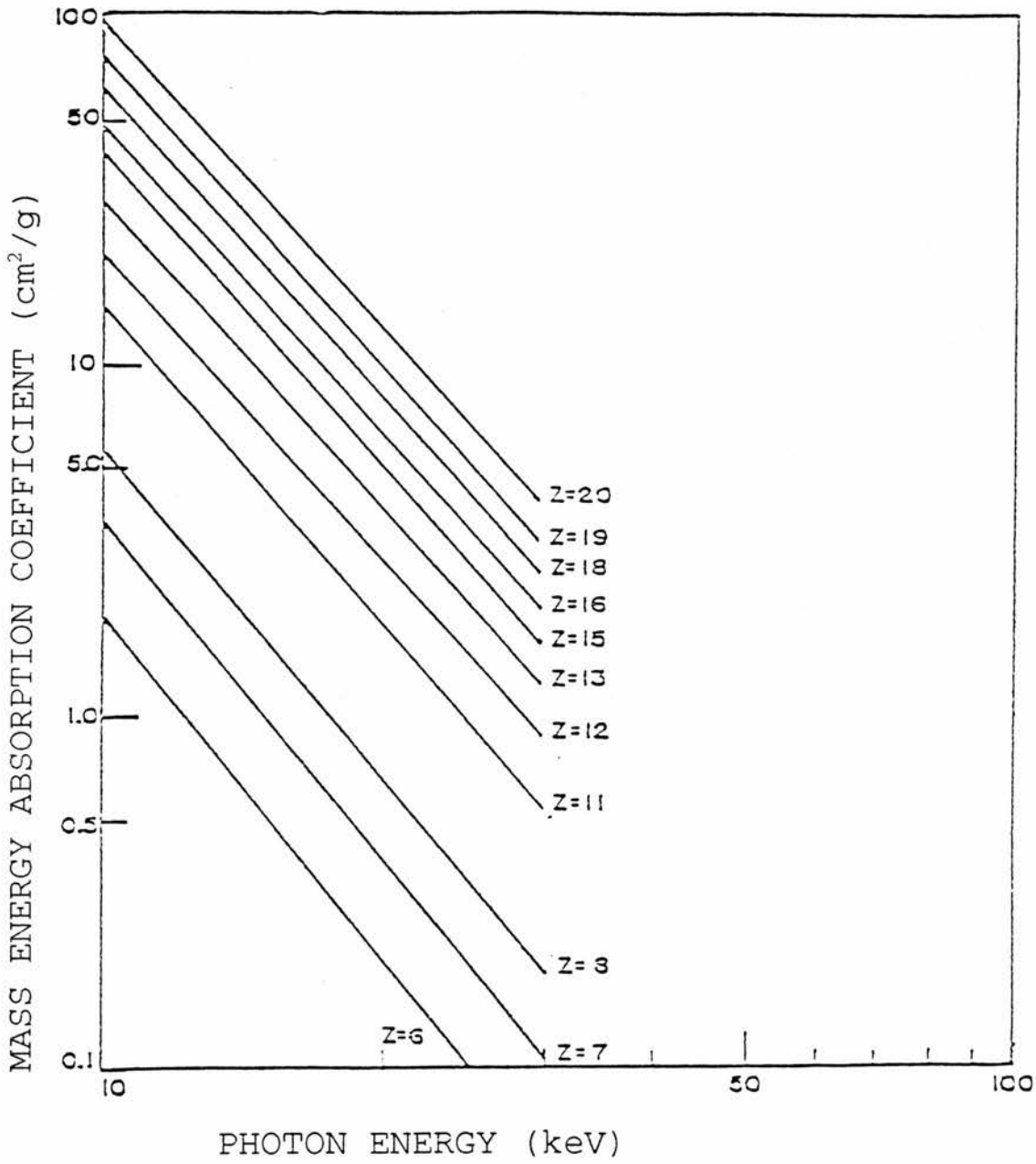

3.2 Measurements of the 60 keV Photons from Americium

The measurement of 60 keV photons (the 59.6 keV photons will be referred to as 60 keV for convenience) emitted by sources located in tissue presents a different problem than the measurement of the low-energy x-rays discussed previously. The following facts must be considered.

The major process of interaction with matter of 60 keV photons in low Z materials is Compton scattering; in oxygen, for example, the Compton scattering cross-section for a 60 keV photon is 4.63 barns/atom including coherent scatter, and 4.36 barns/atom without coherent scatter. The photoelectric cross-section is only 0.448 barns/atom (Hubbell, 1969).

The change in photon energy due to Compton scatter is appreciable and can not be neglected. The maximum possible energy loss for a 60 keV photon in a single collision is 11.3 keV. The change in photon energy, however, for a photon scattered at 90^0 is only 6.0 keV.

The attenuation process causes, therefore, not only reduction of the original number of photons but also degradation of photon energy and changes in photon direction. In the Compton process, the interaction is between the photon and a free electron. If the photon energy is large compared with the electron binding energy

then the electron may be considered to be free (eg Johns and Laughlin, 1956). This is certainly the case for 60 keV photons interacting with tissue, and therefore the Compton scattering cross-section per electron is the same for all elements under consideration. The number of electrons per gram of any material is given by N_E (= Avogradro's number) x Z/A where A = the mass number and Z = the atomic number. The ratio Z/A is nearly constant (and equal to 0.5) for all low-Z elements, with the exception of hydrogen and the Compton scattering cross-section (in cm^2/g) will also be constant.

The electron density (ρ) in tissue and other compounds containing hydrogen is dependent on the hydrogen concentration. Table 6 (Johns, 1964; page 85) gives the electron densities of several elements, namely air, water, muscle, fat and bone. It can be seen that in human tissue the electron density does not vary much and equals 3.3 E23 +/- 10% electrons per gram. It can be said, therefore that the ratio of scattered to non-scattered photons originating from a source within a human body and reaching a detector located at a certain distance from it will be proportional to the depth (expressed in g/cm^2) of the source in the body, and the fraction scattered (within the limits stated above) will not be dependent on tissue composition. The non-scattered photons reaching the detector will be those emitted by the source into the solid angle subtended by

the detector minus those that were scattered and minus those that were absorbed by the photoelectric process. As has been stated, the photoelectric absorption coefficient is strongly dependent upon the atomic number of the absorber.

When the photons emitted by a source of unknown strength within human tissue are measured, the attenuation factor (of this tissue) must be known in order to determine the strength of the source (provided that the efficiency and geometry factors of the detector are known). This can be achieved if the number of scattered photons reaching the detector at an energy lower than 60 keV can be measured and if the atomic number of the absorber is known.

The calculation of the number of scattered photons as a function of source depth is complicated but methods are available for this purpose, the simplest being those that consider the source of radiation to be of regular geometric shape such as a point, line or plane. Taking account of the scattered component can be achieved by using a build-up factor as a correction term in the equation for the uncollided photons (Fitzgerald et al, 1967 and Profia et al, 1979). Many expressions for calculating these build-up factors are found in the literature, some in the form of tables or graphs (Goldstein & Wilkins, 1954; Goldstein, 1959), and some in the form of equations (Chilton, 1965; Trubey, 1966).

The majority of these build-up factors were developed for point sources in infinite homogeneous media and their use in other than point source geometries requires integration over the point source geometry. Although strictly applicable only to infinite homogeneous media, they are often used in finite, inhomogeneous geometries. If the source geometry is complex and irregular, analytical integration of the point source with build-up may be very difficult or impossible. In such cases a numerical point-kernel integration is sometimes used (Profia, 1979).

More exact solutions to the problem of scattered radiation can be achieved by applying the Boltzmann transport equation (Case & Zweifel, 1967) or the Monte Carlo method (Buslinko, 1966, Spainier & Gelbard, 1969). The first method consists in establishing a photon conservation equation and then obtaining a solution for the geometry in question. Derivation of such an equation is usually not difficult, but solving the equation exactly is generally impossible without introducing simplifying assumptions. The solutions are sometimes obtained analytically but often by numerical techniques. The Monte Carlo method simulates the flight and interactions of a photon from birth to absorption or escape from the system. A solution is obtained by averaging the results of simulation of the history of thousands of individual photons. As a rule, establishing

the Monte Carlo simulation is easier than obtaining a solution using the Boltzmann equation. Furthermore, the complexity of the geometry and the number of variables involved in the problem do not usually impose any severe limitations in the method. The disadvantage is that since it is stochastic in nature, a Monte Carlo calculation requires a great number of simulations, or histories eg. 100,000 to obtain a reliable average result. This, in turn, necessitates a very great number of calculations and hence long computer processing time.

In practical cases, using scintillation detectors for measurements of the spectrum, any calculations will be further complicated by the possible non-linear response of the detector to the spectrum in low-energy regions (ie. non-linearity in pulse-height versus photon energy and the limited energy resolution).

In proportional counters the energy resolution is much better, but the efficiency factor of the detector rises sharply with decreasing photon energy. Also, some of the secondary electrons will lose part of their energy in the detector walls, giving rise to pulses corresponding to a lower photon energy.

In the case of plutonium-americium sources, the photons in the energy range 35 - 55 keV (Table 2, page 17) also complicate the analysis and so it would seem very

practical, therefore, to obtain experimental factors relating the observed Compton scatter to the total attenuation.

Figure 14 (page 86) shows the spectra from an Am-241 source obtained with the 0.5 inch x 1 mm NaI(Tl) crystal used in the Dounreay Occupational Health Department. Curve **'a'** is for an unattenuated source (except for air and detector window attenuation), and curve **'b'** is for the same source attenuated by 7.1 g/cm^2 acrylic plastic/polymethylmethacrylate (trade names Lucite, Plexiglass and Perspex). It can be seen that the spectrum from an attenuated Am-241 source is spread over several keV with a large number of counts to the left of the 60 keV peak. The direct measurement of only scattered photons can be seen, therefore, to be quite difficult.

It is possible, however, to measure the relative increase of the low energy part of the 60 keV gamma spectrum due to Compton scatter; or, in other words, the increase in the ratio of counts in the photopeak as a function of attenuation, with the effective atomic number of the absorber as a parameter.

Table 6: Atomic Number and Number of Electrons per Gram of Absorbing Material (Johns, 1964)

Material	Density (g/cm^3)	Effective Atomic Number	Number of Electrons per Gram
Hydrogen	8.99E-5	1	6.01E23
Carbon	2.25	6	3.01E23
Oxygen	1.429E-3	8	3.01E23
Aluminium	2.7	13	2.90E23
Air	1.293E-3	7.64	3.01E23
Water	1.00	7.42	3.34E23
Muscle	1.00	7.42	3.36E23
Fat	0.91	5.92	3.48E23
Bone	1.85	13.8	3.00E23

Figure 14: Comparison of Spectra from Unattenuated (a) and Attenuated (b) Am-241 Sources

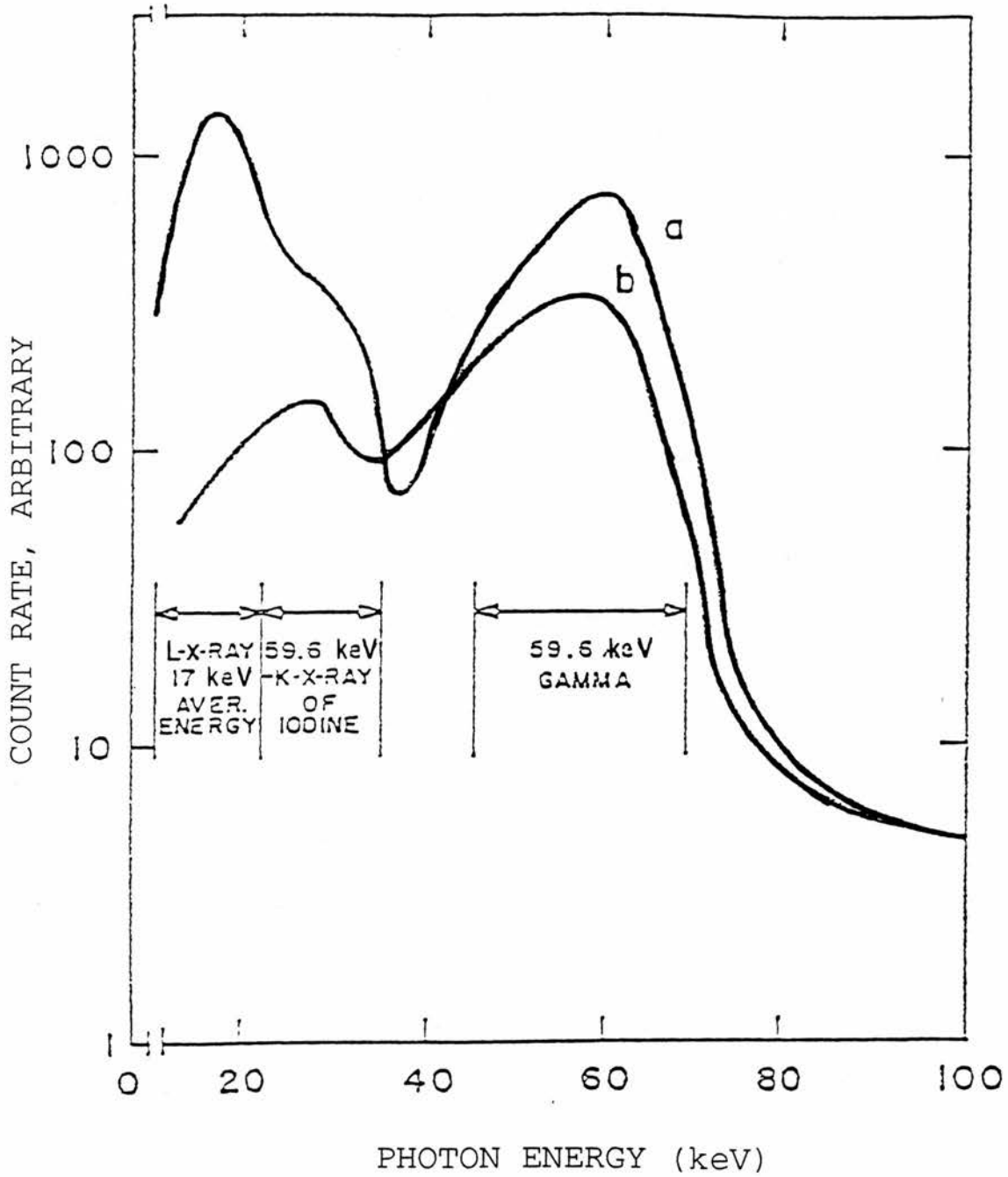

0.5 inch x 1 mm NaI(Tl) crystal

CURVE "a" - NO ATTENUATION

CURVE "b" - 7.1 g/cm^2 ACRYLIC ABSORBER

3.3 Estimation of the Effective Atomic Number

The effective atomic number (Z_{eff}) and densities of various tissues are given in the literature (for example Spiers, 1946; Ter-Pogossian, 1967). The latter paper states that Z_{eff} for human tissues can vary from 6.3 (for fat) to 11.6 (for compact bone). It is conceivable, therefore, that the Z_{eff} for that part of the body over which the measurement is taken can be estimated. It would be more accurate, however, to determine the Z_{eff} directly from the measurements in each case.

When a photon is absorbed in matter by the photoelectric absorption process, an electron is ejected with an energy equal to that of the absorbed photon minus the binding energy of the electron. If the K electron is ejected, which will occur predominantly when the energy of the incoming photon is greater than the binding energy, the vacancy may be filled with an electron from the L, M or N shells. During this process, characteristic x-rays are emitted with an energy equal to the difference between the corresponding binding energies.

The main iodine and mercury K-shell binding energies are shown in Table 7 (Shalev, 1978; page 89). Since those of iodine, but not of mercury, are below the 59.6 keV gamma of Am-241 then the probability of escape of the characteristic x-rays is relatively large. As a result

of this escape peaks are observed at (59.6 keV minus the energies of the escaped x-rays ie. at) 27 and 31 keV (Beinglas et al, 1982). Two such peaks are visible in a spectrum obtained using the mercuric iodide semiconductor detector obtained for use in this study - one at approximately 27 keV and the other at 31 keV (Figure 15, page 90).

The first peak coincides with the 24.6 keV gamma from Am-241, and will be attenuated faster than the 31 keV peak, which will be attenuated at the rate of the 59.6 keV gamma ray.

For a given absorber thickness (in g/cm^2), the ratio of counts in the 27 keV peak to those in the 31 keV peak will be a function of Z_{eff}. Knowing this ratio and the ratio of scatter to photopeak at 60 keV which is also dependent upon both absorber thickness and Z_{eff}, then it should be possible to empirically determine the effective atomic number of the absorber.

Table 7: K-Shell Binding Energies For Mercury and Iodine (Shalev,1978)

	Mercury (Hg)		Iodine (I)	
	Binding Energy (keV)	%	Binding Energy (keV)	%
K_{α_1}	70.8	100.0	28.6	100.0
K_{α_2}	68.9	58.8	28.3	51.0
K_{av}	70.1	158.8	28.5	151.0
K_{β_1}	80.3	35.0	32.3	27.0
K_{β_2}	82.5	9.6	33.0	6.0
K_{av}	80.8	44.6	32.4	33.0

Figure 15: Am-241 Spectrum Obtained Using Mercuric Iodide Detector

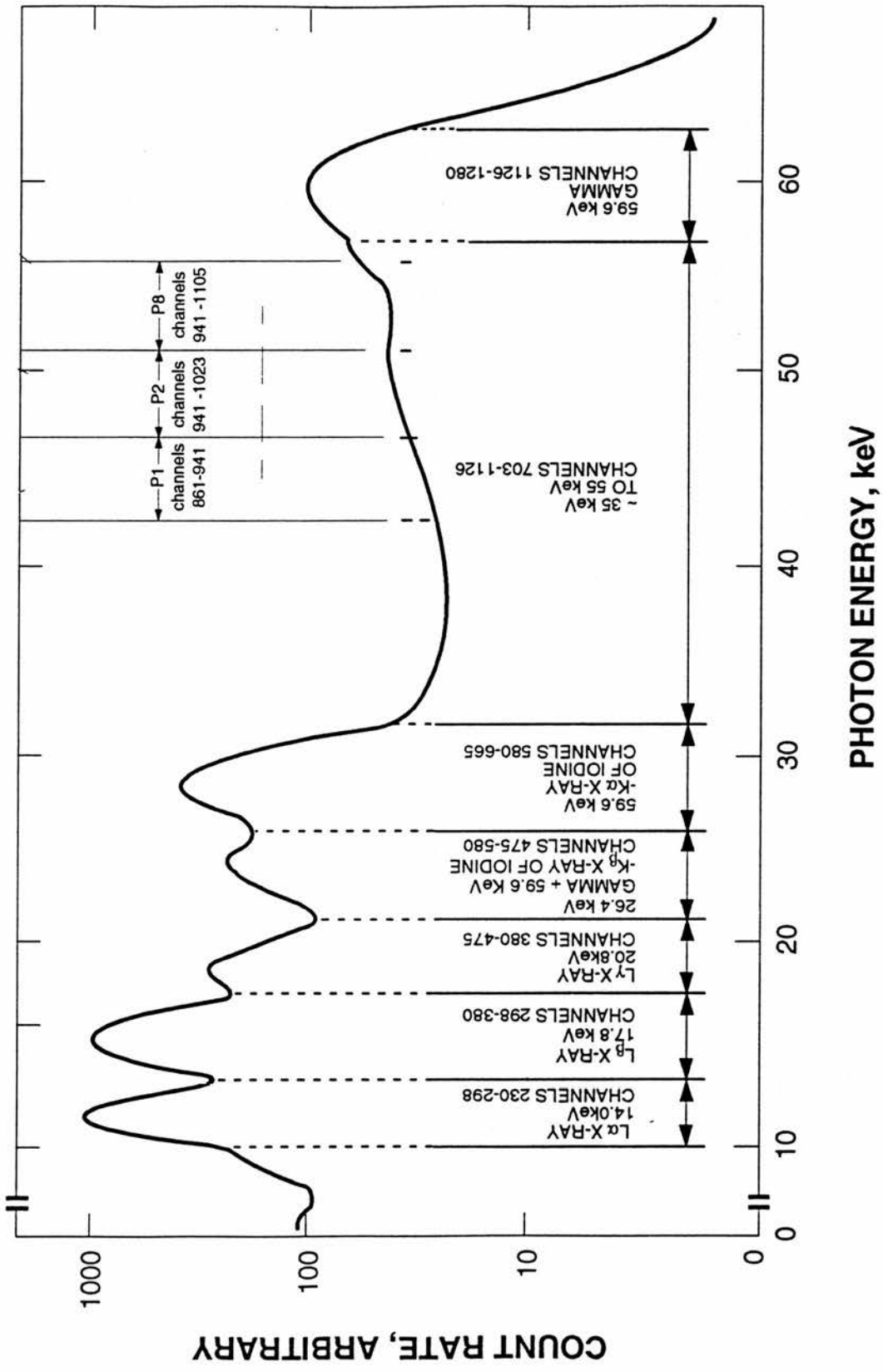

3.4 Successive Approximation of the Pu/Am Ratio

If the ratio $N_{1,0}/N_{2,0}$ = a (Equation 3.6) is unknown, then so is the plutonium to americium ratio. In order to solve equations 3.3 through to 3.5 some arbitrary value for a can be assumed (within the limits of its variation) and so, first approximations of $N_{1,0}$ and $N_{2,0}$ obtained.

From the literature, the ratios of 60 keV photons, 17.75 keV photons and 13.94 keV photons are known. Thus, the fractions of $N_{1,0}$ and $N_{2,0}$ due to americium can be estimated after the number of 60 keV photons have been determined as described in Section 3.2. The proportions of $N_{1,0}$ and $N_{2,0}$ attributable to Pu are then obtained by subtracting those due to Am from the total. Knowing the relative abundances of the low energy photons in plutonium and americium (Table 2, page 17) a first approximation of the plutonium-to-americium ratio can be calculated.

The arbitrarily chosen ratio, a, can now be recalculated as a_1 and equations 3.3 and 3.4 can again be utilised to yield different values of $N_{1,0}$ and $N_{2,0}$. The second estimates of these figures will, in turn, give new values for the plutonium-americium ratio, and consequently a third approximation of a. In this way, a sequence of n successive approximations may be generated to obtain increasingly better estimates of the Pu-Am ratio. A

program can be written to calculate these successive approximations until $| a_n - a_{(n-1)} | < E$, where E is some arbitrarily selected precision to give the final value for the plutonium-americium ratio.

This iterative method was chosen in preference to the computer-assisted methods available for use (some in the form of commercially-available software packages). These programs automatically identify and quantitate radionuclides in a sample that has been analysed by gamma-spectrometric techniques (for example, Putnam et al, 1965; Heath et al, 1965; Gunnink and Niday, 1972; Lima and Atalla, 1974; Cox, 1979; Pearton et al, 1977 and Carpenter et al, 1978). However, these computer methods are often complex and provide results that may be difficult to confirm because of their dependence upon sophisticated computer deconvolution methodology or least-squares fitting techniques. Furthermore, these techniques are also reliant on their being a good response function and good counting statistics, of which the latter may not be available in the case of low-level contamination of a wound. For future work, however, it may be worthwhile reapplying alternative techniques such as deconvolution in order to establish further improvements in these techniques.

4. EXPERIMENTAL PROCEDURES AND RESULTS

4.1 Equipment

4.1.1 The Detector

In selecting the detector to be used in this study various criteria had to be borne in mind. Firstly, there was the requirement for the detector to be used, if possible, at room temperature (generally at temperatures not exceeding 50°C). Secondly, there was the requirement for it to have a high atomic number (Z) so that it had very good stopping power for x- and gamma rays at both high and low energies. Thirdly, a good ratio (in the detector) between photoelectric events to Compton scattering and, finally, good energy resolution were also required.

With the above factors in mind two detectors were purchased for use in this study - a cadmium telluride (CdTe) detector and a mercuric iodide (HgI_2) detector. It rapidly became clear that the former (shown in Figure 16, page 99) was not usable (for reasons which will be discussed later). The mercuric iodide detector, however, fulfilled the necessary criteria and, apart from several recurring problems, could be used for the purposes of this study. It should be noted, therefore, that all of the information obtained from experimental work carried

out during the course of this study was obtained using only the mercuric iodide detector.

The mercuric iodide detector was a standard commercial model obtained from the Yissum Research Development Company of the Hebrew University of Jerusalem. As it is a semi-insulator with a large band gap (2.14 eV) it has a relatively low leakage current (5.0 E-10 amperes) at room temperature and operating bias. The high atomic number (Z) of mercury and iodine means this material has good stopping power for x- and gamma-rays in the energy region of 1.5 keV to 1330 keV.

The detector is a planar type (as shown in Figure 17, page 100) and is fabricated from a slice of high purity and homogeneous HgI_2 single crystal. Both sides of the slice are covered with thin aqua-dag contacts which determine the active volume (the covered area multiplied by the slice thickness). The slice is encapsulated by a polymer to prevent any kind of external damage.

The mechanical construction of the detector is shown in Figure 18 (page 101); the can is made of aluminium with a beryllium window 0.01" thick. For low energies (up to 150 keV) there is a 2 mm lead window to prevent gamma rays impinging on the uncovered area of the slice and thus preventing the edge effects of the contacts from spoiling the resolution. For energies greater than 150

keV the window serves no purpose but the edge effect can be considered to be negligible. The detector can is connected to the pre-amplifier so that the whole system is one unit and electronic noise is kept to a minimum. The detector specifications are as follows;

Active Area;	30.0 mm^2
Detector Thickness;	0.5 mm
Window Thickness (Be);	0.025 mm
Window-Detector Distance;	3.0 mm
Operating Bias;	350 Volts
Bias Polarity;	Negative
Shaping Time Constant;	2 μ sec

The operating bias was supplied by a Harshaw NV-25A unit capable of supplying up to 3000 V (0-10 mA).

4.1.2 The Pre-Amplifier

The Sr-105 pre-amplifier is a low-noise charge-sensitive pre-amplifier designed to operate with mercuric iodide semiconductor radiation detectors. The charge produced by the ionising radiation is integrated on the feedback capacitor and appears at the output, as a voltage pulse having a very short rise time and long decay time. The specifications of this unit are as follows;

(a) Signal Input;

Positive or negative charge pulse up to 6 picocoulomb (approx 85 MeV for HgI_2 detectors).

(b) Test Input;

Positive or negative impulses with short (<1E-6 sec) and long (>1E-4 sec) decay time.

(c) Signal Output;

Positive or negative pulses, inverse of input, with short rise time and long decay time (approx 3 msec); maximum output +/- 5 Volts.

(d) Charge Sensitivity;

0.60 +/- 0.1 Volt/picocoulomb (32 +/- 4mV/MeV for HgI_2 detectors).

(e) Open Loop Gain; >10,000

(f) Output Impedance; 50 ohms

(g) Gain Stability; Better than 0.01% per °C.

(h) Integral Non-linearity;

Less than 0.1% for 0 to +/- 5 Volts.

(i) Test Point;

+24 Volts DC: 3 mA, -24 Volts DC: 20 mA

(j) Connectors;

Input:	BNC
Output:	BNC
Test:	BNC
Test Point:	Miniature binding post
Detector Bias:	MHV
Power:	Amphenol 17-20090

4.1.3 The Amplifier

This was a Silena Model 7612; after a series of experiments the following settings were selected and maintained;

Fine Gain	=	10.00
Coarse Gain	=	50.00
Shaping Time	=	2 μ sec
Input	=	Positive
Output	=	Unipolar

4.1.4 Energy Resolution

The output from the detector was fed into a multi-channel analyser, Type ND-66, manufactured by Nuclear Data UK, Ltd; the number of channels selected was 2048, and the gain was set at 2K. Under these conditions the energy scale of the analyser was from approximately 1.7 keV (channel No. 1) to approximately 97 keV (channel 2048).

The photon energy-versus-channel number calibrations were obtained using a variable energy x-ray source: this is an assembly containing a sealed ceramic primary source (370 MBq Am-241) which excites characteristic x-rays from six different targets in turn. The targets (and associated K_α and K_β x-rays) were copper (8.04 and 8.91 keV), Rubidium (13.37 and 14.47 keV), Molybdenum (17.44 and

19.63 keV), Silver (22.10 and 24.99 keV), Barium (32.06 and 36.55 keV) and Terbium (44.23 and 50.65 keV).

The energy calibration result was 0.0573 keV per channel, and the measured energy resolution (the Full Width at Half Maximum, FWHM, ie the full width of the peak measured at half its maximum height) of the system was as follows;

FWHM at 6.00 keV = 1.708 keV (Fe-55 Source)
FWHM at 13.95 keV = 1.920 keV (Am-241 Source)
FWHM at 59.60 keV = 3.700 keV (Am-241 Source)

Figure 16: The Cadmium Telluride Detector

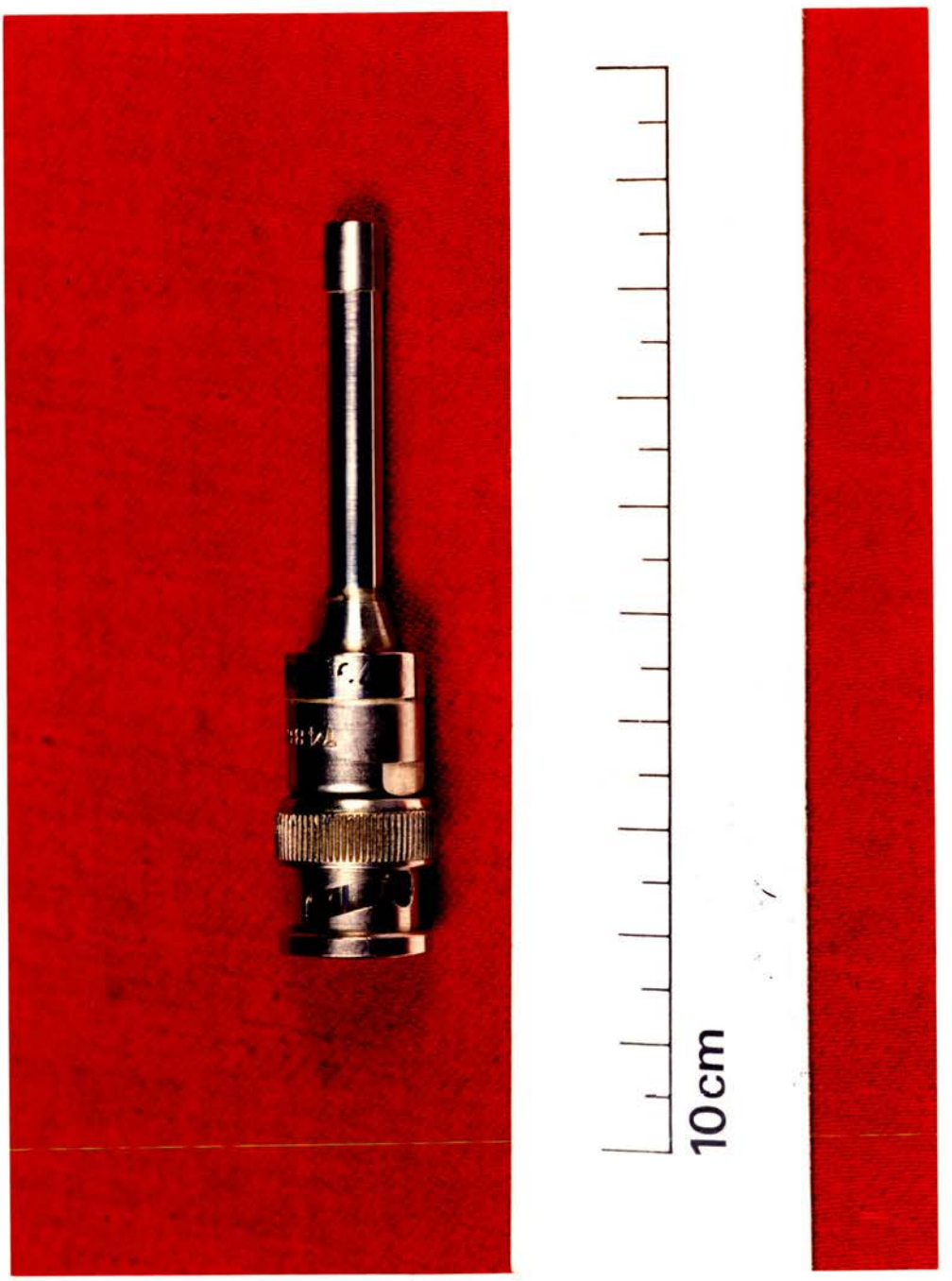

Figure 17: Configuration of Mercuric Iodide Detector

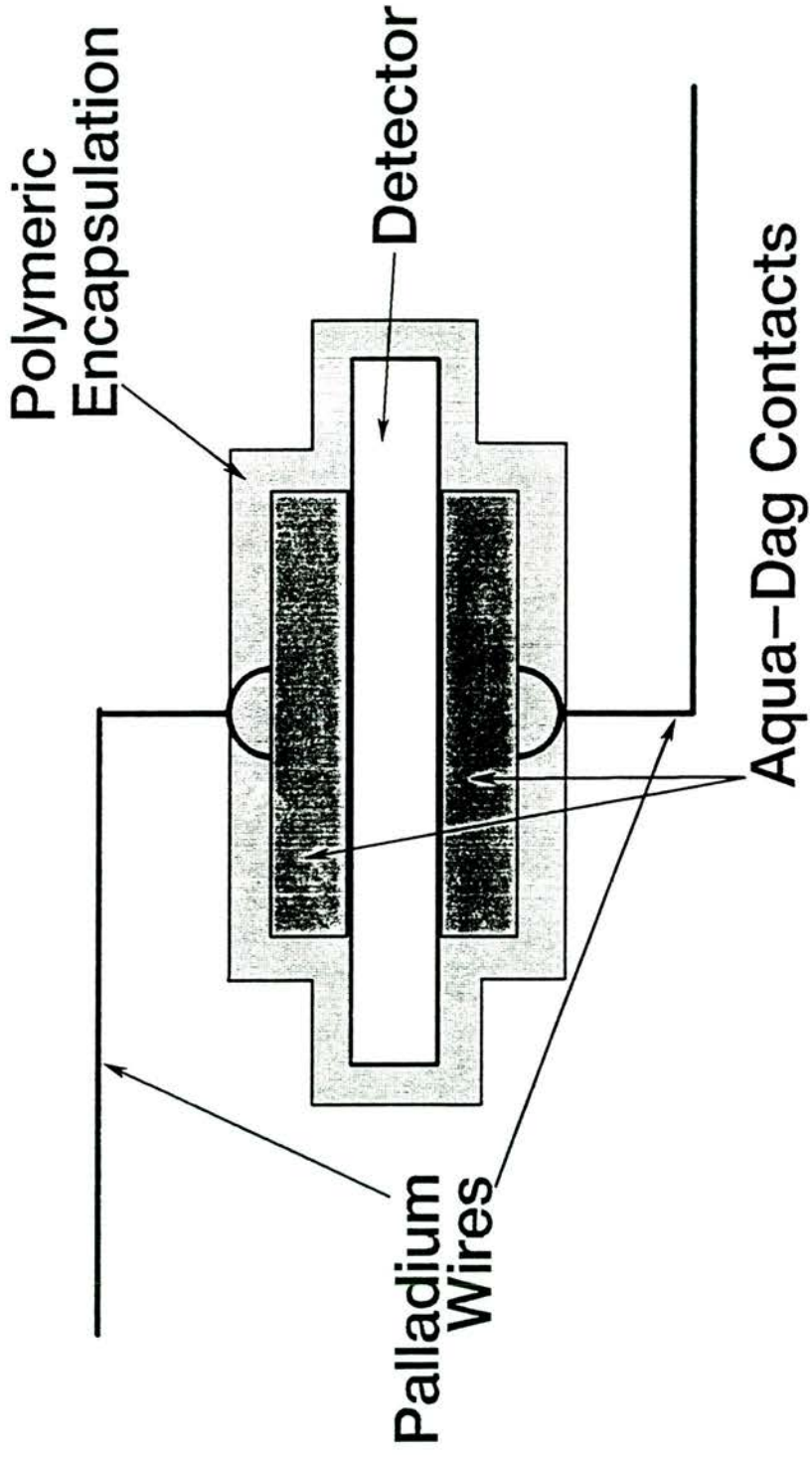

Figure 18: Mechanical Construction of the Mercuric Iodide Detector

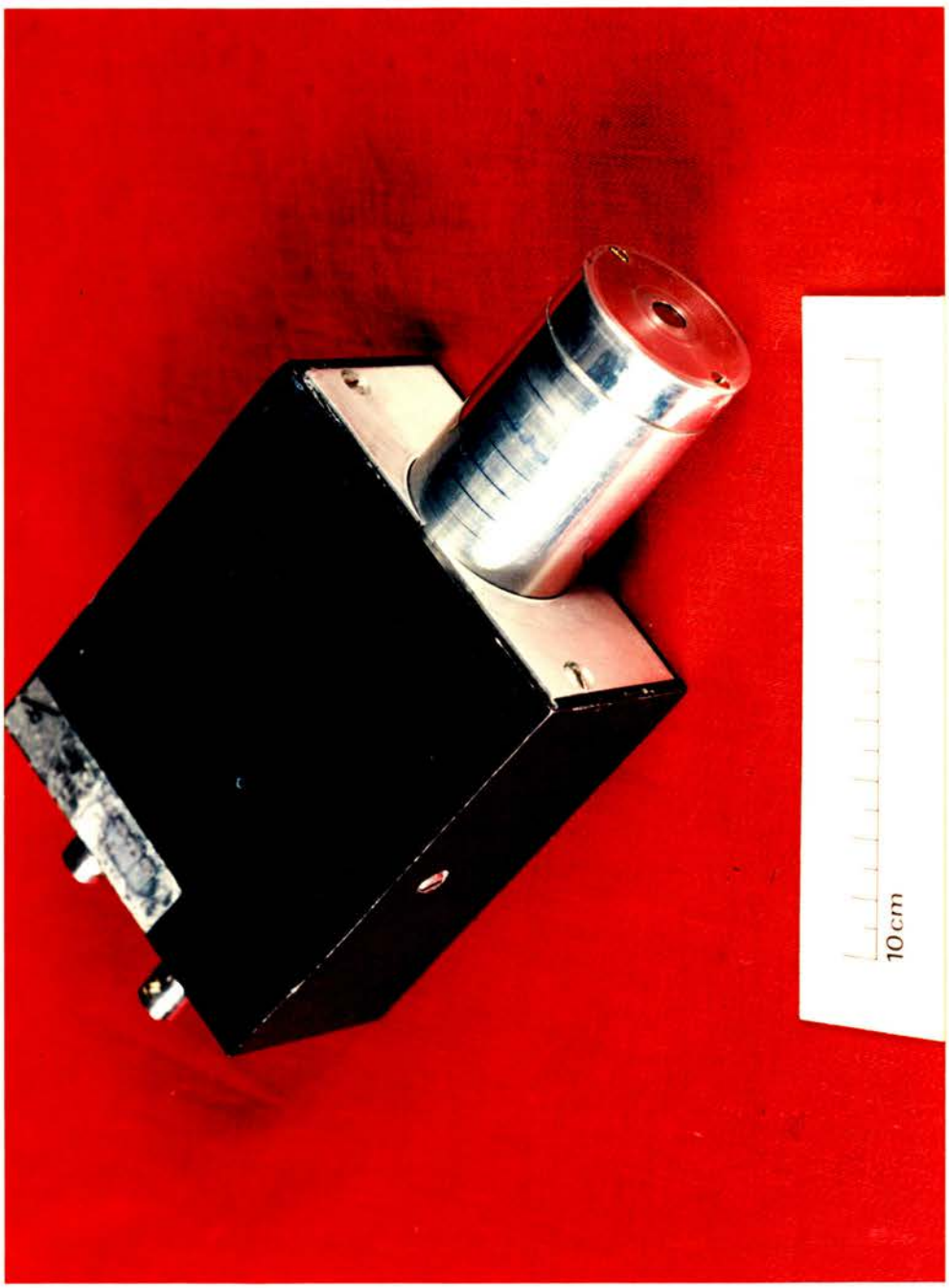

4.2 Determination of the Contribution of Higher Energy Photons to Counts observed in the L X-Ray Region

In an attempt to determine the absorption coefficients of the L x-rays of Am-241 it became apparent that the spectrum obtained with the mercuric iodide detector contained counts in the L x-ray region that were due to high-energy photons. The attenuation did not seem to follow a single exponential, and even after sufficient absorber had been placed between the source and the detector to effectively attenuate the L x-rays a considerable number of counts were still observed (above background) in the L x-ray region when the Am-241 source was present.

It has been seen (Section 3.2 and Figure 14, page 86) that an unattenuated Am-241 source yields a considerable number of counts in the 35 - 55 keV region. When the 59.6 keV gamma-rays are attenuated by a tissue-like absorber, relatively large numbers of photons will reach the detector with energies degraded by Compton scattering, and the number of photons in the energy range 35 - 55 keV will increase relative to the 59.6 keV photopeak and to the L x-ray peaks (see Section 4.6).

Supposing a 43 keV photon is absorbed in mercuric iodide and the iodine characteristic x-rays escape, then the absorbed energy will only be of the order of 11 - 15 keV

and the resulting count will be indistinguishable from a count due to absorption of an L_α x-ray from plutonium or americium, as shown in Figure 15 (page 90). It is not only necessary, therefore to make a correction for the contribution of the 59.6 keV photons to counts in the L x-ray region but also for photons in the 35 - 55 keV region to counts in this region.

Thus, an observed spectrum will appear to contain extraneous photons with energies in the L x-ray region, but those extraneous counts in this region really are a result of the absorption of 35 - 55 and 59.6 keV photons by the detector material followed by the escape of an emitted iodine x-ray. The probability of escape of the characteristic x-ray is a function of the detector size and shape, and the location of the primary interactions within the detector; the distribution of locations of the primary interactions is also a function of photon energy.

On the basis of the arguments presented above the following can be written;

$$N_{net} = N - K.P \qquad (4.1)$$

where;

N = count observed in the L x-ray region;

P = count observed in the energy region of the L x-rays plus the events due to

Compton continuum;

N_{net} = count due to the L x-rays;

K = Correction Factor; the ratio of the number of pulses in the L x-ray peak due to escape of I x-rays per pulse in the (L x-ray-plus-escape) energy region.

NOTE: All counts are minus background.

In order to determine K for the three L x-ray peaks, aluminium and copper absorbers in sufficient quantity to absorb all of the L x-rays were placed between the Am-241 source and the detector. Under these conditions $N_{net} = 0$, and;

$$K = N/P \qquad (4.2)$$

The results are summarised in Table 8 (page 106).

The above method is used for the determination of "escape to photopeak" ratio (Swinth, 1967) but the case here is of a continuous spectrum. In addition, there is more than one escape energy: thus K will be dependent upon the shape of the total spectrum in the 35 -55 keV range. The actual value of K will vary, therefore, not only for different materials but even for different thicknesses of the same material.

As a first approximation, such "average" values of K1, K2 and K8 (for the L_α, L_β and L_γ x-rays, respectively) were selected so that the attenuation of N_{NET} for the three L x-rays followed a single exponential function. (See Section 4.3 and Appendix C.1 for the method of selecting values of K).

The selected average values for the three L x-rays are;

K1 = 2.20

K2 = 2.30

K8 = 2.50

Table 8: Determination of Correction Factors for the Contribution of Higher energy Photons to Counts Observed in the Am L X-Ray Region.

Absorber	N_1 Counts/ 10 min Am Lα X-ray Region	N_2 Counts/ 10 min Am Lβ X-ray Region	N_8 Counts/ 10 min Am L X-Ray Region	P_1 Counts/ 10 min Am Lα I Kα X-Ray Region	P_2 Counts/ 10 min Am Lβ + I Kα X-Ray Region	P_8 Counts/ 10 min Am L + I Kα X-Ray Region	$K_1 = \frac{N_1}{P_1}$	$K_2 = \frac{N_2}{P_2}$	$K_8 = \frac{N_8}{P_8}$
0.27 g/cm^2 copper	20,272	33,606	41,780	12,536	18,469	21,665	1.62	1.82	1.93
0.77 g/cm^2 copper	7,729	12,807	16,277	4,956	7,215	8,353	1.56	1.78	1.95
1.05 g/cm^2 copper	4,413	7,362	9,707	2,864	4,240	5,161	1.54	1.74	1.88
2.7 g/cm^2 aluminum	32,307	48,943	61,857	17,337	23,528	25,709	1.86	2.08	2.41
4.5 g/cm^2 aluminum	24,001	35,738	44,531	12,608	16,754	18,700	1.90	2.13	2.38
6.8 g/cm^2 aluminum	14,356	21,528	26,831	7,446	9,932	11,696	1.93	2.17	2.29

4.3 Determination of Attenuation Coefficients for the L X-Rays

The L x-ray spectrum is complex and consists of many individual lines which are not resolved by standard techniques. Energy values quoted in the literature for L_α, L_β and L_γ x-rays are the main energies of the more prominent lines within their group. The energy differences between the individual lines are considerable - for example, the two most prominent L_β x-ray lines of neptunium are L_{β_1} at 17.76 keV, and L_{β_2} at 16.86 keV. There are lines even further apart - L_{β_6} at 16.14 keV and L_{β_3} at 18.00 keV. For attenuation purposes, the "average" energy of L x-rays would therefore be different for each atomic number and at these low energies any contamination by a higher atomic number material will increase the attenuation coefficient. Therefore, in order to determine the attenuation coefficients of the absorbers used from values quoted in the literature, their elemental composition would have to be known exactly.

It is only the ratios of the attenuation coefficients, however, that are needed for the different L x-rays of plutonium and americium, which are nearly the same for all low atomic number materials (Section 3.1). It was decided, therefore, to obtain our own attenuation coefficients and ratios for the absorber materials used in this study.

For measuring relative attenuation coefficients americium and plutonium sources were placed at a fixed distance from the detector. (The sources consisted of activity that had been electrodeposited onto stainless steel discs; the activity of each source was then determined by cross-calibration with sources which were traceable to NPL.) For each energy interval under consideration counts were obtained from an unattenuated source, and with increasing thicknesses of absorber placed between the source and the detector. The attenuation of the absorbers in each energy range was determined by dividing the count rate obtained with an absorber by the count rate obtained from the unattenuated source. The experimental points obtained for each L x-ray and absorber material were fitted to a single exponential curve by regression-analytic methods (Appendix C.1).

It was necessary to find the "best" average correction factor for each L x-ray for the contribution of higher energy photons to counts observed in the L x-ray region (section 4.2). The value of the correction factor was varied until a minimum χ^2 value was obtained to minimise deviations in determinations of attenuation coefficients for the various L x-rays. The selection process is shown in the computer program given in Table C1 at the end of Appendix C. The results are summarised in Tables 9 to 16 (pages 111 to 118) inclusive. The attenuation curves obtained, together with the experimental points are

presented in Figures 19, 20 and 21 (pages 119 to 121 inclusive).

The largest uncertainty in the determination of the attenuation coefficients is attributable to the uncertainty in the value of the correction factor for the contribution of the higher energy photons to the counts observed in the L x-ray region. It can be seen that the importance of this factor increases with the relative increase in the number of higher-energy photons compared to the number of L x-rays. The L x-rays were attenuated strongly in aluminium. Therefore, meaningful values for americium L x-ray attenuation coefficients in aluminium could not be obtained using the mercuric iodide detector.

By interpolating (linear interpolation on log-log plot) from tables of the mass attenuation coefficients (Evans, 1968, Hubbell, 1969) values for photon energies and materials under consideration were obtained. The interpolated values for acrylic plastic at 13.2 keV, 17.8 keV and 20.2 keV are 1.40 cm^2/g, 0.745 cm^2/g and 0.495 cm^2/g, respectively. This compares very well with the measured results of 1.31 cm^2/g, 0.711 cm^2/g and 0.473 cm^2/g for plutonium L_α, L_β and L_γ x-rays, respectively. Such good agreement was not obtained for the attenuation coefficients for aluminium; Evans' (1968) values are 5.40 cm^2/g and 3.25 cm^2/g for 17.8 keV and 20.2 keV; those obtained in this work are larger: 6.53 cm^2/g and 4.04

cm^2/g for plutonium L_β and L_γ x-rays. This discrepancy may have been due to the aluminium absorbers being contaminated with a higher atomic number element. (The samples of aluminium obtained from Johnson Matthey were nominally 99% pure and thus should not have contained any alloy contaminants; however, careful measurements of two of the aluminium absorbers revealed a small difference in their densities: 2.66 g/cm^3 and 2.72 g/cm^3. In order to have been able to determine the attenuation coefficients from values quoted in the literature, however, the exact elemental composition of the absorbers would have had to have been known.)

The absolute values of the absorption coefficients are not of great interest for the purpose of the present work. Instead, the interest lies in the ratios of the absorption coefficients for the different L x-rays. The ratios of coefficients for the L_α x-rays to the L_β x-rays, and the L_γ x-rays to the L_β x-rays, in acrylic plastic based on this work are 1.84 and 0.665, respectively; calculations from data of Evans (1968) give corresponding values of 1.88 and 0.664. Even in the case of the aluminium absorbers, the agreement of ratios is good: the ratio of (L_β x-ray-to L_γ x-ray) attenuation coefficients from our work is 0.619, and from Evans' data is 0.602.

Table 9: Transmission of Plutonium L-Alpha X-Rays Through Acrylic

X	N	P	Z	SY
0.000	186335	178	1.0000	
0.749	69384	225	0.3705	0.004
1.480	25703	186	0.1360	0.006
2.200	10707	217	0.0550	0.011
2.910	4816	212	0.0234	0.018
3.600	2547	198	0.0114	0.028
5.040	1035	170	0.0036	0.065

K = 2.20

A1 = -1.31

SA1 = 0.002

NOTE: The definitions of the symbols used in this Table are given in Appendix C.1 (page 213).

Table 10: Transmission of Plutonium L-Beta X-Rays Through Acrylic

X	N	P	Z	SY
0.000	194024	237	1.0000	
0.749	113946	236	0.5861	0.003
1.480	67583	208	0.3468	0.004
2.200	39857	229	0.2033	0.005
2.910	24128	212	0.1222	0.007
3.600	15252	199	0.0765	0.009
5.040	6968	164	0.0341	0.013

K = 2.30

A1 = -0.71

SA1 = 0.001

NOTE: The definitions of the symbols used in this Table are given in Appendix C.1 (page 213).

Table 11: Transmission of Plutonium L-Gamma X-Rays Through Acrylic

X	N	P	Z	SY
0.000	33675	357	1.0000	
0.749	23345	345	0.6858	0.007
1.480	17081	375	0.4924	0.009
2.200	12281	287	0.3527	0.010
2.910	8937	330	0.2474	0.013
3.600	6619	297	0.1793	0.016
5.040	3980	241	0.1030	0.022

K = 2.50

A1 = -0.47

SA1 = 0.002

NOTE: The definitions of the symbols used in this Table are given in Appendix C.1 (page 213).

Table 12: Transmission of Americium L-Alpha X-Rays Through Acrylic

X	N	P	Z	SY
0.000	1127506	23967	1.0000	
0.749	479392	26546	0.3917	0.002
1.480	227986	28703	0.1534	0.004
2.200	132418	29791	0.0622	0.008
2.910	94792	30135	0.0265	0.017
3.600	77398	29640	0.0113	0.039
5.040	64191	27818	0.0028	0.149

K = 2.20

A1 = -1.26

SA1 = 0.002

NOTE: The definitions of the symbols used in this Table are given in Appendix C.1 (page 213).

Table 13: Transmission of Americium L-Beta X-Rays Through Acrylic

X	N	P	Z	SY
0.000	1206136	31816	1.0000	
0.749	775433	36201	0.6109	0.001
1.480	518500	37488	0.3815	0.002
2.200	346649	36708	0.2314	0.003
2.910	245440	35886	0.1438	0.004
3.600	180742	34209	0.0901	0.006
5.780	101648	30228	0.0284	0.016

K = 2.30

A1 = -0.66

SA1 = 0.001

NOTE: The definitions of the symbols used in this Table are given in Appendix C.1 (page 213).

Table 14: Transmission of Americium L-Gamma X-Rays Through Acrylic

X	N	P	Z	SY
0.000	279825	35642	1.0000	
0.749	240166	41617	0.7137	0.005
1.480	210302	41907	0.5533	0.007
2.200	175472	39800	0.3983	0.009
2.910	150410	37894	0.2919	0.011
3.600	130331	34439	0.2319	0.013
5.780	94526	29826	0.1047	0.027

K = 2.50

A1 = -0.41

SA1 = 0.002

NOTE: The definitions of the symbols used in this Table are given in Appendix C.1 (page 213).

Table 15: Transmission of Plutonium L-Beta X-Rays Through Aluminium

X	N	P	Z	SY
0.000	194024	237	1.0000	
0.224	43949	237	0.2243	0.005
0.439	11825	194	0.0588	0.010
0.662	3223	189	0.0144	0.023
0.888	1160	214	0.0034	0.072

K = 2.30

A1 = -6.53

SA1 = 0.014

NOTE: The definitions of the symbols used in this Table are given in Appendix C.1 (page 213).

Table 16: Transmission of Plutonium L-Gamma X-Rays Through Aluminium

X	N	P	Z	SY
0.000	33675	357	1.0000	
0.224	13737	346	0.3926	0.010
0.439	6438	338	0.1706	0.017
0.662	3136	326	0.0708	0.031
0.888	1707	288	0.0302	0.061
1.334	849	275	0.0049	0.314

K = 2.50

A1 = -4.04

SA1 = 0.022

NOTE: The definitions of the symbols used in this Table are given in Appendix C.1 (page 213).

Figure 19: Transmission of Plutonium X-Rays Through Acrylic

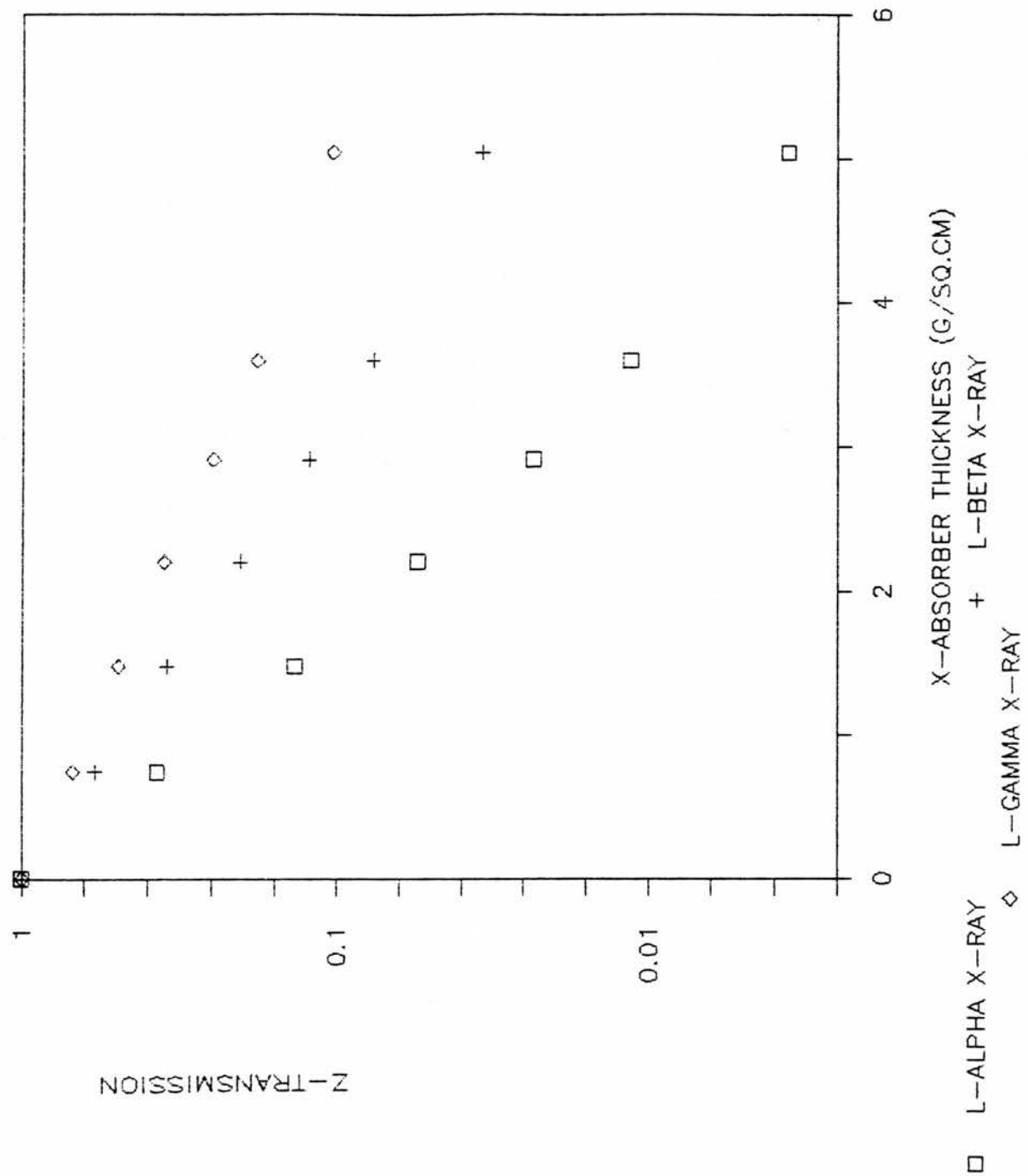

Figure 20: Transmission of Americium X-Rays Through Acrylic

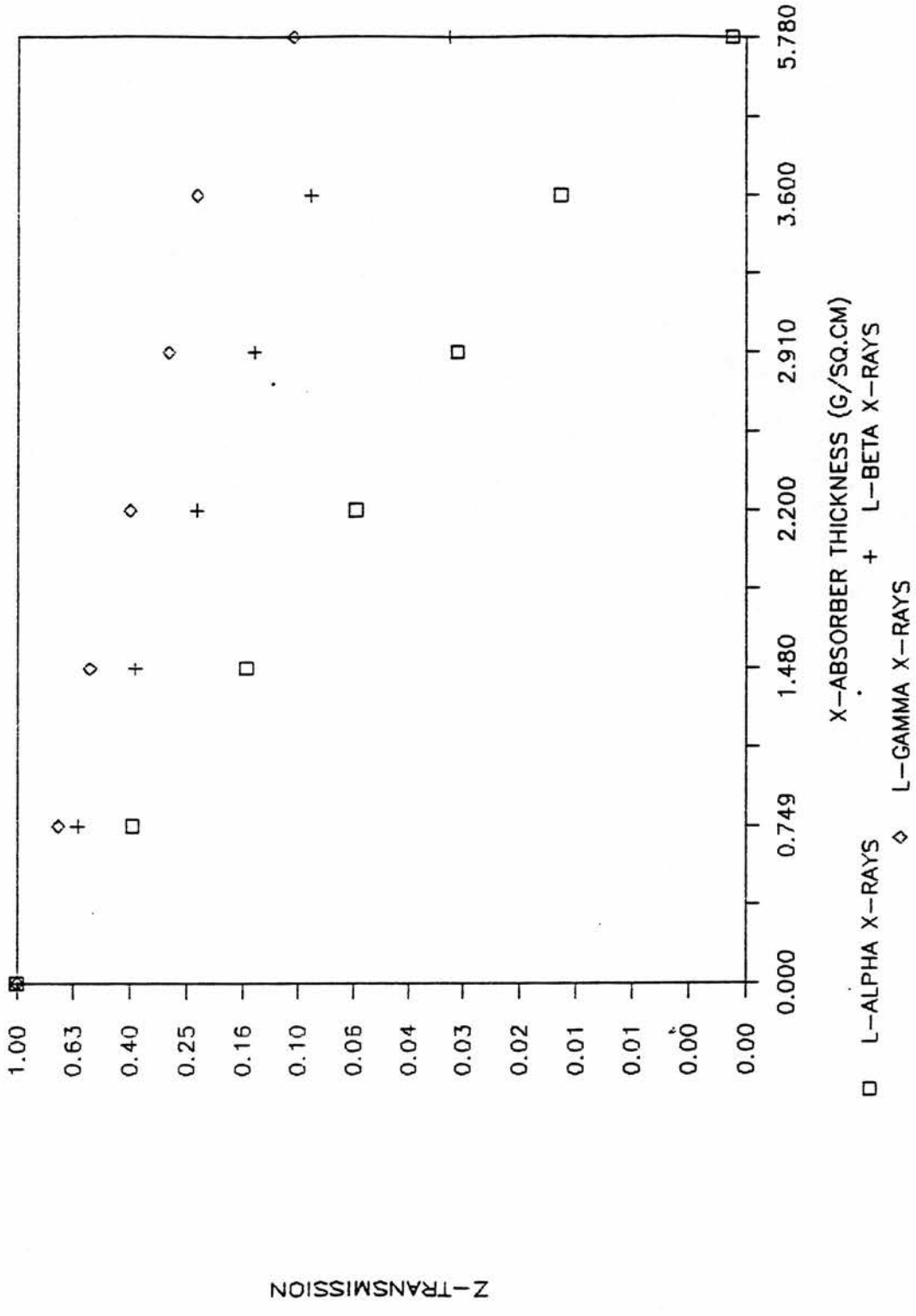

Figure 21: Transmission of Plutonium L_β and L_γ X-Rays Through Aluminium

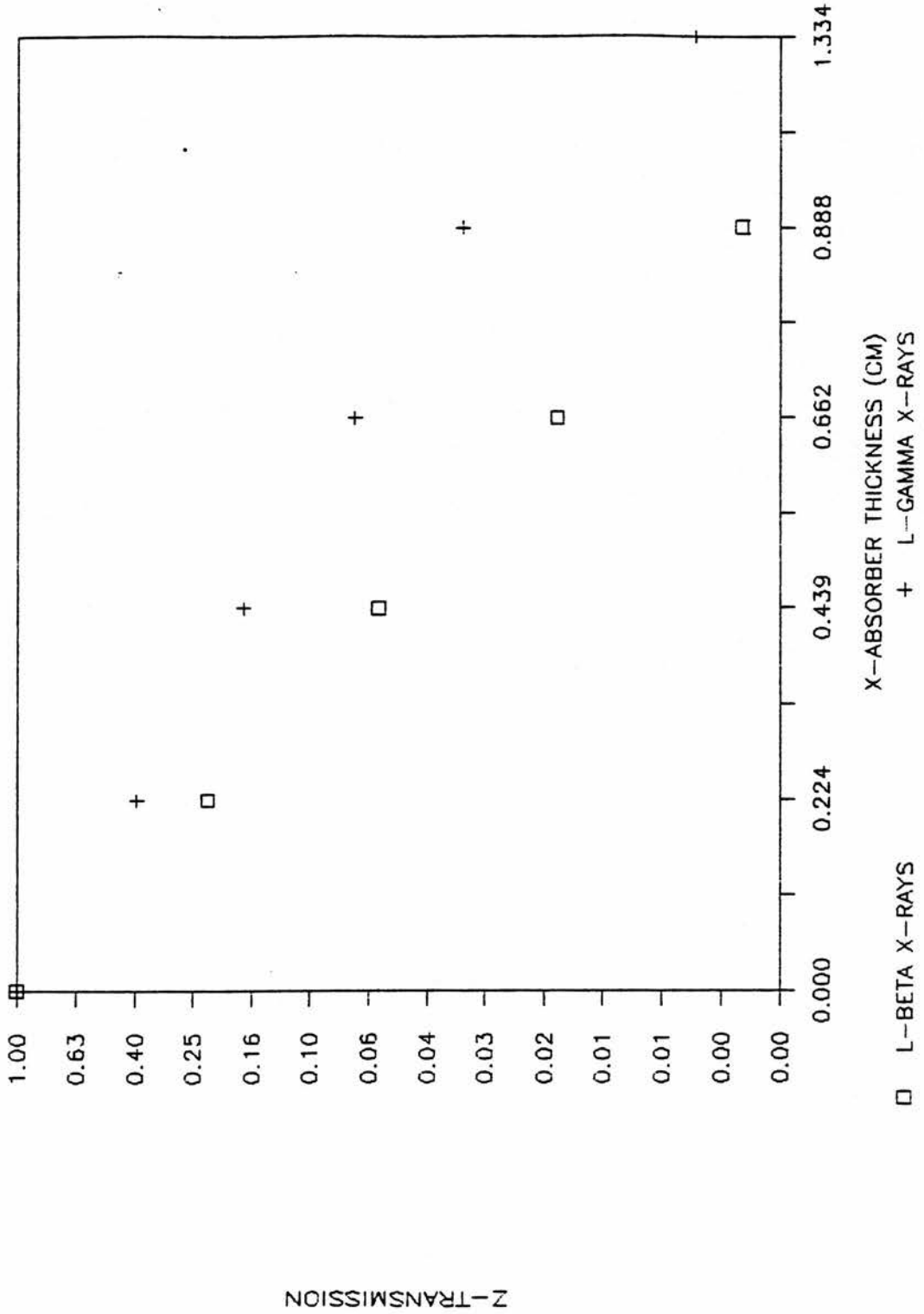

4.4 ESTIMATING TRANSMISSION OF THE 60-keV GAMMA-RAYS FROM AMERICIUM-241 THROUGH THE ABSORBER

For the purpose of this section transmission is defined as the ratio of counts obtained with the source placed behind an absorber, (with the other side of the absorber touching the detector) to those obtained with the source placed in very close proximity to the surface of the detector.

The transmission, 'Z', is, therefore, defined by:

$$Z = (1-A)g(x) \qquad (4.3)$$

where; A is the attenuation factor for the absorber, and;
g(x) is the geometry factor (see Section 4.7).

The escape peak of the 60-keV gamma, which appears between channels 580 and 665 (as shown in Figure 15, page 90) should have been attenuated at the same rate as the 60 keV photopeak (Section 3.3). In order to check whether or not this was true the attenuation in aluminium absorber of the sum of counts under these two peaks was measured. (The same experimental set-up and data treatment as in Section 4.3 were used). The results are given in Table 17 (page 126). The value of 0.25 cm^2/g obtained for the attenuation coefficient of aluminium is

in good agreement with the value given by Hubbell (1969) of 0.277 cm^2/g.

In order to increase the count rate, and thus improve the statistical precision of the method it was decided to use in all the calculations the sum of counts under the escape peak and photopeak (even though this was probably unnecessary as sufficient counts had appeared to have been obtained in the photopeak alone). This sum can thus be referred to as the "count in the 60-keV photopeak".

The theoretical reasons for the increase in the ratios of counts in the 35-55 keV region to counts in the 60-keV photopeak, with increasing attenuation, are given in Section 3.2. The experimental procedure to obtain these relationships for acrylic, water and aluminium absorbers will now be described.

The count rates in the 60-keV photopeak (N3) and in the 35-55 keV region (N4) were obtained with the source (1.1E4 Bq americium-241) placed in very close proximity to the surface of the detector, and with the absorbers, of known thickness, placed between the source and the detector. The absorber was placed touching the surface of the detector, with the source being directly behind the absorber. The "water absorbers" were prepared as follows: plastic rings of approximately 10 cm in diameter

and 2, 4, 6, 8 and 10 cm height were obtained by cutting away the top and bottom of plastic bottles. The ring was then sealed on one side by a thin plastic film ['cling film'] and placed on top of the source. The ring was filled with distilled water and covered by another sheet of this plastic film. The detector was then lowered until it touched the ring. The acrylic and aluminium absorbers were simply placed on top of the source, and the detector was then lowered until it touched the absorber.

The transmission in each case was determined by dividing the counts obtained with the absorber in place by the counts obtained when the source was placed directly against the detector surface (the case of transmission being equal to one).

The "scatter-to-photopeak" ratio was obtained by dividing N4 by N3 in each count. The separation between the photopeak and the scatter region was selected arbitrarily, from the appearance of the unattenuated spectrum as shown in Figure 15 (page 90).

To avoid discrepancies resulting from slightly different conditions in different experimental runs, the scatter-to-photopeak ratio was normalised to 1.0 by dividing all the scatter-to photopeak ratios by that obtained when transmission was unity. The experimental points (thus

normalised) appeared to fit a straight-line on a semi-log plot. The final fits were obtained by regression analysis which yielded the following equations ;

a) acrylic absorbers

$$z = e^{-1.95(x-1)} \qquad (4.4)$$

b) water absorbers

$$z = e^{-2.54(x-1)} \qquad (4.5)$$

c) aluminium absorbers

$$z = e^{-3.94(x-1)} \qquad (4.6)$$

where; Z is the transmission as defined above;

x is the normalised scatter-to-photopeak ratio.

The details of the regression analysis calculation are given in Appendix C.2. The experimental results are summarised in Tables 18, 19 and 20 (pages 127 to 129 inclusive). Equations (4.4), (4.5) and (4.6), together with the experimental points, are plotted in Figure 22 (page 130).

Table 17: Transmission of Americium 60 keV Gamma Rays Through Aluminium

X	N	P	Z	SY
0.000	588890	0.0	1.0000	
0.439	526539	0.0	0.8941	0.001
0.904	471989	0.0	0.8015	0.001
1.334	427005	0.0	0.7251	0.002
1.794	377081	0.0	0.6403	0.002
1.812	377361	0.0	0.6408	0.002
2.251	318109	0.0	0.5402	0.002
2.716	299319	0.0	0.5083	0.002

K = 0.00

A1 = -0.25

SA1 = 0.0000

NOTE: The definitions of the symbols used in this Table are given in Appendix C.1 (page 213).

Table 18: Transmission of 60 keV Photons Versus Scatter-to Photopeak Ratios - Acrylic Absorbers

N3	N4	X	Z	S
116870	38430	1.000	1.000	
82431	32845	1.212	0.705	0.016
60541	27346	1.374	0.518	0.020
46137	23117	1.524	0.395	0.024
36283	19262	1.614	0.310	0.029
29651	16280	1.670	0.254	0.032
36580	19477	1.619	0.313	0.029
29621	16619	1.706	0.253	0.033
20078	12215	1.850	0.172	0.042
13916	8738	1.910	0.119	0.052
14058	9254	2.002	0.120	0.053

A1 = -1.95

SA1 = 0.016

NOTE: The definitions of the symbols used in this Table are given in Appendix C.2 (page 217).

Table 19: Transmission of 60 keV Photons Versus Scatter-to-Photopeak Ratios - Water Absorbers

N3	N4	X	Z	S
116870	38430	1.000	1.000	
44664	20875	1.421	0.382	0.031
23268	12509	1.635	0.199	0.047
13254	8124	1.864	0.113	0.067
8057	5218	1.970	0.069	0.091
5351	3648	2.073	0.046	0.114

A1 = -2.54

SA1 = 0.037

NOTE: The definitions of the symbols used in this Table are given in Appendix C.2 (page 217).

Table 20: Transmission of 60 keV Photons Versus Scatter-to-Photopeak Ratios - Aluminium Absorbers

N3	N4	X	Z	S
116870	38430	1.000	1.000	
103923	35220	1.031	0.889	0.025
92081	32606	1.077	0.788	0.028
76102	28664	1.145	0.651	0.031
61543	24258	1.199	0.527	0.036
50190	20832	1.262	0.429	0.041
41526	17163	1.257	0.355	0.045
41850	17104	1.243	0.358	0.045
29098	12810	1.339	0.249	0.056
29578	12995	1.336	0.253	0.056
26046	11322	1.322	0.223	0.059
18853	8590	1.386	0.161	0.071
13239	6585	1.513	0.113	0.090

A1 = -3.94

SA1 = 0.056

NOTE: The definitions of the symbols used in this Table are given in Appendix C.2 (page 217).

Figure 22: Transmission of 60 keV Photons Versus Scatter-to-Photopeak at 60 keV.

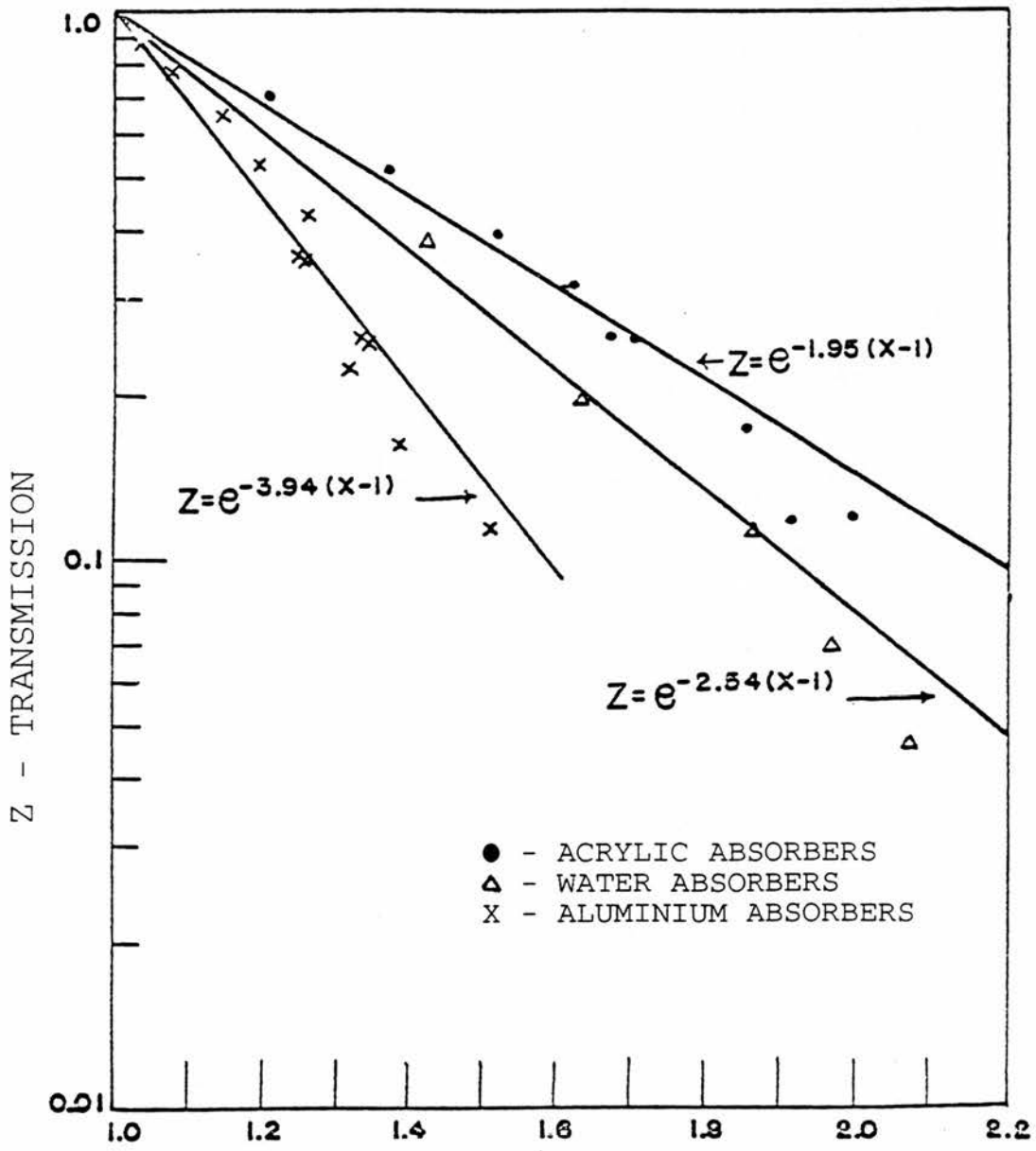

4.5 ESTIMATION OF ABSORBER THICKNESS

The transmission obtained in Section 4.4 was plotted against the absorber thickness (g/cm^2). The data appeared to fit a single curve regardless of absorber. This is not surprising since in Section 4.4 the transmission was defined as a product of (1 minus attenuation factor) and geometry factor (Equation 4.3).

If the Z_{eff} is increased for a given absorber thickness (in g/cm^2) then the attenuation factor will increase. It is reasonable to assume, therefore, that the transmission, as defined, will not vary by an appreciable amount.

By regression analysis and computer calculations (given in Appendix C.5) the following relationship was obtained:

$$X = (1/-0.58)\ln [(Z-0.14)/0.86)] \qquad (4.7)$$

Where; x is absorber thickness in g/cm^2 and;
z is the transmission.

Equation (4.7), together with the experimental points, is plotted in Figure 23 and the data given in Table 21 (pages 133 and 132, respectively).

Table 21: Transmission of 60 keV Photons Versus Absorber Thickness (in g/sq. cm)

X	N3	N3/N30	S	ABSORBER
0.000	116870	1.000		ALUMINIUM
0.224	103923	0.889	0.004	ALUMINIUM
0.439	92081	0.788	0.004	ACRYLIC
0.749	82431	0.705	0.004	ALUMINIUM
0.888	76102	0.651	0.005	ALUMINIUM
1.334	61543	0.527	0.005	ALUMINIUM
1.794	50910	0.436	0.006	ALUMINIUM
2.000	44664	0.382	0.007	WATER
2.251	41526	0.355	0.008	ALUMINIUM
2.906	36381	0.311	0.009	ACRYLIC
3.604	29621	0.253	0.012	ACRYLIC
4.000	23268	0.199	0.020	WATER
5.042	20078	0.172	0.032	ACRYLIC

A1 = -0.58

SA1 = 0.002

C = 0.14

NOTE: The definitions of the symbols used in this Table are given in Appendix C.5 (page 231).

Figure 23: Transmission of 60 keV Photons Versus Absorber Thickness

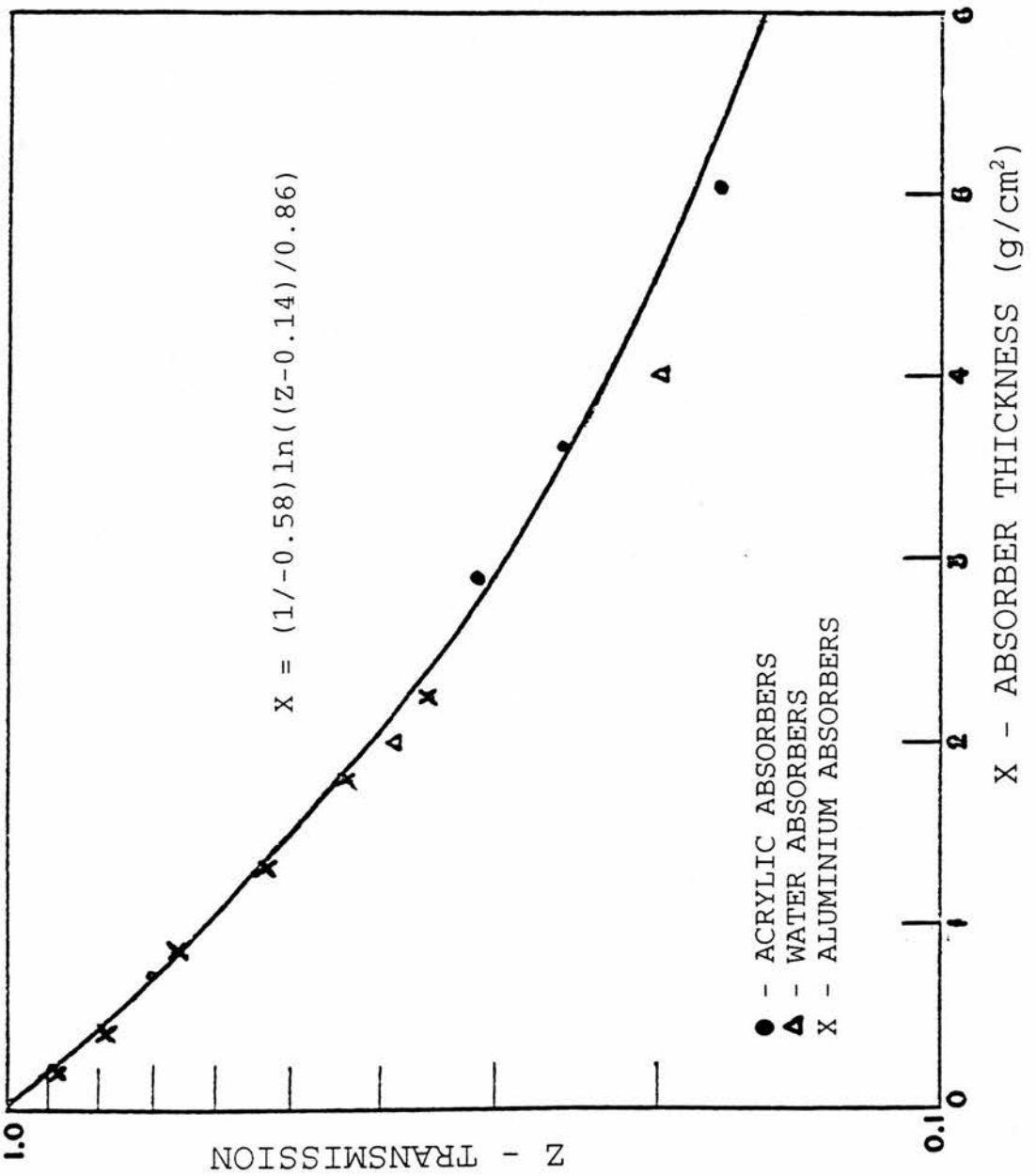

4.6 ESTIMATION OF THE EFFECTIVE ATOMIC NUMBER OF THE ABSORBER

It was seen in Section 3.3 that it should be theoretically possible to estimate the Z_{eff} directly from the spectrum. The experimental procedure for testing this idea was similar to the one described in Section 4.4, only in this case the interest lay in;

(a) the relationship between the ratio of the 27 keV to the 31 keV peak (N_6/N_5) and;
(b) the ratio of scatter-to-photopeak at 60 keV (N4/N3).

Examining the experimental data as shown in Tables 22 to 24 (pages 137 to 139) inclusive and Figure 24 (page 140) it can be seen that for aluminium, as predicted, the 27-keV peak was attenuated faster than the 31 keV peak, but only for absorber thicknesses up to approximately 2 g/cm^2. For absorber thicknesses greater than this the relationship appeared to reverse. The attenuation coefficient for 26.4 KeV gamma rays in aluminium is approximately 1.5 cm^2/g (as obtained by linear interpolation on log-log plot of data from Hubbell (1969)). Thus, less than 5% of the 26.4 keV gammas remain after attenuation in 2 g/cm^2 aluminium, while more than 60% of the 60-keV gammas remain. The relative number of photons reaching the detector at an energy reduced from 60 keV by Compton scatter increases under

those conditions, and the escape process described in Section 3.3 causes the 27-keV peak to decrease more slowly than the 31-keV peak. In low Z materials, where for 60-keV photons Compton scattering is the predominant mode of interaction (Section 3.3), the escape process in the detector causes the 27-keV peak to decrease more slowly than the 31-keV peak at all absorber thicknesses. Thus, the ratio of counts in the 27-keV peak to the counts in the 31-keV peak is a function of Z_{eff}, but in the case of aluminium it ceases to be a monotonic function for absorber thicknesses greater than 2 g/cm^2.

Preliminary plots indicated that a linear relationship existed between the ratio of "27-keV peak to the 31 keV peak" and the scatter-to-photopeak ratio at 60 keV, for each material examined (limited to 2 g/cm^2 in the case of aluminum). As in Section 4.4, both ratios were normalised to unity at zero absorber thickness and the ratios obtained with the various absorbers divided by the corresponding ratio obtained without an absorber. The final fit of the data was obtained by regression analysis and the following equations were obtained;

a) acrylic absorbers

$$y = 0.32x - 0.68 \qquad (4.8)$$

b) water absorbers

$$y = 0.23x + 0.77 \qquad (4.9)$$

c) aluminium absorbers

$$y = -0.78x + 1.78 \qquad (4.10)$$

where; y = normalised ratio of 27-keV peak to 31-keV peak;

x = normalised scatter-to-photopeak ratio at 60 keV.

The details of the regression analysis calculations and the computer program used to obtain the numerical results are given in Appendix C.3. The summaries of the experimental results are given in Tables 22, 23 and 24 (pages 137 to 139 inclusive). Equations (4.8), (4.9) and (4.10), together with the experimental points, are plotted on Figure 24 (page 140). Equation (4.10) is plotted for values of x and y corresponding to absorber thicknesses from 0 to 2 g/cm^2. Beyond that, the relationship between x and y is shown by a broken line. In practical cases, the highest possible Z would be found in bone which contains elements such as calcium (Z=20). However, the equivalent Z of bone is still lower than that of aluminium (Section 3.3). Equation (4.10) cannot be used in the case of the absorber having a Z_{eff} equal to that of aluminium and thicker than 2 g/cm^2; however, by utilising the relationship between the counts in the different L x-ray peaks, such a case can be recognised and assigned the proper Z_{eff} (see Section 4.9).

Table 22: The ratios of 27 keV Peak to 31 keV Peak Versus Scatter-to-Photopeak Ratios of 60 kev Photons - Acrylic Absorbers

N3	N4	N5	N6	X	Y	S
116870	38430	89656	47409	1.000	1.000	
82431	32845	62543	36012	1.212	1.089	0.008
60541	27346	45482	27100	1.374	1.127	0.009
46137	23117	34646	21766	1.524	1.188	0.011
36283	19262	27370	17592	1.614	1.216	0.013
29651	16280	22299	14291	1.670	1.212	0.014
36580	19477	27529	17743	1.619	1.219	0.013
29621	16619	22192	14598	1.706	1.244	0.014
20078	12215	15109	10036	1.850	1.256	0.018
14058	9254	10457	6955	2.002	1.258	0.021
10209	6729	7719	5202	2.004	1.274	0.025
7557	5285	5704	3911	2.127	1.297	0.030

A1 = 0.32

SA1 = 0.007

NOTE; The definitions of the symbols used in this Table are given in Appendix C.3 (page 222).

Table 23: The Ratios of 27 keV Peak to 31 keV Peak Versus Scatter-to-Photopeak Ratios of 60 keV Photons - Water Absorbers

N3	N4	N5	N6	X	Y	S
116870	38430	89656	47409	1.000	1.000	
44664	20875	33815	19706	1.421	1.102	0.010
23268	12509	17557	10567	1.635	1.138	0.015
13254	8124	9945	6234	1.864	1.185	0.020
8057	5218	6014	3957	1.970	1.244	0.027
5351	3648	3995	2608	2.073	1.235	0.033

A1 = 0.23

SA1 = 0.011

NOTE; The definitions of the symbols used in this Table are given in Appendix C.3 (page 222).

Table 24: The Ratios of 27 keV Peak to 31 keV Peak Versus Scatter-to Photopeak Ratios of 60 keV Photons - Aluminium Absorbers

N3	N4	N5	N6	X	Y	S
116870	38430	89656	47409	1.000	1.000	
103923	35220	79174	39154	1.031	0.935	
92081	32606	69862	34015	1.077	0.921	0.008
76102	28664	57453	27105	1.145	0.892	0.008
61543	24258	46354	22270	1.199	0.090	0.009
100148	33768	75741	37274	1.025	0.931	0.010
86522	31087	65367	31660	1.093	0.916	0.008
80286	28778	60625	28109	1.090	0.877	0.008
69456	26123	52382	24372	1.144	0.880	0.009
56185	21581	42254	19618	1.183	0.878	0.011

A1 = -0.78

SA1 = 0.027

NOTE; The definitions of symbols used in this table are given in Appendix C.3 (page 222).

Figure 24: The Ratios of 27 keV Peak to 31 keV Peak versus Scatter-to-Photopeak Ratios of 60 keV Photons

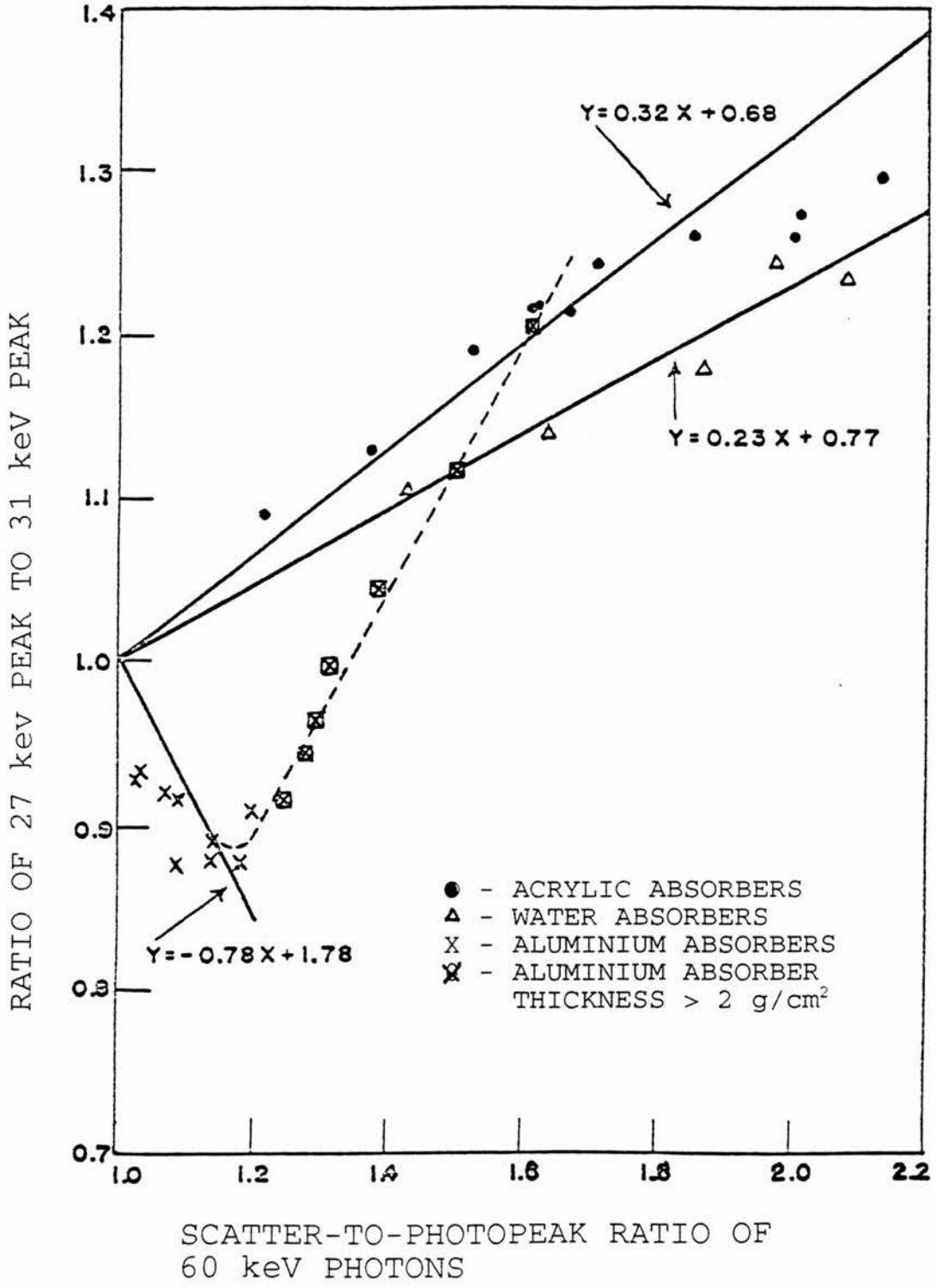

4.7 DETERMINATION OF THE GEOMETRY FACTOR

The geometry factor (also called the geometrical attenuation factor), g(x), for a point source can be generally represented by the equation (eg Tait, 1980):

$$g(x) = A/4\pi x^2 \qquad (4.11)$$

where: A is the detector area;
x is the linear source-detector distance.

For the detector used in this case the area "seen" of the detector by the source will vary with the source-to-detector distance. Since the width and length of the detector surface are different a simple relationship between the area 'seen' and source-to-detector distance is difficult to develop.

It was decided, therefore, to develop an empirical relationship between the geometry factor and the perpendicular distance between the source and the detector surface. This relationship, of course, is only valid for the mercuric iodide detector used.

The attenuation of several thicknesses of absorber material was determined as in Section 4.3. The source was then placed in close proximity to the detector surface (as in the procedure described in Section 4.4)

and the count rate N at zero distance was determined. Absorber material of known thickness (and attenuation) from previous measurements was then placed between the source and the detector, the absorber touching the detector and the source directly behind the absorber. Count rates N_i were obtained under these conditions. The index i (i = 1,2,3 ..... n) refers to count rates obtained whilst using absorber thickness x_i.

For a given absorber thickness x_i, $N_i/N_o = g(x_i)$ times the attenuation of the absorber. The geometry factor is thus obtained by dividing N_i/N_o by the known attenuation of the absorber. The results are given in Table 25 (page 143). By regression analysis (Appendix C.4) the following relationship was obtained:

$$g(x) = 0.64e^{-0.54x} + 0.36 \qquad (4.12)$$

Equation 4.12, together with the experimental points, is plotted in Figure 25 (page 144).

As already discussed in Section 3.1 the geometry factor under conditions of "good" (narrow or ideal broad beam) geometry can be considered to be independent of energy or atomic number. The 59.6 keV gamma-rays from americium-241 were used in the determination of g(x) as they are the most abundant photons at greater absorber thickness and hence give rise to the smallest statistical errors.

Table 25: Geometry Factor versus Source-to-Detector Distance (in centimetres)

X	N3	M	GEOM. F.	S	ABSORBER
0.000	116870	588890	1.000		
0.082	103923	553039	0.947	0.005	ALUMINIUM
0.162	92081	526539	0.881	0.005	ALUMINIUM
0.326	76102	471989	0.812	0.006	ALUMINIUM
0.632	82431	548953	0.757	0.006	ALUMINIUM
1.252	60541	493850	0.618	0.008	ALUMINIUM
1.859	46137	438892	0.530	0.011	ACRYLIC
2.453	36283	368721	0.496	0.014	ACRYLIC
3.040	29621	355167	0.420	0.021	ACRYLIC
4.220	20078	282667	0.358	0.045	ACRYLIC

A1 = -0.54

SA1 = 0.004

C = 0.36

Note: The definitions of symbols used in this Table are given in Appendix C.4 (page 226).

Figure 25: Geometry Factor Versus Source-to-Detector Distance

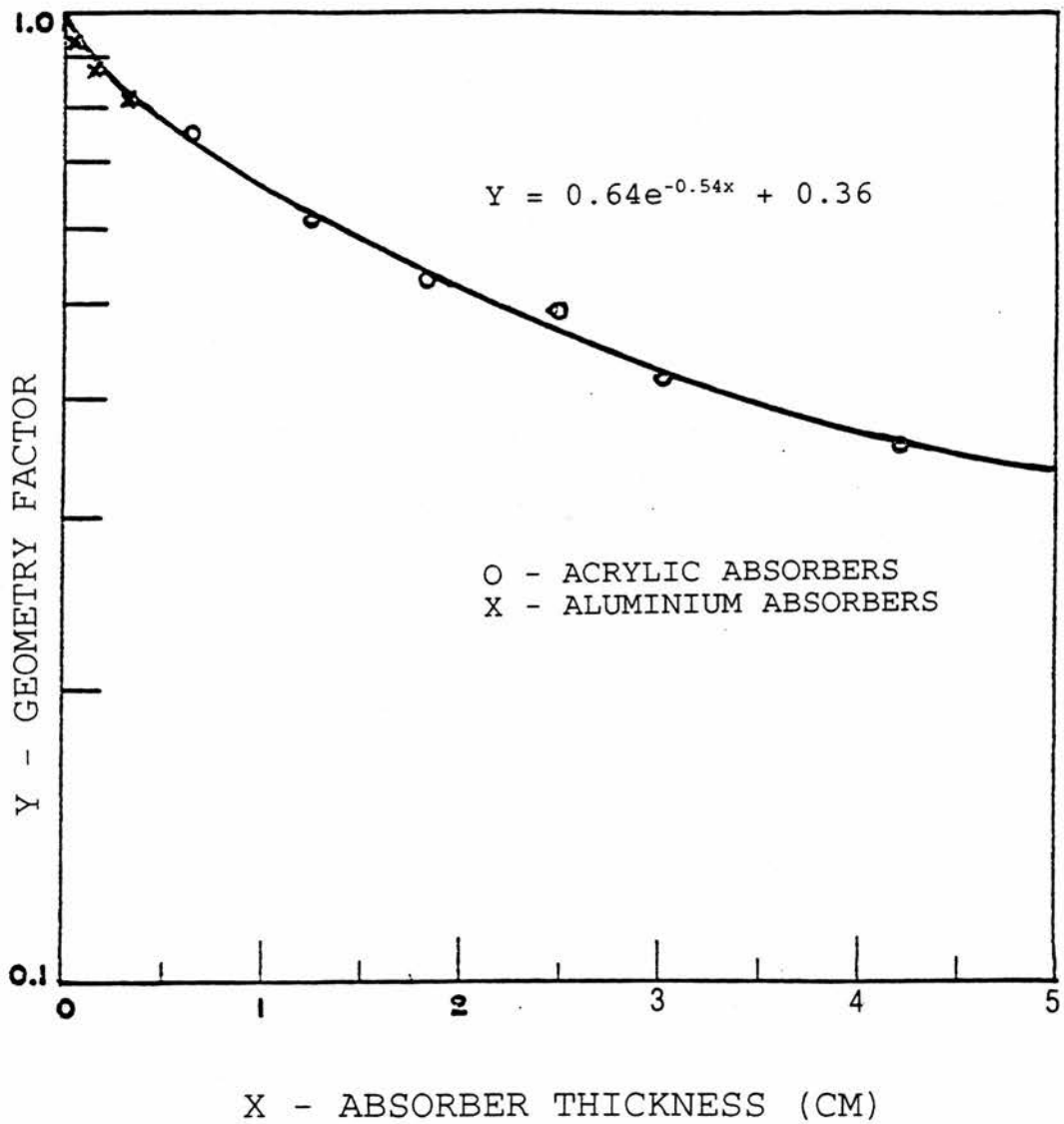

4.8 DETERMINATION OF THE DETECTION EFFICIENCIES OF THE COUNTER FOR THE L_α, L_β, L_γ X-RAYS AND THE 60-keV GAMMA-RAYS

For the determination of counter efficiencies one americium-241 and one plutonium source were used. These were standard calibration sources (traceable to a national standard) in which the alpha activities had been previously determined.

The alpha activities of the two sources were as follows:

Source (a) - Plutonium-238; 2.22E6 dpm
Source (b) - Americium-241; 5.60E5 dpm

The number of photons emitted per unit time by each source in each energy interval of interest was calculated using the known photon abundances per alpha decay (as per Table 2, page 17).

Each source was positioned under the detector so that the detector surface was in very close proximity to the source and then counted for a time period such that the counting error was less than 1%. The observed numbers of counts per unit time, with the background count subtracted, in each energy region, were divided by the calculated number of photons emitted per unit time emitted by the appropriate source. The energy regions

for the L x-rays were as shown in Figure 15 (page 90). Results obtained for the efficiency factors are 25%, 19%, 14% and 48% for the L_α, L_β, L_γ x-rays and 60-keV gamma rays respectively. (This surprising change in efficiency may indicate some layering of the sensitive region of the detector.)

The factors thus obtained are the overall efficiency factors for the detector; they are a product of the intrinsic efficiency, window attenuation and the geometry factor for the small distance between the detector surface and window.

4.9 PROGRAMMING THE METHOD FOR COMPUTER CALCULATIONS

All symbols used perviously are redefined in this section with notations introduced that can be used in the DEC FORTRAN computer program.

4.9.1 Definition of Symbols.

T = counting time (minutes);

N1 = count rate in the L_α x-ray region;

N2 = count rate in the L_β x-ray region;

N3 = count rate in the 60-keV photopeak;
N3 = N5 + N7;

N4 = count rate in the scatter region (approximately 35 - 55 keV);

N5 = count rate in the 31 keV peak;

N6 = count rate in the 27 keV peak;

N7 = count rate in the actual 60 keV peak;

N8 = count rate in the L_γ x-ray peak;

N10 = number of L_α x-rays emitted by the source in time T;

N20 = number of L_β x-rays emitted by the source in time T;

N30 = number of 60 keV photons emitted by the source in time T;

N80 = number of L_γ x-rays emitted by the source in time T;

N3P = count rate that would be observed in the

60-keV photopeak if the source were located directly under the detector;

N10PU = number of L_α x-rays emitted by plutonium alone;

N20PU = number of L_β x-rays emitted by plutonium alone;

N80PU = number of L_γ x-rays emitted by plutonium alone;

N10AM = number of L_α x-rays emitted by americium alone;

N20AM = number of L_β x-rays emitted by americium alone;

N80AM = number of L_γ x-rays emitted by americium alone;

P1 = count rate in the energy range that equals the L_α x-ray plus the iodine escape energy;

P2 = count rate in the energy range that equals the L_β x-ray plus the iodine escape energy;

P8 = count rate in the energy range that equals the L_γ x-ray plus the iodine escape energy;

K1 = factor giving the fractional contribution of P1 to N1;

K2 = factor giving the fractional contribution of P2 to N2;

K8 = factor giving the fractional contribution

of P8 to N8;

N1NET = N1 - K1.P1;

N2NET = N2 - K2.P2;

N8NET = N8 - K8.P8;

RN4N30 = ratio of N4 to N3 in the unattenuated source;

RN6N50 = ratio of N6 to N5 in the unattenuated source;

X = (N4/N3)/RN4N30;

Y = (N6/N5)/RN6N50;

A = slope of the curve of: "ratios of 27 keV photopeak to the 31 keV peak versus scatter-to-photopeak ratios for 60 keV photons";

B = slope of the curve of: "transmission of 60 keV photons versus scatter-to-photopeak ratios";

Z = transmission of 60 keV photons;

F1 = detector efficiency for the L_{α} x-rays emitted by the source at the detector surface;

F2 = detector efficiency for the L_{β} x-rays emitted by the source at the detector surface;

F3 = detector efficiency for the 60 keV gamma rays emitted by the source at the detector surface;

F8 = detector efficiency for the L_{γ} x-rays

emitted by the source at the detector surface;

BQAM = Bq of americium;

BQPU = Bq of plutonium;

Q = absorber thickness between source and detector (g/cm^2);

AQ = slope of the curve of: "transmission of 60 keV photons versus absorber thickness";

C1 = constant subtracted from A (Appendix C.5);

L = absorber thickness between source and detector (in cm);

RHO = density (g/cm^3);

GL = geometry factor;

AL = slope of the curve: "geometry factor versus source-to-detector distance";

C2 = constant subtracted from GL (Appendix C.4);

MU1X = number of mean free paths of the L_α x-rays;

MU2X = number of mean free paths of the L_β x-rays;

MU8X = number of mean free paths of the L_γ x-rays;

H1 = MU1X/MU2X;

H2 = MU8X/MU2X;

AO = arbitrarily assumed value for N10/N20;

BO = arbitrarily assumed value for N80/N20;

AN = calculated value for N10/N20;

BN = calculated value for N80/N20;

PUAMR = plutonium-to-americium ratio;

S = (in front of any of the above-defined symbols) the standard deviation of the respective quantity.

4.9.2 Computation of Americium Quantity and Plutonium-to-Americium Ratio.

The initial calculations in the method described are based on the 60-keV gamma rays from Am-241, and the method does not apply to cases of essentially pure plutonium. If the americium content in a mixture is less than about 2% by alpha activity, the contribution of the low abundance plutonium gamma rays at 39 keV, 44 keV and 53 keV (Table 2, page 17) to the count rate observed in the scatter region (N4) becomes significant. Under those circumstances the relationships described in Section 4.4, 4.5 and 4.6 cannot be used. In such a case, however, the contribution of Am-241 to the count rates observed in the L x-ray region can be neglected. In such cases, alternative methods are available (for example, Yamaoka, et.al., 1966) for quantitative evaluations in cases of internal contamination by pure plutonium when it is located in soft tissues within several millimetres of the surface.

From the spectrum, it is possible to determine if the

americium content is very low. In such a case, N4 is greater than N5. However, this condition can also occur if the americium content is higher than 2% and the source is strongly attenuated by a low atomic number material (Section 4.4). If this happens, the L_α x-rays will be practically totally attenuated. Therefore, an instruction has been placed in the computer program that, whenever N4 > N5, and at the same time N1 > N5, the following comment is printed: "less than two percent americium."

In Appendix C.3 the following equation was obtained;

$$Y = A(X-1) + 1 \qquad (4.13)$$

and from the computer calculations the values of A are a_1 = 0.32; a_2 = 0.23, and a_3 = -0.78 for acrylic, water and aluminium absorbers, respectively. In Appendix C.2, the following equation was obtained;

$$\ln(A) = B(X-1) \qquad (4.14)$$

and from computer calculations the values of B are: b_1 = -1.95; b2 = -2.54; and b3 = -3.94, for acrylic, water and aluminium, respectively.

It is necessary to determine Z from knowledge of X and Y (obtained from measurements). In each case A can be determined. On the basis of the arguments presented in

Section 3.3 it can be assumed that a relationship exists between A and B in the form;

$$B = f(A) \tag{4.15}$$

Assuming Equation (4.15) is expanded in a Taylor series and using the first three terms yields,

$$B = R1 + A.R2 + A^2.R3 \tag{4.16}$$

where R1, R2 and R3 are constants, and for the three materials tested:

$$\begin{aligned} b_1 &= R1 + a_1R2 + a_1^2R3 \\ b_2 &= R1 + a_2R2 + a_2^2R3 \\ b_3 &= R1 + a_2R3 + a_3^2R3 \end{aligned} \tag{4.17}$$

From the three known values of A and B, the following set of linear equations can be written:

$$\begin{aligned} -1.95 &= R1 + 0.32R2 + (0.32)^2R3 \\ -2.54 &= R1 + 0.23R2 + (0.23)^2R3 \\ -3.94 &= R1 - 0.78R2 + (0.78)^2R3 \end{aligned} \tag{4.18}$$

Solving this set of linear equations by the method of determinants yields the following results;

$$\begin{aligned} R1 &= -3.64 \\ R2 &= 3.81 \end{aligned}$$

$$R3 = 4.42$$

Thus, after determining A from Equation (4.13) B can be determined from Equation (4.16) and the transmission of the 60-KeV photons (Z) obtained from Equation (4.14).

Equation (4.13) is not valid in the case of an absorber having an effective atomic number equal to or greater than that of aluminium and a thickness in excess of 2 g/cm^2 (although this particular situation is unlikely to occur in practice). By observation of the data collected, it can be seen that in such a case the following relationship takes place: N8 > N2 and N8 > 1.7N1. An instruction has thus been placed into the computer program so that whenever the above condition occurs, the value of B is set equal to -3.94 and Z is calculated accordingly. Thus,;

$$N3P = N3/Z \qquad (4.19)$$

and

$$N30 = N3P/F3 \qquad (4.20)$$

The quantity of americium (in Bq) is then given by

$$BQ = N30/(T.60.0.359) \qquad (4.21)$$

where 60 is the number of disintegrations per minute per Becquerel and 0.359 is the abundance of 60-keV photons per alpha decay.

Knowing the relative abundances of the L_α, L_β and L_γ x-rays and 60-keV gamma rays in americium (Table 3, page xx), N10AM, N20AM, N80AM can be calculated, followed by N1NET, N2NET and N3NET. If N2NET is equal to or less than zero, it is impossible to continue the calculations, since all the L x-rays have been absorbed. An appropriate instruction is included in the computer program to stop the calculations and print a comment that indicates that all the L x-rays have been absorbed. If the above condition does not occur, the program proceeds.

The absorber thickness ('Q') in g/cm^2 can now be calculated. In Appendix C.5, the following equation was obtained;

$$Q = (1/AQ).\ln((Z - C1)/(1 - C1)) \qquad (4.22)$$

The absorber thickness in centimetres, L, is given by

$$L = Q/RHO \qquad (4.23)$$

In Appendix C.4 the following relationship between the geometry factor GL and L was obtained;

$$GL = (1-C2)\mathrm{Exp}(AL.L) + C2 \qquad (4.24)$$

Knowing GL, Equations (3.3) through (3.6) for the L x-rays can be solved using the method of successive approximations described in Section 3.4. Obviously it is

best to use the most prominent L x-ray peaks in the analysis. Hence, in the programme the L_α and L_γ x -ray peaks are compared and the more prominent selected. The L_β peak is always used in the analysis. Only the equations for a case when the L_α peak is used will be shown here. When the L_γ peak is used, the equations are similar but the values appropriate to L_γ x-rays are utilised instead of those of the L_α x-rays.

N1NET and N2NET are calculated. From Equations (3.3) and (3.4) and the definitions of H1 and A0 the following equation is obtained;

$$MU2X = \frac{\ln(N1NET/N2NET).(F2/F1).(1/A0)}{(1 - H1)} \quad (4.25)$$

and $$MU1X = MU2X.H1 \quad (4.26)$$

Substituting these values back into Equations (3.3) and (3.4), yields;

$$N10 = N1NET.Exp(MU1X)/(F1.GL) \quad (4.27)$$

$$N20 = N2NET.Exp(MU2X)/(F2.GL) \quad (4.28)$$

and $$N10PU = N10 - N10AM \quad (4.29)$$

$$N20PU = N20 - N20AM \quad (4.30)$$

AO was arbitrarily selected for use in the computations. The value AN is calculated from the following equation;

$$AN = 0.667.N20PU/N20 + 0.734.N20AM/N20 \quad (4.31)$$

The constants 0.667 and 0.734 were obtained from the relative abundances of L_α and L_β x-rays in Pu-239 and Am-241, respectively (see Table 4 and Section 3.4). If AN-AO > 10^{-3} (10^{-3} is the arbitrarily-selected precision), then AN is substituted in place of AO in Equation (4.25). This process continues until the desired precision is reached.

If the value of N10PU, or N20PU, becomes zero or negative, then this indicates (within the limits of the accuracy of the method) that all L x-rays detected were due to americium and no plutonium is present. The computer is instructed to print a statement "no plutonium detected" and stop the calculations. If N10PU and N20PU are both greater than zero the amount of plutonium (in Bq) can be calculated as follows;

```
BQPU = N20PU/(T.60.*.0.021)                    (4.32)
```

where 0.021 is the abundance of Pu-239 L_β x-rays per alpha decay.

Finally, the plutonium-to-americium ratio is given by;

```
PUAMR = 8.60.N20PU/N20AM                       (4.33)
```

where 8.60 is the ratio of the abundances of L_β x-rays per alpha decay in Am-241 and Pu-239.

4.9.3 Computation of Standard Deviations

On the basis of the assumptions presented in Appendices B and C.3, using Equation B.8, the standard deviations of X and Y are given by;

$$SX = N30/N40 \sqrt{[N4/(N3)^2 + (N4)^2/(N3)^3]} \quad (4.34)$$

$$SY = N50/N60 \sqrt{[N6/(N5)^2 + (N6)^2/(N5)^3]} \quad (4.35)$$

Equation (4.13) is differentiated with respect to X and Y, making the assumptions that $(\partial A/\partial X)dX$ and $(\partial A/\partial Y)dX$ are stochastically independent of each other, and their standard deviations SX and SY are small compared to the values of X and Y, respectively. Then, let dX = SX and dY = SY. Then the variance of A is given by the sum of squares of $(\partial A/\partial X)SX$ and $(\partial A/\partial Y)SY$. The result is;

$$SA = \sqrt{[(SX(1-Y)/(1-X)^2)^2 + (SY/(1-X))^2]} \quad (4.36)$$

This assumption of independence is not entirely valid. Both X and Y contain the term N5; (N3 = N5 + N7). Thus, when N5 gets bigger X, Y, SX and SY get smaller, i.e., there is a positive correlation between X and Y. The standard deviation of A will therefore be smaller than the value calculated from Equation (4.36).

A similar situation occurs in several other instances as the calculations continue; however, the assumption of independence will be retained. This will lead to the

overestimation of the standard deviation of the detected quantities of americium and plutonium. Hence, the calculated values will represent the worst case. A comparison between the calculated and experimentally obtained values of the standard deviations of measured amounts of americium and plutonium is given.

Differentiating Equation (4.16) with respect to R1, R2, R3 and A and making assumptions similar to those made in the calculation of SA yields;

$$SB = \sqrt{[(SR1)^2 + (A/SR2)^2 + (A^2.SR3)^2 + ((R2+2.A.R3)SA)^2]} \quad (4.37)$$

SR1, SR2 and SR3 were calculated by differentiating the analytical values of R1, R2 and R3 obtained from the solution of the set of Equations (4.17) with respect to a_1, a_2, a_3, b_1, b_2, and b_3, in each case. The values of $(SR1)^2$, $(SR2)^2$ and $(SR3)^2$ were obtained by squaring each of the six differentials, each containing the appropriate variance as a factor, and summing the terms. For numerical calculations of SR1, SR2 and SR3 the values of a_1, a_2, a_3, b_1, b_2, b_3, σ_{a1}, σ_{a2}, σ_{a3}, σ_{b1}, σ_{b2}, and σ_{b3} were obtained from the computer calculations described in Appendices C.2 and C.3. The results are as follows;

$$SR1 = 0.215$$

$$SR2 = 0.442$$

$$SR3 = 0.921$$

The first three terms under the square root in Equation (4.37) are a result of the errors in the calculations of the regression-line parameters (Appendix C); the fourth term represents fluctuations in counting statistics. Included in the computer program (Appendix D) is the possibility of calculating SB as given in Equation (4.37), and a separate calculation giving the contribution of counting statistics alone (by equating SR1, SR2 and SR3 to zero). The same possibility exists in the computer program for all of the calculations of the standard deviations that depend on counting statistics and regression-line parameter errors. Those standard deviations are flagged up in the programme using the index I. Whenever I = 0 the calculations are for the errors due to counting statistics alone, and when I = 1 all the errors are included.

Differentiating Equation (4.14) with regard to B and X, and again applying the assumptions discussed previously yields;

$$SZ = Z \sqrt{[(B.SX)^2 + [(X-1)SB]^2]} \qquad (4.38)$$

Substituting Equation (4.19) into Equation (4.20) yields;

$$N30 = N3/(Z.F3) \qquad (4.39)$$

Differentiating Equation (4.39) with regard to N3 and Z, again applying the same assumptions and taking N3 as the

variance of N3 yields;

$$SN30 = (Z.F3)^{-1}.\sqrt{[N3 + (N3P.SZ)^2]} \qquad (4.40)$$

Equation (4.22) is differentiated with regard to Z and AQ, Equation (4.23) with regard to Q, and Equation (4.24) with regard to L and AL. The results are:

$$SQ = (AQ)^{-1}.\sqrt{[(Q/SAQ)^2 + [SZ/Z-C1)]^2]} \qquad (4.41)$$

$$SL = SQ/RHO \qquad (4.42)$$

and $$SGL = [(GL-C2)\sqrt{(AL.SL)^2 + (L.SAL)^2}] \qquad (4.43)$$

The numerical values of C1, AQ and SAQ were obtained from the calculations described in Appendix C.5 and the values of C2, AL and SAL from the calculations described in Appendix C.4. The variance of N1NET is simply the sum of the variances of the count rates NQ and k1.P1; the variances of N2NET and N3NET are obtained in the same way.

To obtain SMU2X Equation (4.25) is used. The differentiation is with respect to N1NET and N2NET. Hence;

$$SMU2X = \frac{\sqrt{[(SN1NET/N1NET)^2 + (SN2NET/N2NET)^2]}}{(1 - H1)} \qquad (4.44)$$

From Equation (4.25);

$$SMU1X = H1/SMU2X \quad (4.45)$$

SN1O is calculated from Equation (4.27). The variables in this case are N1NET, MU1X and GL. The result is;

$$SN10 = N10\sqrt{[(SN1NET/N1NET)^2 + (SMU1X)^2+(SGL/GL)^2]} \quad (4.46)$$

SN20 is obtained from Equation (4.28). The expression is similar to that in Equation (4.46), except that only terms relevant to L_β x-rays are used in this case. Equation (4.30) can be written in the form;

$$N20PU = N20 - 0.512.N30 \quad (4.47)$$

where 0.512 is the abundance ratio of the L_β x-rays and the 60 KeV photons in Am-241. From Equation (4.47) can be written;

$$SN2PU = \sqrt{[(SN20)^2 + (0.512.SN30)^2]} \quad (4.48)$$

Equation (4.33) can be rewritten in the form;

$$PUAMR = 8.60\ N20PU/0.512.N30 = 16.78.N20PU/N30 \quad (4.49)$$

Differentiating Equation (4.48), with regard to N20PU and N30 yields the final result;

$$SPUAMR=(16.78/N30)\sqrt{[(SN20PU)^2+(N20PU.SN30/N30)^2}$$

4.10 EXPERIMENTAL TESTS AND EVALUATIONS OF THE METHOD

To simulate experimentally the characteristics of human tissue, tissue-equivalent sections of material were used. These sections were taken from samples of the types of tissue-equivalent materials which are used in the manufacture of "Lawrence Livermore Phantoms". These samples of material had been supplied with the "Lawrence Livermore" calibration body phantom currently used for calibration tests in the Dounreay Whole Body Monitoring facility. Hence, they were not part of the basic phantom or its additional components, but had been included with it in the form of cylindrical blocks of material.

The basic construction material of these samples was commercial polyurethane, with calcium carbonate [$CaCO_3$] added in the concentrations necessary for tissue simulation. The three types of material available were; C2-163 (muscle equivalent material representing the liver envelope), B-126 (muscle equivalent material representing the torso) and E-136 (material equivalent to rib bone representing torso bone components). The densities of these materials were, (approximately) 1.11, 1.14 and 1.41 gram/cm^3 respectively.

The sections of tissue-equivalent material prepared varied in thickness from 0.1 cm to 1.5 cm, with variations in thickness (across their area) ranging from 0.01 to 0.3 cm. These relatively large variations were

due to the problems associated with the sectioning of the material, as it was different to cut without deformation and consequent shearing of the material. Various techniques were tried (including freezing with liquid nitrogen and embedding in wax before cutting), but the technique eventually used was that described in Appendix A as this was the technique that yielded the best results.

Three radioactive sources were prepared (by electrodeposition of radioactive material onto small stainless steel discs) containing the following amounts of plutonium and americium as follows;

(1) 1.1E4 Bq americium;
(2) 3.6E3 Bq americium and 3.5E4 Bq plutonium;
(3) 1.7E4 Bq americium and 1.7E5 Bq plutonium;

The activity of these three sources was checked using a solid-state detector which had previously been calibrated using sources that were traceable back to the National Physical Laboratory.

For the purposes of experimental assessment of the method one of the sources was placed in a perspex jig. The detector was then lowered until the surface of the detector was in very close proximity to the surface of the source. (The perspex jig was designed so that the position of the centre of the source, relative to that of

the centre of the surface of the detector remained constant, even if the source-to-detector distance was altered. A background count was carried out on the jig prior to each test.) The source was then counted for ten minutes. The source was then removed and another background count carried out.

The source was then replaced and sections of tissue-equivalent material placed between the source and the detector, material type C2-163 being used for this purpose as this had the least variations in thickness across the areas of each section. The depths at which the source could be located were dictated by this need to use those sections of material showing the least variations in thickness across their area. Hence, the following total thicknesses of material were used; 1.0 cm, 2.1 cm, 3.9 cm and 5.1 cm. The source was then counted under each total thickness of material in turn. This procedure was repeated for each of the prepared sources. In order to mimic (as far as possible) a "real" wound a section of tissue-equivalent material was also placed behind the source for each count.

Between each of these measurements the sources and tissue-equivalent material were removed and replaced, and the detector repositioned. Furthermore, background counts were carried out (on the jig and tissue-equivalent material in use at that time) after each test.

The reasons for the above were two-fold; firstly, to observe the possible errors resulting from the slightly different configurations of the source/material/detector arrangement in each test. Secondly, to reduce the errors caused by the fluctuations in background which, by this stage of the study, were leading to severe problems in the acquisition and analysis of data.

Because of the increasing severity of the problems associated with the operation of the mercuric iodide detector (see Section 5; Discussion) only a limited number of experimental tests and repeat measurements could be carried out.

The counts obtained for each source and position were, after subtraction of the background, were analysed using the program described in Section 4.9 and shown in Appendix D. It was not possible to obtain meaningful estimates of Pu-239 for sources at a depth of 5.1 cm. The remainder of the results are summarised in Table 26 (page 168), in which the known quantities of Pu-239 and Am-241 are compared with the quantities determined by the method developed during this study together with the standard deviations in the determinations of plutonium and americium calculated using the assumptions and equations presented in Section 4.9.3.

The standard deviations were calculated considering only counting errors, as well as for the estimated upper

limits of error involving all of those in the regression analyses. In cases of repeated counts, pooled standard deviations from the analytical calculation are presented in Table 26 (page 168). These were obtained by taking the square root of the mean of the variance, calculated for each set of measurements. The standard deviations were also determined empirically from seven repeated overall determinations, each including both the experimental and computer-method errors ie;

$$S = \sqrt{[\Sigma (x - \bar{x})^2/(n-1)]} \text{ where } n = 7.$$

The comparisons between the calculated and empirically-determined standard deviations show that in the case of americium, where the errors are relatively small, their values are very close. As expected, the empirical standard deviation is smaller in the case of plutonium.

The computer calculated depths were, in all cases, greater than the actual depths. For example, the calculated depths using source 1 were 1.1 cm, 2.3 cm, 4.1 cm and 5.2 cm for the 1.0 cm, 2.1 cm, 3.9 cm and 5.1 cm depths, respectively. This may have been due to backscatter of the x- and gamma-rays from the stainless steel disc on which the activity had been deposited (a situation which would not occur with a real wound) or errors in the figures input into the computer program caused by the fluctuations in the background counts.

TABLE 26: RESULTS OF EXPERIMENTAL TESTS OF THE METHOD

		Counts - bkgd.		Amounts of Pu and Am as determined from analysis of spectra							
				Bq Pu				Bq Am			
Source Used[a]	Depth (cm)	Lβ x-rays (N2)	60 keV photopeak (N3)	Pu	±S Pu (0)[b]	±S Pu (1)[c]	±S Pu [d]	Am	±S Am (0)[b]	±S Am (1)[c]	±S Am [d]
1.08 E4 Bq Am	Surface	178,635	105,697					1.02E4	2.96E2	3.70E2	
	1.0	63,904	60,369					1.08E4	6.66E2	1.11E3	
	2.1	21,360	35,112					9.36E3	8.51E2	1.67E3	
	3.9	9,393	19,754					1.07E4	1.33E3	2.18E3	
	5.1	5,577	12,634					9.14E3	1.15E3	2.18E3	
3.48 E4 Bq Pu	Surface	106,093	32,570	2.45E4	5.00E3	5.25E3		3.26E3	3.33E3	3.70E2	
+	1.0	37,902[e]	19,324[e]	2.12E4	5.22E3	7.03E3[f]	1.15E3	3.22E3	4.07E2	5.55E2	5.55E2
3.59 E3 Bq Am	2.1	13,744	12,232	2.85E4	7.47E3	9.66E3		2.44E3	3.33E2	4.81E2	
	3.9	4,895	6,608	1.95E4	1.14E4	1.34E4		2.74E3	5.18E2	7.77E2	
1.74 E5 Bq Pu	Surface	464,633	129,519	1.57E5	9.14E3	1.04E4		1.48E4	5.92E2	9.99E2	
+	1.0	183,706[e]	90,614[e]	1.39E5[e]	1.21E4[f]	2.55Er[f]	5.22E3	1.82E4[f]	9.25E2[f]	2.00E3[f]	7.77E2
1.73 E4 Bq Am	2.1	61,895	52,529	1.64E5	1.80E4	4.00E4		1.66E4	1.22E3	3.37E3	
	3.9	22,140	30,421	1.74E5	3.60E4	5.62E4		1.49E4	1.55E3	4.00E3	

Continued ...

NOTES TO TABLE 26

a. Measured using calibrated solid-state detector.

b. S(O) = theoretically calculated standard deviation only counting errors included.

c. S(1) - theoretically calculated standard deviations, all errors included.

d. S = empirically determined standard deviation from 7 repeated overall determinations, including both experimental and computer-method errors, ie

$$S = \sum_{i=1}^{n} (x-\bar{x})^2/(n-1), \text{ where } n=7$$

e. Mean of 7 determinations.

f. Pooled from 7 individual determinations.

4.11 PROCEDURAL SUMMARY OF THE METHOD

This section summarises the procedures used for analysing the spectra obtained from Pu-Am contaminated wounds, using a mercuric iodide (HgI_2) semiconductor detector.

By comparison of the ratio of the counts in the 27-keV peak to those in the 31-keV peak (N4/N3) with the scatter-to-photopeak ratio (N6/N5), the effective atomic number of the absorber (Figure 24, page 140) is obtained, which, in turn, yields the slope of the curve relating the transmission of the 60 keV photons to the scatter-to-photopeak ratio of 60 keV photons (Figure 22, page 130). Knowing the transmission and detector efficiency for the 60 keV photons, the number of 60 keV photons emitted by the source (N30) is calculated from the count rate in the 60 keV peak (N3). Since the counting time (T) and the abundance of 60 keV photons per decay of Am-241 are known, the americium activity can then be calculated.

From Figure 23 (page 133), relating transmission to absorber thickness, the absorber thickness between source and detector in g/cm^2 (Q) can be obtained. Then, dividing this quantity by the density gives the approximate linear distance between the source and the detector. From Figure 25 (page 144) the geometry factor (GL) for the case under consideration is then obtained.

In order to determine the amount of plutonium, the count

rates observed in the L x-ray region (N1, N2, N8) must next be corrected for the contributions of higher energy photons. After this correction is performed the two most prominent L x-ray peaks are selected for future computations.

The experimentally-determined efficiency factors of the detector for the L x-rays, the geometry factor, as determined above, and the known ratio of the absorption coefficients for the photon energies under consideration have now been established. Next, an initial value of the ratio of the number of photons emitted by the source in the L_α and L_β x-ray regions (AO) is estimated, followed by the calculation of the first approximation of the number of photons emitted by the source in these energy regions (N10 and N20).

Since the quantity of americium has already been calculated, the number of L x-rays due to americium (N10PU and N20PU) can then be calculated; subtracting N10AM from N10 and N20Am from N20 yields the first approximations of the number of L x-rays due to plutonium (N10PU and N20PU).

Now the ratio of the number of photons emitted by the source in the L_α and L_β x-ray regions can be recalculated, the new value of (AN) obtained and the calculation repeated. This process is continued until a desired precision is obtained. Finally, knowing the abundance of

L_β x-rays per decay of Pu-239 the quantity of plutonium can be calculated from N20PU.

5. DISCUSSION

During the course of this work, the objectives (as defined in Section 2) have been partially achieved. Firstly, one of the detector types (mercuric iodide) has been assessed for the purpose of measurement of plutonium in wounds. Secondly, a method has been developed (utilising the mercuric iodide detector) that permits the evaluation, in certain cases, of the quantities of plutonium and americium in wounds at various depths without any a priori knowledge of the position of the contaminant. This evaluation is based exclusively on the electromagnetic radiations emitted from the site of the contaminant. It has also been demonstrated that it is possible to determine (utilising the same detector) the attenuation by human tissue of the Am-241 60 keV gamma-rays based upon the ratio of the counts observed in the photopeak and the scatter region of that peak, without phantom calibration as a part of each examination.

It should be possible to extend this method to other low-energy gamma- and x-ray emitters by relationships similar to those described in Sections 4.4, 4.5 and 4.6, and by calibrating the detectors to be used for each energy under consideration.

There are several limitations to the method as presented. In the case of a plutonium-americium mixture, the americium content should be greater than about 2% by

alpha activity for determinations in soft tissue depths no greater than about 4 cm. The reasons for this limitation were given in Section 4.9. If there is also significant contamination by other isotopes, the evaluation might become impossible. If the other isotopes emit photons in the energy range of 10 to 60 keV, it is clear that this will interfere with the evaluations. If, however, the energy of the radiation emitted by the other contaminant is greater than 60 keV then Compton scatter might cause some photons to appear below 60 keV.

For the measurement of the L x-rays, the method is self-limiting to an absorber thickness of about 5 g/cm^2. The constant C1 in Equation (4.22), obtained by regression analysis (Appendix C.5) is 0.14. If the transmission of the 60 keV photons is less than 14%, the argument of the logarithm in Equation (4.22) becomes negative and the evaluation of the absorber thickness and the geometry factor becomes impossible. This happens at an absorber thickness of about 5 g/cm^2 as shown in Figure 25 (page 143). At absorber thicknesses approaching this depth, statistical fluctuations will require an increase in the counting time (of ten minutes) to effect detection.

Equation (4.22) does not, however, limit the evaluation of americium. The absorber thickness does not need to be evaluated in order to estimate the attenuation of the 60 keV photons, given by Equation (4.14). It is possible to

develop a different equation to relate the absorber thickness to transmission of 60 keV photons, but it is questionable whether one could expect (or even need) to measure the L x-rays from contaminants in a wound at a depth greater than 5 g/cm^2. The attenuation coefficient of plutonium L_β x-rays in muscle is approximately 1.1 cm^2/g (Evans, 1968). Thus, the attenuation in 5 g/cm^2 muscle will remove 99.6% of the photons, and the geometry factor will further reduce the number of photons reaching the detector.

It was not possible to quantify the amount of plutonium located at depths greater than 4 cm in the tissue-equivalent material (Section 4.10). In addition to the limitation described above, several other factors interfered with the measurements. At greater depths, because of the very strong attenuation of the L x-rays, the contribution of higher-energy photons to counts observed in the L x-ray region becomes very important (Section 4.2).

For example, measuring the source containing 3.48E4 Bq plutonium and 3.59E3 Bq americium located at a depth of 3.9 cm gave results of 4895 counts/10 minutes and 1125 counts/10 minutes in the L_β x-ray region (N2) and the energy interval equal to the L_β x-ray plus the iodine escape energy (P2). Using the "average" correction factor K = 2.3 (Section 4.2) the calculated count due to the L_β x-rays alone is only 2307 counts/10 minutes. The

total number of L_β x-rays emitted by the source was in this case calculated as 4.65E5 photons/10 minutes and the number of americium L_β x-rays emitted by the source was calculated as 2.20E5 photons/10 minutes. A 10% change in the value of K will cause a 23% change in the calculated quantity of plutonium in this particular case. As the depth increases even further, a slight deviation of the "average" K from its true value will cause a much greater change in the calculated plutonium quantity since N2 decreases more quickly than P2.

There is a difference in the absorption coefficients of plutonium and americium L x-rays, because of the slight difference in their photon energies (plutonium L x-rays have the lower energy). This was not corrected for as the composition of the absorber was not known exactly. This type of error increases with increasing depth of the contaminant and could be the reason for the low values obtained for plutonium measured in the experimental tests (Table 26, page 168).

The intrinsic efficiency of the detector is less than 100% for the L x-rays. If the position of the contaminant changes relative to the detector, more photons will reach the detector at angles different from the perpendicular, and the efficiencies at various energies will differ from those measured in Section 4.8.

Although no difficulties were encountered in the

measurement of americium in the experimental tests, the quantities determined were less than the known quantities when measured at depths of a few centimetres (Table 26, page 168). A possible explanation of this fact could be that for larger ratios of scatter-to-photopeak the transmission of the 60-keV photons can be smaller than predicted by Equations (4.4) through (4.6) which were obtained by weighted regressions. This is indicated in Figure 24 (page 140) by the points at the right-hand side of the graph being below the curves, and illustrates the importance of the contribution of higher-energy photons to counts observed in the region of interest.

In the spectroscopic evaluation of electromagnetic radiation one should evaluate not only the energy range of interest, but also the energy range above it. This is a well-known and logical principle. Numerous processes, for example Compton scattering, the escape of characteristic x-rays, the escape of secondary electrons after partial loss of energy, to mention only a few factors, can affect the observed count rates at lower energies. Even in the case of pure plutonium, there are photons emitted in the energy range from 39 keV to 53 keV (Table 2, page 17). Although the abundance of these photons is very low, their contribution to counts observed in the L x-ray region might become significant if the L x-rays are strongly attenuated.

For additional research, it should be possible to develop

a mathematical formula that will permit the evaluation of the contribution of higher-energy photons to counts observed in the L_α, L_β and L_γ x-ray regions for each case under consideration. Such a formula could be based on the analysis of the total scatter region (35 keV to 55 keV), by evaluating separately the contributions of small intervals within the scatter region to the counts observed in each of the L x-ray peaks. This would help to increase the depth at which plutonium could be measured and the accuracy of the method described in this work.

As mentioned earlier, there are other factors also affecting the accuracy of the described method. These were, in essence, the deficiencies of the mercuric iodide detector used. In principle, this detector possessed the capabilities required for the measurement of plutonium in wounds in an operational environment. However,the problems associated with the use of this detector from the beginning of this work, and which gradually increased (possibly due to increasing polarisation of the detector material) in severity mean that (for the moment, at least) this type of detector is not suitable for use as operational radiological protection instrumentation (RPI).

For example, the high voltage bias could not be raised to the operating level required for this detector at a rate greater than 100 V/minute (as per the manufacturer's

instructions). Furthermore, it was recommended that operation of the detector did not begin until twenty minutes had elapsed after the raising of the bias. This was to allow time for the detector to stabilise. In practice, it was found to be necessary to wait for a period of approximately one hour before the detector could be used.

In comparison, the sodium iodide detector in use in the Dounreay Occupational Health Department can be brought into use quickly and easily. The time taken to prepare the detector for use is no longer than ten minutes; this includes the raising of the bias to the operating level, followed by a calibration check and a background measurement.

In all the stages of this work there were problems with electrical noise leading to spurious counts in the energy region up to 60 keV. In the early stages this problem only tended to occur after the detector had been left in an operational condition for approximately 120 hours. Various solutions to this problem were tried eg irradiation of the detector with a high-activity source. It was found, however, that in order to temporarily resolve the problem it was necessary to reduce the bias to zero and not operate the detector for twenty-four hours.

As the work progressed the severity of this problem

increased such that by the end of the work;

(a) the generation of noise occurred at least every thirty minutes;

(b) the detector could not be left in an operational condition for more than twenty-four hours, and;

(d) in order to reduce the problem such that the detector could be operated satisfactorily for short periods of time, it was necessary to have periods of "down-time" between use for up to forty-eight hours.

As previously stated, this problem resulted in only a limited number of experimental tests of the method. The system was tested, however, on a "real" wound on one occasion near to the end of the work. Prior assessment of the wound using the sodium iodide detector had indicated that a small amount of activity was located at the wound site. When the mercuric iodide detector was used (having been in operation for one hour) a large number of spurious counts were generated in the region of interest. Not only was it not possible to quantify the activity at the wound site, but it also lead to some distress on the part of the individual concerned. It was therefore decided that the system was not reliable enough to be used in an operational environment.

The technique developed for use in this work utilised a

mercuric iodide detector. The cadmium telluride (CdTe) detector could not be used for any practical purpose during the course of this work, simply because it suffered from the knock-induced signals known as microphonics. This detector was so sensitive that such phenomena such as doors slamming, items being placed on a bench and (even) a telephone (placed on the same bench) ringing led to the generation of tens of thousands of counts in the region of interest.

Various solutions, including the use of mains and voltage filters, were tried. The most extreme solution was to design and manufacture a jig to provide acoustic protection. This jig was based on a design used by Aeronutronic Ford in 1973 to provide protection to a CdTe detector in a severe vibration/acoustic environment (with an "acoustic" power spectral density in the order of 120 dB/Hz (Baxter, 1976). Despite all these efforts, however, this problem could not be resolved and the detector was not used further in the study.

It is surprising that the problems associated with the operation of these two types of detectors have not been mentioned in the literature, apart from Austin (1989), although it appears that these problems have been reported to the manufacturers (for example, Manson, 1979). It is perhaps unfortunate that these detectors have been marketed as operational RPI when it is apparent that further development work is required on them. As

such there is still no "ideal" detector available for the measurement of plutonium in wounds. In this respect it is obvious that the assessment of activity in contaminated wounds has not progressed much further on from the situation outlined by Hesp (1968), who reviewed the requirements for a measurement system to be used for this purpose.

It is also clear that more work needs to be done on the assessment of uptake of activity from contaminated wounds and the resulting radiological consequences (both to tissues and organs within the body and the local area of tissue surrounding the contamination in the wound site). The International Commission on Radiological Protection (ICRP) have assessed the various routes of uptake of plutonium into the human body, and the resulting consequences (ICRP, 1972; ICRP, 1986). The uptake of plutonium via contaminated wounds is not considered in these documents, only absorption through intact skin and skin damaged by acids or organic solvents. (Some consideration is given to the problem of "local" doses in Appendix E.)

6. CONCLUSIONS

The conclusions from this study are as follows;

1. It was not possible to assess the cadmium telluride detector obtained for this study due to the severity of the operational problems encountered.

2. The mercuric iodide detector obtained for use in this study has been successfully assessed for the proposed application of plutonium-in-wound monitoring.

3. Using the mercuric iodide detector a method has been developed for the evaluation of plutonium and americium point sources containing more than 2% americium by alpha activity up to a depth of about 4 cm in soft tissue.

4. The limitations of the mercuric iodide detector used put a certain limit on the usefulness of the developed method. These limitations indicate that this detector type, although suitable for experimental work, is not suitable for use as operational radiation protection instrumentation.

5. The most important single factor that appears to affect the sensitivity and the accuracy of the method is the contribution of higher energy photons to count rates observed in the L x-ray region due to the escape of iodine characteristic x-rays.

6. It is to be hoped that the development of mercuric iodide for use as radiation detectors will continue so that the current limitations are overcome, as this detector type is, in principle, close to the "ideal" detector for plutonium-in-wound monitoring.

7. PROPOSED FURTHER WORK

Based on the information obtained from the work carried out on this study it is possible to make the following recommendations for proposed further work;

1. The method as described relies on the manual inputting of data for analysis by the computer program; this method should be streamlined by incorporation of the program into a "jobstream" (a series of commands and programs that can be run on the Dounreay Whole Body Monitor DEC computer system) such that intervention by the operator is reduced to a minimum.

2. The experimental tests used radioactive sources with a stainless steel disc backing; the effects of backscatter from this disc may have been responsible for the uncertainties in the calculation of the depths of the activity. Efforts should be made to determine a method of depositing activity directly on to tissue-equivalent material so that the experiment is akin to a "real" wound and the potential effect of backscatter on the measurements and the calculation can be quantified.

3. Further work should be done to carry out experiments using plutonium-americium sources sealed in small glass tubes. This would simulate the situation in which contaminated slivers of glass have been driven into surface tissue, and would allow the method to be tested

for a distributed source configuration.

4. The method described in this work should be extended to other low-energy gamma- and x-ray emitters by using relationships similar to those described in Sections 4.4, 4.5 and 4.6, and by calibrating the detectors to be used for each energy under consideration.

5. A mathematical formula should be derived that will permit the evaluation of the contribution of higher-energy photons to counts observed in the L_α, L_β and L_γ x-ray regions for each case under consideration. Such a formula could be based on the analysis of the total scatter region (35 keV to 55 keV), by evaluating separately the contributions of small intervals within the scatter region to the counts observed in each of the L x-ray peaks. This would help to increase the depth at which plutonium could be measured and the accuracy of the method described in this work.

6. Alternative techniques, such as deconvolution of spectra and least-square fitting techniques, should be reapproached in order to assess improvements in these techniques and reassess their potential for use in plutonium-in-wound monitoring.

8. REFERENCES

Austin, J G. (1989). The Investigation of Alternative Detectors for Plutonium-in-Wound Monitoring. Proceedings of the 25th Anniversary Symposium of the Society for Radiological Protection, pp 165 - 168.

Austin, J G. (1991). AEA Dounreay Internal Document.

Austin, J G. (1992). Contaminated Wounds at Dounreay: A History. AEA-D-002.

Axiel, P. (1954). Intensity Corrections for Iodine X-rays Escaping from Sodium Iodide Scintillation Crystals. Review of Scientific Instruments **25**, p 391.

Bair, W J, Willard, D H, Nelson D C and Case, A C. (1973). Comparative Distribution and Excretion of Pu-237 and Pu-239 Nitrates in Beagle Dogs. Health Physics **27**, pp 392 - 396.

Bair, W J, and Thompson, R C. (1974). Plutonium: Biomedical Research. Science **183**, pp 715 -721.

Baxter, R D. (1976). Miniature Hybrid Preamplifier for CdTe Detectors. IEEE Transactions on Nuclear Science. **NS-23** (1), pp 493 - 497.

Beck, S M. (1969). Lithium-Drifted Silicon Detectors as Low-Energy Photon Spectrometers. NASA TN D-5056. National Aeronautics and Space Administration, Washington DC.

Beinglas, I, Dishon, G, Holzer, A, Ofer, S and Schieber, M. (1982). High-Energy Gamma Spectra Detected with Improved HgI_2 Spectrometers at Room Temperature. Applied Physics Letters, **30**(11), pp 611 - 613.

Bell, R O, Entine, G and Serreze, H B. (1974). Time-Dependent Polarization of Mercuric Iodide Detectors. Nucl. Instr. and Meth. **112**, pp 267 - 274.

Bell, R O, Wald, F V and Goldner, R B. (1975). Study of the Behaviour of Traps in Cadmium Telluride Nuclear Detectors by Optical Methods. IEEE Trans. Nucl. Sci., **NS22**(1), pp 241 - 245.

Bistline, R W and Tyree W H. (1967). A Comparison of Low-Energy Photon Detectors for Plutonium and Americium Wound Counting. RFP-1068, Rocky Flats Division, The Dow Chemical Company.

Bistline, R W, Watters, R L, and Lebel, J L. (1972). A Study of Translocation Dynamics of Plutonium and Americium from Simulated Puncture Wounds in Beagle Dogs. Health Physics **22**, pp. 329 - 337.

Boss, M R and Mann J R. (1967). Body Counter Evaluation of Plutonium Exposures. Health Physics **13**, pp 259 - 266.

Brodsky, A. (1967). Personal communication to Tyler, G R.

Buslinko, N P. (1966). The Monte Carlo Method. The Method of Statistical Trials. Pergamon Press, Elmsford, NY.

Case, K M and Zweifel, P F. (1967). Linear Transport Theory. Addison-Wesley, Reading, MA.

Chilton, A B. (1965). Two-Parameter Formula for Point-Source Build-Up Factors. Nucleonics **23**(8), pp 119 - 127.

Cooke, N. (1987). BNF Springfields. Personal communication to Austin, J G.

Cox, L E. (1979). ESCADT: A Fortran Code for Computing the Positions and Areas of X-Ray Photoelectron Spectral Peaks. Report LA-7910, Los Alamos Scientific Laboratory, Los Alamos, NM 94550.

Dabrowski, A J, Chwaszczewska, J, Triboulet, R and Marfaing, Y. (1976). Spectrometer Performance of N-Type Cadmium Telluride X- and γ-Ray Detectors. IEEE Trans.

Nucl. Sci. **NS23**(1), pp 171 - 176.

Dawson, F G, Deonigi, D E and Eschback, E A. (1965). Plutonium Buildup and Depletion. Nucleonics **23**, pp 101 -105.

Drexler, G and Perzl, F. (1967). Spectrometry of Low-Energy Gamma- and X-Rays with Ge(Li) detectors. Nucl. Inst. and Meth. **48**, pp 332 - 334.

Ehret, R, Kiefer, H, Maushart, R and Mohrle, G. (1964). Performance and Arrangement of Several Large-Area Proportional Counters for the Assessment of Pu-239 Lung Burdens. Assessment of Radioactivity in Man, Volume 1, pp 141 - 149. IAEA, Vienna.

Entine, G. (1976). Nuclear Applications of CdTe Detectors. Proceedings, ERDA X- and Gamma-Ray Symposium, (CONF 760539), Ann Arbor, MI, pp 68 - 70.

Epstein, R J, and Johanson, E W. (1966). Apparatus for Measuring Pu-239 in Wounds. Health Physics **12**, pp 29 - 35.

Erkilla, B H. (1984). Automatic Material Identifier. LA-UR-84-2222, Los Alamos National Laboratory.

Farnsworth, A. (1987). NE Technology Ltd.

Personal communication to Austin, J G.

Fessler, H, Kiefer, H and Maushart, R. (1961). Zur Messung von Quantenstrahlung in Engeriefereich von 3-30 keV mit Grossflächigen Proportionalzahlröhren. Atompraxis **7**, pp 410 - 407.

Fischer, E. (1985). AEA Dounreay Internal Document.

Fitzgerald, J J, Brownell G L and Mahoney F J. (1967). Mathematical Theory of Radiation Dosimetry. Gordon and Breach Science Publishers, New York.

Forbes, P D. (1975). Damage and Repair in Skin Following Exposure to Radioactive Particles. COO-2366-4, Temple University, Philadelphia.

Foster, P P. (1986). AEA Technology Winfrith. Personal communication to Austin, J G.

Fromhein, O, Ohlenschläger, L and Rapp, W. (1975). IAEA-SR-6/4, Diagnosis and Treatment of Incorporated Radionuclides. IAEA, Vienna.

Gale, H J, Peaple, L H J, and Richards, J E. (1960). A Detector for the Measurement of Plutonium-239 in Wounds. AERE-M-595.

Gibbon, J and Howes, J H. (1972). High Purity N-Type Gallium Arsenide for Nuclear Detectors. AERE-R7033.

Goldstein, H and Wilkins, J R. (1954). Calculations of the Penetration of Gamma-Rays. US AEC Report NYO-3075.

Goldstein, H. (1959). Fundamental Aspects of Reactor Shielding. Addison-Wesley, Reading, MA.

Gomez, L S, Label, J L and Walters, R L. (1972). The Effect of Lymph Node Removal On PuO_2 Translocation. Health Physics **22**, pp 833 - 842.

Griffith, W C. (1983). A Bioassay Model for Estimating Body Burdens of Am-241 from Excretion Analysis. Health Physics **44**, Supplement No 1, pp 545 - 554.

Gunnink, R and Nidey, J B. (1972). Description of the Gaminal Program. Report UCRL-51061. Lawrence Livermore National Laboratory, CA 94550.

Hadwin, M. (1986). BNF Sellafield. Personal communication to Austin, J G.

Hartwell, J K. (1972). Detection Limits for Radioisotopic Counting Techniques. ARH-2537.

Harvey, J R. (1971). Alpha Radiation, an External Radiation Hazard. Health Physics **21**(6), pp 866 - 868.

Health & Safety Executive (HSE). (1986). The Ionising Radiations Regulations 1985. HMSO, London.

Heath, R L. (1966). Computer Techniques for the Analysis of Gamma-Ray Spectra Obtained with NaI and Lithium-Ion Drifted Germanium Detectors. Nucl. Inst. and Meth. **43**, pp 209 - 229.

Heath, R L, Holmer, R G, Schmittbroth, L A and Cozier, G A. (1965), Calculation of Gamma-Ray Shapes for Sodium Iodide Scintillation Spectrometers. Report IDO-17017. AEC Research & Development, Idaho Falls, ID 83401.

Hempelmann, L H, Langham, W H, Richmond C R and Voelz, G L. (1973). Manhattan Project Plutonium Workers: A Twenty-Seven Year Follow-Up Study of Selected Cases. Health Physics **25**, pp 461 - 467.

Hesp, R. (1968). Some Aspects of the Measurement of Plutonium in Wounds. Report W.B.C. 27. UKAEA Windscale, Cumberland.

Hill, I D, Church, E L and Mihelich, J W. (1952). The Determination of Gamma-Ray Energies from Beta-Ray Spectroscopy and a Table of Critical X-Ray Absorption

Energies. Rev. Sci. Instr. **23**, pp 523 - 528.

Hogg, R V and Craig A T. (1965). Introduction to Mathematical Statistics, (2nd Edition). The Macmillan Company, New York.

Howes, J H and Totterdell, D H J. (1973). CdTe as a Room Temperature Semiconductor Detector. AERE-R9151.

Hubbell, J H. (1969). Photon Cross Sections, Attenuation Coefficients, and Energy Absorption Coefficients from 10 keV to 100 GeV. Report NSRDS-NBS29, US National Bureau of Standards.

Hubbell, J H. (1982). Photon Mass Attenuation and Energy-Absorption Coefficients from 1 keV to 20 MeV. Int. J. Appl. Rad. Isot., **33**, pp 1269 - 1290.

Huth, G C. (1969). Avalanche Photomultiplying Diode. Semiconductor Nuclear Particle Detectors and Circuits, publication no. 1593, pp 323 - 327, National Academy of Sciences, Washington DC.

ICRP. (1972). The Metabolism of Compounds of Plutonium and Other Actinides. A report prepared by a Task Group of Committee 2 of the International Commission of Radiological Protection. ICRP Publication 19, Pergamon Press, Oxford.

ICRP. (1977). Recommendations of the ICRP. A report prepared by a Task Group of Committee 2 of the International Commission of Radiological Protection. ICRP Publication 27, Pergamon Press, Oxford.

ICRP. (1979a, 1979b, 1980, 1981a, 1981b, 1982a, 1982b). Limits for Intakes of Radionuclides by Workers, Parts 1 - 4. Reports prepared by a Task Group of Committee 2 of the International Commission of Radiological Protection. ICRP Publication 30, Parts 1 - 4, Pergamon Press, Oxford.

ICRP. (1984). Non-stochastic Effects of Ionising Radiation. A report prepared by a Task Group of Committee 4 of the International Commission of Radiological Protection. ICRP Publication 41, Pergamon Press, Oxford.

ICRP. (1986). The Metabolism of Plutonium and Related Elements. A report prepared by a Task Group of Committee 2 of the International Commission of Radiological Protection. ICRP Publication 48, Pergamon Press, Oxford.

ICRP. (1988). Individual Monitoring for Intakes of Radionuclides: Design and Interpretation. A report prepared by a Task Group of Committee 4 of the International Commission of Radiological Protection. ICRP Publication 54, Pergamon Press, Oxford.

ICRP. (1990). 1990 Recommendations of the International Commission on Radiological Protection. ICRP Publication 60, Pergamon Press, Oxford.

ICRU. (1971). Radiation Quantities and Units. ICRU Report 19. International Commission on Radiation Units and Measurements, Washington.

Johanson, J L and Lawrence, J N P. (1974). Plutonium Contaminated Wound Experience and Assay Techniques at the Los Alamos Scientific Laboratory. Health Physics **27**, pp 55 -59.

Johns, H E and Laughlin, J S. (1956). Interaction of Radiation with Matter. (Ed. Hine, G J and Brownell, G L.) Radiation Dosimetry. Academic Press, Inc., New York, pp 49 - 123.

Johns, H E. (1964) The Physics of Radiology. Charles C Thomas, Illinois.

Jones, E W, and Saxby, W N. (1968). Detection and Measurement of Plutonium Contamination in Wounds. (Eds., Snyder, W S, Abee, H H, Burton, L K, Maushart, R, Benco, A, Duhamel, F and Wheatley, B M.) Proceedings of the First International Congress of Radiation Protection, pp 1295 - 1307. Pergamon Press, Oxford.

Jones, S R. (1985). Derivation and Validation of

a Urinary Excretion Function for Plutonium Applicable Over Tens of Years Post Uptake. Radiation Protection Dosimetry, **10**, pp 19 -27.

Judd, A M. (1981). Fast Breeder Reactors: An Engineering Introduction. Pergamon Press, Oxford.

Kobayushi, T and Sugita, T. (1972). Gallium Arsenide Surface Barrier Detectors. Nucl. Instrum. and Meth. 213, pp 179 - 180.

Kobayushi, T, Kuru, I, Hojo, A and Sugita, T. (1976). Fe-Doped High Purity GaAs as a Room Temperature Gamma-Ray Spectrometric Detector. IEEE Trans. Nucl. Sci. **NS-24**(1), pp 97 - 101.

Kiefer, H and Maushart, R. (1962). Determination of Plutonium-239 Body Burden Using Gamma Spectrometry with Proportional Counters. Whole Body Counting, pp 289 - 293. IAEA, Vienna.

Kiefer, H and Maushart, R. (1964). Nachweis von Pu-239. Strahlenschutzmesstechnik. (Abschnit 3.629) Braun-Verlag. Karlsruhe.

Kiefer, H and Maushart, R. (1968). Plutonium-Inkorporationsnachweis durch Direktmessung. Atompraxis **14**, pp 338 - 339.

Knoll, G F. (1989). Radiation Detection and Measurement (2nd ed.) John Wiley and Sons, New York.

Konishi, E and Yoshzawa, Y. (1985). Estimation of Depth of Basal Cell Layer of Skin for Radiation Protection. Radiat. Prot. Dosim. **11**(1), pp 29 - 33.

Krebs, J S. (1967). Response of Mammalian Skin to Irradiation with Particles of Reactor Debris. USNRDL-TR-67-118.

Lansiart, A and Morucci, J P. (1964). Nouveau Compteur Proportionnel Destine à la Detection In Vivo de Traces de Plutonium dans les Poumons. Assessment of Radioactivity in Man, Volume 1, IAEA, Vienna.

Laurer, G R and Eisenbud, M. (1967). In Vivo Measurements of Radionuclides Emitting Soft Penetrating Radiation. Proceedings of a Symposium on Diagnosis and Treatment of Deposited Radionuclides. (Eds. Kornberg, H A and Norwood, W D.) Excerpta Medica Foundation. pp 189 - 207.

Leggett, R W. (1985). A Model of the Retention, Translocation and Excretion of Systemic Pu. Health Physics **49**, pp 1115 - 1137.

Lima, F W and Atilla, A T. (1974). A Simple Program in BASIC Language for Analysis of Gamma-Ray

Spectra Using an On-Line Minicomputer. Journal of Radioanalytical Chemistry **20**, pp 769 - 777.

Lister, B J. (1964). Health Physics Aspects of Plutonium Handling. Report AERE L-151. UKAEA Harwell, Oxfordshire.

Loevinger, W. (1950). Distribution of Absorbed Energy Around a Point Source of Beta Radiation. Science **112**, pp 30 - 32.

Lushbaugh, CC and Langham, J. (1962). A Dermal Lesion from Implanted Plutonium. Arch. Dermatol. **86**, pp 461 - 465.

Lushbaugh, C C, Cloutier, R J and Humason, G. (1967). Histopathologic Study of Intradermal Plutonium Deposits: Their Conjectural Fate. Ann. N.Y. Acad. Sci **145**, p 791.

Magnusson, L B. (1957). Intensities of X-Ray and Gamma-Ray in Am-241 Alpha Decay. Physical Review **107**, pp 213 -227.

Maldofsky, P J and Swinth, K L. (1972). Avalanche Detector Arrays for <u>In Vivo</u> Measurement of Plutonium and Other Low-Activity Low-Energy Emitters. IEEE Trans. Nucl. Sci. **NS-19**(1), pp 55 - 63.

Malm, H L and Martini, M. (1974). Polarization Phenomena in Cadmium Telluride Radiation Detectors. IEEE Trans. Nucl. Sci., **NS23**(1), pp 322 - 330.

Manson, A J. (1985). AEA Technology Dounreay. Personal communication to Austin, J G.

Manson, A J, and Austin, J G. (1985). AEA Dounreay Internal Document.

Manson, P. (1979). AEA Dounreay Internal Document.

NCRP. (1980). The Management of Persons Accidentally Contaminated with Radionuclides. National Council on Radiation Protection and Measurements Publication 65.

NBS. (1964). Physical Aspects of Irradiation. National Bureau of Standards Handbook 85. ICRU Report 10b.

Norwood, W D. (1972). Plutonium (Pu-239) Toxicity, Diagnosis and Therapy. J. Occup. Med. **14**, pp 37 - 44.

Palmer, H E, Wogman, N A and Cooper, J A. (1967). The Determination of the Depth and Amount of Pu-239 in Wounds with Si(Li) Detectors. Nucl. Med. Biol. **2**, pp 164 -170.

Palmer, H E and Rieksts, G A. (1980). The Use of

M X-Rays from Pu-238/239 and Am-241 to Study Shallow Depositions in Body Surfaces. Health Physics **38**, pp 71 - 73.

Pearton, D C G, Eddy, B T and Watterson, W I J. (1977). The Rapid Reduction of Gamma-Ray Spectra with a Desk-Top Calculator. Report 1873, National Institute for Metallurgy, Randburg, South Africa.

Powell, H J. (1985). AEA Dounreay Internal Document.

Profio, A E. (1979). Radiation Shielding and Dosimetry. John Wiley and Sons, New York.

Putnam, Marie, Gipson, D H, Halmer, R G and Heath, R L. (1965). A Nonlinear Least Square Program for the Determination of Parameters of Photopeaks by the Use of a Modified Gaussian Function. Report IDO-17016. AEC Research & Development, Idaho Falls, ID 83401.

Putzier, E A, Mann, J R, and Johnson, V P. (1958). Use of a Gamma-Ray Spectrometer for Investigation of Plutonium Contaminated Wounds. Am. Ind. Hyg. Ass. J. **19**, pp 384 - 385.

Putzier, E A. (1966). Data Used in Health Physics Considerations for Plutonium and Americium. RFP-795. Dow Chemical Corp., Golden, Colorado.

Ramsden, D. (1969). The Measurement of Pu-239 In Vivo. Health Physics **16**, pp 145 - 154.

Ramsden, D and Speight, R G. (1967). The Measurement of Pu-239 In Vivo: A Progress Report. (Eds., Kornberg, H A and Norwood, W D.) Proceedings of a Symposium on Diagnosis and Treatment of Deposited Radionuclides, pp 171 - 188. Excerpta Medica Foundation.

Randtke, P J, Ortale, C, Whited, R C and Van den Berg, L. (1976). Proceedings, ERDA X- and Gamma-Ray Symposium, Ann Arbor, MI, (CONF 760539), pp 71 -76.

Roesch, W C and Baum, J W. (1958). Detection of Plutonium in Wounds. Proceedings of the Second United Nations International Conference. United Nations, Geneva. pp 142 - 144.

Roesch, W C and Palmer, H E. (1962). Detection of Plutonium In Vivo by Whole Body Counting. Health Physics **8**, pp 773 -775.

Ross, J S. (1968). Evaluation of Plutonium Exposures in Man. Health Physics **14**, pp 373 - 389.

Rossi, H H. (1967). Energy Distribution in the Absorption of Radiation. Adv. Biol. Med. Phys. **11**, pp 27 - 30.

Schieber, M. (1977). Fabrication of HgI_2 Nuclear Radiation Detectors. Nucl. Instr. and Meth., **144**, pp 469 - 477.

Shalev, S. (1978). Gamma-Ray Spectrometry with Mercuric Iodide Detectors with Application to Medical Imaging. Nucl. Inst. and Meth., **150**, pp 79 - 82.

Sharma, R C, and Somasundaram, S. (1971). Detection and Measurement of Pu-239 in Wounds. BARC-559, Bhabha Atomic Research Centre, Bombay.

Siffert, P, Cornidec, J P, Cornet, A, Bell, R O and Wald, F V. (1974). Full Energy Peak Efficiency of CdTe Gamma-Ray Spectrometers. Nucl. Inst. and Meth., **115**, pp 13 - 21.

Siffert, P, Cornet, A, Stuck, R, Triboulet, R,and Marfaing, Y. (1975). Cadmium Telluride Nuclear Radiation Detectors. IEEE Trans. Nucl. Sci., **NS 22**(1), pp 211 - 225.

Siffert, P, Berger, J, Scharager, C, Cornet, A, Stuck, R, Bell, R O, Serreze, H B and Wald, F.V. Polarization in Cadmium Telluride Nuclear Radiation Detectors. IEEE Trans. Nucl. Sci., **NS23**(1), pp 159 -176.

Slapa, M, Huth, G C, Seibt, W, Schieber, M M and Randtke, P J. (1976). Capabilities of Mercuric Iodide

as a Room Temperature X-Ray Detector. IEEE Trans. Nucl. Sci., **NS23**(1), pp 102 - 111.

Splichal (Jnr), W F. (1966). Plutonium Wound Monitor. Report DP-1059, Savannah River Laboratory, E.I. Pont de Nemours & Co., Aiken S.C. 29801.

Spanier, J and Gelbard, E M. (1969). Monte Carlo Principles and Neutron Transport Problems. Addison-Wesley, Reading, MA.

Swierkowski, S P. (1976). A Comprehensive Model for Predicting Semiconductor Detector Performance. IEEE Trans. on Nucl. Sci., **NS-23**(1), pp 131 - 137.

Swinth, K L. (1967). Wound Counting with Solid-State Detectors. Report BNWL-481-4, pp 23 - 25. Battelle-Northwest, Richland, Wash., Northwest Lab.

Taylor, D M. (1973). Chemical and Physical Properties of Plutonium. In: Uranium, Plutonium, Transplutonic Elements (Eds., Hodge, H C, Stannard, J C and Hurst, J B). Hand. Exp. Pharmacol. **XXXVI**, pp 321 - 347.

Tait, W H. (1980). Radiation Detection. Butterworths, London.

Toohey, R E, Keane, A T and Rundo, J. (1983).

Measurement Techniques for Radium and the Actinides in Man at the Centre for Human Radiobiology. Health Physics **44** (Supplement No. 1), pp 323 - 341.

Totterdell, D H J. (1984). AEA Technology Harwell. Personal Communication to Austin, J G.

Trubey, D K. (1966). A Summary of Empirical Functions Used to Fit Gamma-Ray Build-Up Factors. Report ORNL-RSIC-10, Oak Ridge National Laboratory, Oak Ridge, Tennessee.

Tyler, G R. (1966) Self-Absorption of X-Rays with Special Reference to Plutonium-in-Wound Monitoring. Health Physics **12**, pp 509 - 519.

Vasilik, D G, Martin, R W and Umbarger, C J. (1978). A Sensitive, Yet Simple, Plutonium Wound Monitor. Health Physics **35**, pp 577 - 578.

Vaughan, J, Bleaney, B and Taylor, D M. (1973). Distribution, Excretion and Effects of Plutonium as a Bone Seeker. Uranium-Plutonium-Transplutonic Elements, (eds. Hodge, H C, Stannard, J N and Hursh, J D), pp 349 - 502. Springer-Verlag, New York.

Voelz, G L, Ziegler W , Lawrence T, Vasilik T E and Moss, O R. (1984). Management of a Plutonium-Contaminated Wound: A Case Study. Presented at the 29th

Annual Meeting of the Health Physics Society, June 3 - 8, 1984, New Orleans, Louisiana.

Waechter, D A, Brake R J, Vasilik, D G and Erkilla, B H. A Computer-Based Plutonium Wound Monitor. IEEE Transactions on Nuclear Science **NS31**(1), pp 679 - 681.

Watters, R L and Lebel, J L. (1972). Progress in the Beagle Studies at Colorado State University. Health Physics **22**, pp 811 -819.

Webb, P P and Jones, A R. (1974). Large-Area Reach-Through Avalanche Diodes for Radiation Monitoring. IEEE Trans. Nucl. Sci., **NS-21**(1), pp 151 - 158.

Webb, P P and McIntyre, R J. (1976). Large-Area Reach-Through Avalanche Diodes for X-Ray Spectroscopy. IEEE Trans. Nucl. Sci., **NS-23**(1), pp 138 - 144.

Whitton, J T. (1973). New Values for Epidermal Thickness and their Importance. Health Physics **24**(1), pp 1 - 8.

Yamoaka, A, Kuroda, H and Tatsuta, H. (1968). A Trial Production of Plutonium Contaminated Wound Counters. Proceedings of a Symposium on Diagnosis and Treatment of Deposited Radionuclides. (Eds. Kornberg, H A and Norwood, W D.) Excerpta Medica Foundation, pp 1003 - 1009.

APPENDIX A METHOD USED TO SLICE TISSUE - EQUIVALENT SAMPLE MATERIAL

1. Trepan discs of 35 mm diameter using hole saw in drilling machine.
2. Fit the trepanned disc in the split collet with screw-adjusting backstop.
3. Set up collet assembly in lathe.
4. Part-off slice to approximate thickness using 0.65 mm wide parting tool.
5. Remove collet assembly from machine and repeat operations 3 and 4 after adjusting backstop to achieve the thickness required for the next part-off.
6. Repeat operation 5 as required.

APPENDIX B ESTIMATION OF THE STANDARD DEVIATION FOR A RATIO OF TWO COUNTS

For a given function f(x,y), a small variation δf can be represented by

$$\delta f = (\partial f/\partial x)dx + (\partial f/\partial y)dy \qquad (B.1)$$

It can be assumed that $(\partial f/\partial x)dx$ and $(\partial f/\partial y)dy$ are independent of each other. If dx and dy can fluctuate independently in the plus or minus direction, then dx and dy are independent random variables. For small variations of x and y, $(\partial f/\partial x)$ and $(\partial f/\partial y)$ are approximately constants.

The standard deviations of x and dx, and y and dy are equal;

$$\sigma_x = \sigma_{dx} \qquad (B.2)$$

$$\sigma_y = \sigma_{dy} \qquad (B.3)$$

because the respective frequency distributions of the variables are translations of each other along the x axis.

Therefore;

$$\mathrm{Var}(\partial f/\partial x)dx = (\partial f/\partial x)^2\,\mathrm{Var}(dx) = (\partial f/\partial x)^2\sigma_x^2$$

or $$\sigma_{(\partial f/\partial x)dx} = (\partial f/\partial x)\sigma_x \qquad (B.4)$$

and in a similar way;

$$\sigma_{(\partial f/\partial y)dy} = (\partial f/\partial y)\sigma_y \qquad (B.5)$$

Since the variance of the sum of two independent random variables is given by the sum of the variances, then;

$$\sigma_{f(x,y)} = \sqrt{((\partial f/\partial x)\sigma_x)^2 + ((\partial f/\partial y)\sigma_y)^2} \qquad (B.6)$$

If $f(x,y) = x/y$, then;

$$\partial f/\partial x = 1/y: \quad \partial f/\partial y = -x/y^2$$

Substituting these values into Equation (B.6) then;

$$\sigma_{x/y} = \sqrt{[(\sigma_x/y)^2 + ((x/y^2)\sigma_y)^2]} \qquad (B.7)$$

The standard deviation of a count N is $\sqrt{N}$. (If the count is large enough, then the value of the standard deviation of the count approximates the standard deviation of a normally distributed variate having the same mean and variance, and then μ +/- $\sqrt{N}$ approximates 68% of the area under the frequency distribution. Now, if;

$x = N_A$ = counts in interval A of the spectrum;

$y = N_B$ = counts in interval B of the spectrum, then;

$\sigma_x = \sqrt{N_A}$; $\sigma_y = \sqrt{N_B}$

$1/y = 1/N_B$; $x/y^2 = N_A/N_B^2$

Substituting these values into Equation (B.7) then;

$$\sigma_{NA/NB} = \sqrt{[N_A/N_B^2 + N_A^2/N_B^3]} \qquad (B.8)$$

It can be seen from Equation (B.8) that the value of $\sigma_{NA/NB}$ will be large when the ratio N_A/N_B will be large and N_B will be small. As a result of the assumptions in this derivation, however, Equation (B.8) is a good estimate of $\sigma_{NA/NB}$ only when the relative errors $\sqrt{N_A}/N_A$ and $\sqrt{N_B}/N_B$ are small.

APPENDIX C: CALCULATION OF REGRESSION LINE PARAMETERS

If there is a set of observations X_1, X_2 .....X_n that are stochastically independent and it is assumed that a dependent variable y(x) is linearly related to x then the parameters of a regression line.

$$y = a_o + a_1 x \qquad (C.1)$$

can be obtained by minimising

$$\chi^2(n-1) = \sum ((y_i - y)^2/S_i^2) \qquad (C.2)$$

where $y = f(x_i)$ and S_i^2 is the observed variance of y_i. (Hogg and Craig, 1965). (The notation $\sum$ has been used to denote;

$$\sum_{i=1}^{n}$$

as an aid to legibility. This convention has been adhered to in all Appendices unless otherwise stated.)

The value of χ^2 is minimised by setting;

$$\partial\chi^2/\partial a_o = 0, \text{ and;} \qquad (C.3)$$

$$\partial\chi^2/\partial a_i = 0 \qquad (C.4)$$

in order to obtain the parameters of the regression line most likely to have produced the observed data.

In the calculation it is assumed that the background is known without error and is subtracted prior to the analysis.

APPENDIX C.1: TRANSMISSION OF L X-RAYS THROUGH ABSORBER MATERIAL IN "GOOD GEOMETRY" CONDITIONS

Definition of symbols: Let

N_i = count rate in the energy range under consideration for absorber thickness x;

x_i = absorber thickness (g/cm^2);

P_i = count rate in energy range that equals energy range under consideration plus iodine escape energy;

K = factor correlating the contribution of P_i to N_i;

N_{iNET} = $N_i - K.P_i$;

N_o, P_o = count rates in the appropriate energy ranges without the absorber;

S_i = standard deviation of Y_i;

i = 1,2,3 .....n.

Assumptions: N_o, P_o, and x are known without error from previous measurements. K is a constant.

Since the photon attenuation of each L x-ray under conditions of "good geometry" approximates an exponential curve, then a straight line is anticipated on a semi-logarithmic plot ie.

$$y = a_o + a_1 x \qquad (C.1.1)$$

where; $y_i = \ln z_i$

$$= \ln((N_i - K.P_i)/(N_o - K.P_o)) \qquad (C.1.2)$$

When $x = 0$, $z = 1$ and $y = 0$ then $a_o = 0$ and

$$y = a_1 x \qquad (C.1.3)$$

Since one point (the y intercept) and the slope, a, were fixed using the data then for χ^2 there are only (n - 2) degrees of freedom. Substituting Equation (C.1.3) into Equation (C.1.2) then yields;

$$\chi^2 (n - 2) = \sum ((y_i - a_1 x_i)/S_i)^2 \qquad (C.1.4)$$

Differentiating Equation (C.1.4) with respect to a, and setting the derivative equal to zero then gives;

$$\sum ((a_1 x_i^2 - y_i x_i)/S_i^2) = 0 \qquad (C.1.5)$$

Solving for a_1 produces;

$$a_1 = \sum (x_i y_i / S_i^2) / \sum (x_i^2 / S_i^2) \qquad (C.1.6)$$

Since x is known without error, S_i^2 is equal to the variance of y attributable only to variations in measuring the transmitted radiation. The variance of x, $(S_{i,x})^2 = 0$.

From Equations (C.1.3) and (C.1.2);

$$\delta y = (\partial y/\partial z)\delta z$$
$$= (\partial(\ln z)/\partial z).\delta z$$
$$= ((N_o - K.P_o)/(N_i - K.P_i))\delta z \qquad (C.1.7)$$

Since Var(a-b) = Var(a) + Var(b), and the estimated variance of a count is equal to the count, then from Equation (C.1.2.);

$$\text{Var } \hat{c} = \text{Var}(N_i/N_o - K.P_o) + \text{Var}(K.P_i/N_o - K.P_o)$$

and the estimate of δz is;

$$\delta z = \sqrt{\text{Var}Z}$$
$$= (\sqrt{N_i + K^2 .P_i})/(N_o - K .P_o) \qquad (C.1.8)$$

Substituting Equation (C.1.8) into (C.1.7) then yields;

$$\delta y = S_i$$
$$= S_{i,y}$$
$$= \sqrt{(N_i + K^2.P_i)/(N_i - K.P_i)} \qquad (C.1.9)$$

The estimated variance of a_1 is similarly obtained from the relationship;

$$(S_{a_i})^2 = \sum (\partial a_1/\partial y_i)^2.\delta_{y_i})^2 \qquad (C.1.10)$$

Differentiating Equation (C.1.6) with respect to y_i yields;

$$(\partial a_1/\partial y_i) = (x_i/S_i^2) / \sum (x_1^2/S_i^2 \qquad \text{(C.1.11)}$$

Substituting Equation (C.1.11) into (C.1.10), letting $S_i = \delta y_i$, and then simplifying, yields;

$$(S_{a1})^2 = 1/ \sum (x_i^2/S_i^2) \qquad \text{(C.1.12)}$$

It has been assumed that K is a constant, but it is known that K is a function of Z_{eff} and absorber thickness. The exact relationships are not known, however, and the true value of K for each x_i cannot be determined. An average value of K for this detector must then be determined. This can be done by changing the value of K until the minimum numerical value of χ^2 is obtained as follows.

The value of K will be changed in the computer until the minimum numerical value of χ^2 is obtained. In this way an "average" value of K is determined that yields the best fit of the experimental points to a straight line on a semi-logarithmic plot. The computer program for the above calculation is presented in Table C.1 (page 233).

(It should be noted that P(0) and N(0) are referred to as P(1) and N(1) in the program ie the first set of results obtained when no absorber is present. This is because the subscript '(0)' is invalid in DEC FORTRAN and will not be recognised).

APPENDIX C.2 TRANSMISSION OF 60 keV PHOTONS VERSUS SCATTER-TO-PHOTOPEAK RATIO

Definition of symbols;

$N_{3,i}$ = count rate in the 60 keV photopeak;

$N_{4,1}$ = count rate in the scatter region (approximately 35-55 keV);

$N_{3,0}$, $N_{4,0}$ = count rates in the appropriate regions without an absorber and with the source placed against the detector;

i = 1,2,3.....n;

$\hat{a}$ = estimate of the slope from an "eyeball" fit;

y_i = $\ln z_i$

= $\ln (N_{3,i}/N_{3,0})$; (C.2.1)

x_i = $(N_{4,i} /N_{3,i})/(N_{4,0} /N_{3,0})$; (C.2.2)

Assumptions: $N_{3,0}$ and $N_{4,0}$ are known without error.

Preliminary graphs of y versus x indicated that an exponential relationship would yield a reasonable fit to the data (Figure 23, page 137). Here an objective "best fit" to an assumed straight line on a semi-logarithmic plot is wanted. The actual value of a_1 was determined by reiterations as shown in the computer program in Table C.2 (page 236) of this Appendix.

When z = 1, x = 1 and y = 0. Substituting these values into Equation (C.1) the result is $a_o = -a_1$ and the regression line equation is;

$$y = a_1(x-1) \qquad \text{(C.2.3)}$$

Substituting Equation (C.2.3) into Equation (C.2) yields

$$\chi^2(n-2) = \sum [(y_i - a_1 (x_i - 1))/S_i]^2 \qquad \text{(C.2.4)}$$

Differentiating Equation (C.2.4) with respect to a_1, and equating to zero yields;

$$\sum [S_i^{-2} (y_i - a_1.x_i + a_1)(x_i - 1)]=0 \qquad \text{(C.2.5)}$$

and solving for a_1 produces;

$$a = \sum [(Y_i/S_i^2)(x_i - 1)]/\sum [(1/S_i^2)(x_i - 1)^2] \qquad \text{(C.2.6)}$$

Appropriate values of S_i^2 must now be obtained for use in Equation (C.2.6). Since both x and y have non-zero variances in this case then;

$$(S_i)^2 = (S_{i,y})^2 + (S_{i,x}.\hat{a})^2 \qquad \text{(C.2.7)}$$

where $S_{i,y}$ is the standard deviation of y_i and $S_{i,x}$ is the standard deviation of d_i. From Equation (C.2.1) and using

$$\delta z = \sigma_z$$
$$= \sqrt{N_{3,i}/N_{3,0}} \text{ then;}$$

$$S_{i,y} = \delta y$$
$$= (\partial y/\partial z)\delta z$$
$$= (\partial(\ln z)/\partial z)\delta z$$
$$= (1/z)\delta z$$
$$= (N_{3,0}/N_{3,i}).\sqrt{(N_{3,i}/N_{3,0}}$$
$$= \sqrt{N_{3,i}/N_{3,0}} \qquad (C.2.8)$$

which is an approximation to the component $S_{i,y}$ of the variation in y resulting from counting errors alone.

The evaluation of the standard deviation for a ratio of two counts has been given in Appendix B. In order to obtain the contribution $S_{i,x}$ to the random error in y resulting from errors in determining x, Equation (B.8) can be used as follows;

$$S_{i,x} = S_{(N4,i/N3,i)/(N4,0/N3,0)}$$
$$= \sqrt{N_{4,i}/(N_{3,i})^2 + ((N_{4,i})^2/(N_{3,i})^3)/(N_{3,0}/N_{4,0})} \qquad (C.2.9)$$

since $N_{3,0}$ and $N_{4,0}$ have been assumed to be constant. Now, to obtain an initial estimate of the slope a,

$$\hat{a} = (y_t - y_0)/(x_t - x_0) \qquad (C.2.10)$$

where t is some chosen value of i. Setting $x_0 = 1$ at $y_0 = 0$ and, by definition

$$Y_t = \ln(N_{3,t}/N_{3,0})$$

then;

$$a = (\ln(N_{3,t}/N_{3,0}))/(x_t - 1) \qquad \text{(C.2.11)}$$

By substituting Equations (C.2.8), (C.2.9) and (C.2.11) into Equation (C.2.7) then the final value of (S_i^2) is obtained. The actual value of a, is determined by reiterations as shown in the computer program given in Table C.2 (page 236).

The variance of a_1 in this case is given by;

$$(S_{a1})^2 = \sum ((\partial a_1/\partial y_i)\delta y_i)^2 + \sum ((\partial a/\partial x_i)\delta x_i)^2 \qquad \text{(C.2.12)}$$

Differentiating Equation (C.2.6) with respect to y_i and x_i yields;

$$\partial a_1/\partial y_i = ((1/S_i^2)(x_i - 1))/\sum ((1/S_i^2)(x_i - 1)^2) \qquad \text{(C.2.13)}$$

$$(\partial a_1/\partial x_i) =$$
$$((y_i/S_i^2)\sum (1/S_i^2)(x_i - 1)^2)/(\sum(1/S_i^2)(x_i - 1)^2)^2$$

$$- 2(1/S_i^2)(X_i - 1)\sum(y_i/S_i^2)(x_i - 1)^2/(\sum(1/S_i^2)(x_i - 1)^2)^2 \qquad \text{(C.2.14)}$$

Substituting Equations (C.2.13) and (C.2.14) into

Equation (C.2.12), cancelling (whenever possible) the term $\Sigma(1/S_i^2)(x_i - 1)^2$, and substituting a_1 for the expression given in Equation (C.2.6) (when applicable) then the following result is obtained;

$$(S_{a_1})^2 =$$

$$\frac{\left[\sum (1/S_i^4)(x_i - 1)^2(S_{i,y})^2 + \sum (y_i^2/S_i^4)(S_{i,x})^2\right.}{\left[\sum (1/S_i^2)(x_i - 1)^2\right]^2}$$

$$\frac{-4a_1 \sum (y_i/S_i^4)(x_i - 1)(S_{i,x})^2 + 4a_1^2 \sum (1/S_i^4)(x_i-1)^2(S_{1,x})2}{\left[\sum (1/S^{i2})(x_i - 1)^2\right]^2} \qquad (C.2.15)$$

APPENDIX C.3: THE RATIOS OF 27 keV PEAK TO 31 keV PEAK VERSUS SCATTER-TO-PHOTOPEAK RATIOS OF 60 keV PHOTONS.

Definition of symbols;

$N_{5,1}$ = count rate in the 31 keV peak;

$N_{6,1}$ = count rate in the 27 keV peak;

$N_{5,0}$, $N_{6,0}$ = count rates in the appropriate regions without absorber and with the source placed against the detector;

y = $(N_{6,i}/N_{5,i}) / (N_{6,0}/N_{5,0})$;

x = $(N_{4,i}/N_{3,i}) / (N_{4,0}/N_{3,0})$;

Note; x is defined as in Appendix C.2 and the other symbols remain as defined previously.

Assumptions: $N_{3,0}$; $N_{4,0}$; $N_{5,0}$; $N_{6,0}$; are known without error.

When X=1 , y=1, and the relationship between y and x in this case is illustrated in Figure 25 (page 144). Substituting the boundary conditions x=1 when y=1 into Equation (C.1) yields;

$$a_o = 1 - a_1 \qquad (C.3.1)$$

and the regression line equation is;

$$y = a_1(x-1) + 1 \qquad (C.3.2)$$

Substituting Equation (C.3.2) into Equation (C.2) produces;

$$\chi^2(n - 2) = \sqrt{\ ((y_i - a_1(x_i - 1)^{-1})/S_i)^2 \qquad (C.3.3)$$

Equation (C.3.3) is similar to Equation (C.2.4) except for the term "-1". Thus, differentiating Equation (C.3.3) with respect to a_1, equating to zero and solving for a_1, as in Appendix C.2 then the following is obtained.

$$a_i = \frac{\sum (1/S_i^2)\ (Y_i - X_i - Y_i + 1)}{\sum (1/S_i^2)\ (X_i - 1)^2} \qquad (C.3.4)$$

(S_i^2) is in this case defined as in Appendix C.2 and is given by Equation (C.2.7).

$S_{i,x}$ is given by Equation (C.2.9) and $S_{i,y}$ is obtained in a similar way.

$$S_{i,y} = \sqrt{[(N_{6,i}/(N_{5,i}^2) + ((N_{6,i})^2/(N_{5,i})^3).(N_{5,0}/N_{6,0})]} \qquad (C.3.5)$$

Since when $x_o = 1$, $y_o = 1$ then from Equation (C.2.10) is obtained;

$$\hat{a} = (y_t - 1)/(x_t - 1) \qquad (C.3.6)$$

where t is some chosen value of i.

The final value of (S_i^2) is obtained by substituting Equations (C.2.9), (C.3.5) and (C.3.6) into Equation (C.2.7). The actual value of a_1 was determined by reiterations as shown in the computer program in Table C.3 (page 239) of this Appendix.

The variance of a_1 is calculated in the same way as that in Appendix C.2 and given by Equation (C.2.12). Differentiating Equation (C.3.4) with respect to y_i and x_i yields;

$$(\partial a_i/\partial y_i) = \frac{(1/S_i^2)(x_i - 1)}{\sum (1/S_i^2)(x_i - 1)^2} \qquad (C.3.7)$$

$$(\partial a_1/\partial x_i) = \frac{(1/S_i^2)(y_i - 1) \sum (1/S_i^2)(x_i - 1)2}{[\sum (1/S_i^2)\ (x_i - 1)^2]\,2}$$

$$- \frac{2(1/S_i^2)(x_i - 1) \sum (1/S_i^2)(y_i x_i - x_i - y_i + 1)}{[\sum (1/S_i^2)(x_i - 1)_2]^2} \qquad (C.3.8)$$

Substituting Equations (C.3.7) and (C.3.8) into Equation (C.2.12) and using the same cancellations and substitutions as in Appendix C.2 the following result is obtained;

$$(Sa_i)^2 = \frac{\sum (1/S_i^4)(x_i - 1)^2 (S_{i,y})^2 + \sum (1/S_i^4)(y_i - 1)^2 (S_{i,x})^2}{[\sum (1/S_i^2)(x_i - 1)^2]^2}$$

$$- [4a_1 \sum (1/S_i^4)(x_i - 1)(y_i - 1)(S_{i,x})^2 + 4a_i^2 \sum (1/S_i^4)(x_i 1)^2 (S_{i,x}) 2] / [\sum (1/S_i^2)(x_i - 1)^2]^2$$

(C.3.9)

APPENDIX C.4: "GEOMETRY FACTOR" VERSUS SOURCE-TO-DETECTOR DISTANCE

The experimental data do not fit a straight line on a linear, semi-log nor full logarithmic plot. By subtracting a constant, c, from the "geometry factor" a straight line fit is obtained on a semi-logarithmic plot. This constant must be determined from the data.

Definition of symbols:

x_i = absorber thickness (cm) for i^{th} data point;

$N_{3,i}$ = count rate in the 60 keV photopeak with the source-detector distance $x = x_i$ as set for the i^{th} data point, and with the absorber of thickness x_i between the source and the detector;

$N_{3,0}$ = count rate in the 60 keV photopeak with the source placed against the detector ie $x = 0$ (no absorber between source and detector);

M_i = count rate in the 60 keV photopeak with the source placed at some arbitrary fixed distance from the detector, and absorber of thickness x between the source and detector, with the side opposite the detector placed against the source;

M_o = count rate in the 60 keV photopeak with

the source-detector distance the same as in the measurement of M_i but with no absorber between the source and detector;

$g(x_i)$ = geometry factor, $g(x_i) = (N_{3,i}/N_{3,0})/(M_i/M_0)$;

$\hat{c}$ = "eyeball" estimate of the constant, c, to be subtracted from $g(x_i)$ to obtain a function y(x) that is exponential in x;

i = 1,2,3,.....n.

Assumptions: $N_{3,0}$, M_o, x are known without error. The variance of c is small compared to the variance of y. If y_i is set as follows;

$$y_i = \ln z_i$$
$$= \ln ((N_{3,i}N_{3,0})/(M_i/M_0 - c) \qquad (C.4.1)$$

then a linear function y(x) is obtained as shown in the following diagram:

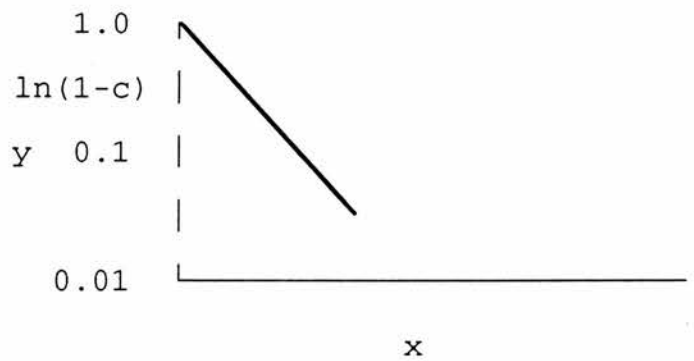

When x = 0, z = (1 - c) and y = ln(1 - c). Substituting these values into Equation (C.1) produces;

$$\ln(1 - c) = a_o$$

and the regression line equation is;

$$y = a_1 x + \ln(1 - c) \qquad \text{(C.4.2)}$$

Substituting Equation (C.4.2) into Equation (C.2) yields;

$$\chi^2(n - 2) = \sum [y_i - a_i x_i - \ln(1 - c)/S_i]^2 \qquad \text{(C.4.3)}$$

Differentiating Equation (C.4.3) (with respect to a_1 and c, respectively), and equating to zero thus yields the normal equations;

$$\sum (1/S_i^2)(-x_i y_i + a_1 x_i + x_i \ln(1 - c)) = 0 \qquad \text{(C.4.4)}$$

$$\sum (1/S_i^2)(y_i - a_1 x_i - \ln(1 - c)) = 0 \qquad \text{(C.4.5)}$$

From the above equations is obtained;

$$a_1 = \frac{\sum (x_i y_i/S_i^2) \sum (1/S_i^2) - \sum (y_i/S_i^2) \sum (x_i/S_i^2)}{\sum (1/S_i^2) \sum (x_i^2/S_i^2) - \sum (x_i/S_i^2)^2} \qquad \text{(C.4.6)}$$

$$c = 1 - \exp \frac{\sum (y_i/S_i^2) - a_1 \sum (x_i/S_i^2)}{\sum (1/S_i^2)} \qquad \text{(C.4.7)}$$

These equations cannot be solved because both S_i and y_i contain x. If it is assumed that;

$$y_i = \ln z_i = \ln((N_{3,i}/M_i)(M_o/N_{3,0})) - \hat{c}) \qquad \text{(C.4.8)}$$

then on the basis of this assumption;

$$\delta z_i = (M_o/N_{3,0})\,\delta(N_{3,i}/M_i)$$
$$= (M_o/N_{3,0})\,S_{(N3,i/Mi)} \qquad (C.4.9)$$

Using Equation (B.8) for the evaluation of the standard deviation for the ratio of two counts then;

$$\delta z_i = (M_o/N_{3,0})\sqrt{(N_{3,i}/M_i^2) + (N_{3,i}^2/M_i^3)} \qquad (C.4.10)$$

From equation (C.4.8);

$$\delta y_i = (\partial y/\partial z)\,\delta z_i$$
$$= (\partial \ln z/\partial z)\,\delta z_i$$
$$= ((N_{3,1}.M_0)(M_i.N_{3,0}) - \hat{c})^{-1}\delta z_i \qquad (C.4.11)$$

Since x is known without error (S_i^2) is equal to the variance of y.

Combining Equations (C.4.10) and (C.4.11) then;

$$S_i = S_{i,y}$$
$$= \delta y_i$$
$$= (M_i.M_o)\,/\,(N_{3,i}M_0 - cM_i.N_{3,0})\sqrt{(N_{3,i}/M_i^2)+(N_{3,i}^2/M_i^3)}$$
$$= \delta z_i/z_i \qquad (C.4.12)$$

Now, from Equations (C.4.8), (C.4.12), (C.4.6) and (C.4.7), the first approximations of y_i, S_i, a_1 and c can be calculated. If $|\ c - \hat{c}\ | > E$, where E is some chosen

accuracy then the computer value of c will become $\hat{c}$ and by the method of successive approximations the value of c is determined. The variance of a_1 is, in this case;

$$Sa_{a1} = \sum ((\partial a/\partial y)\, dy_i)^2 \qquad (C.4.13)$$

Differentiating Equation (C.4.6);

$$(\partial a_1/\partial y_i) = \frac{(x_i/S_i^2) \sum (1/S_i^2) - (1/S_i^2) \sum (x_i/S_i)^2}{\sum (1/S_i^2) \sum (x_i^2/S_i^2) - \sum (x_i/S_i^2)} \qquad (C.4.14)$$

Substituting Equation (C.4.14) into Equation (C.4.13) then;

$$(Sa_1)^2 = \frac{\sum (1/S_i^4)}{\sum (1/S_i^2) \sum (x_i^2/S_i^2) - (\sum (x_i/S_i^2))^2} \qquad (C.4.15)$$

The computer program for the above calculations is presented in Table C.4 (page 242) of this Appendix.

APPENDIX C.5: TRANSMISSION OF 60 keV PHOTONS VERSUS ABSORBER THICKNESS BETWEEN SOURCE AND DETECTOR

This curve is similar to the one described in Appendix C.4 and the same analysis will be used.

Definition of Symbols;

$N_{3,i}$, $N_{3,o}$, i, c, $\hat{c}$ - as defined previously;

x = absorber thickness between source and detector (g/cm^2).

Assumptions: $N_{3,0}$ and x are known without error. The variance of c is small compared to the variance of y.

If y is set as follows;

$$Y_i = \ln z_i$$

$$= \ln(N_{3,i} / N_{3,0} - c) \qquad (C.5.1)$$

then a linear function y(x) is obtained as shown in the diagram in Appendix C.4.

The equations of the regression line, χ^2 (n - 2), a_1, c, and ($S_{a_1}^2$) are the same as in Appendix C.4 and are given by Equations (C.4.2), (C.4.3), (C.4.6), (C.4.7) and (C.4.15) respectively. If it is assumed that;

$$y_i = \ln z_i$$

$$= \ln(N_{3,1}/N_{3,0} - \hat{c}) \qquad \text{(C.5.2)}$$

Then;

$$\delta z_i = \sqrt{N_{3,i}/N_{3,0}} \qquad \text{(C.5.3)}$$

From Equation (C.5.2);

$$\delta y_i = (\partial y/\partial x)\delta z_i$$

$$= (\partial \ln z/\partial z)\delta z_i$$

$$= (N_{3,0}/(N_{3,i} - N_{3,0}.\hat{c}))\delta z_i \qquad \text{(C.5.4)}$$

Again, as in Appendix C.4, $S_i = S_{i,y} = \delta y_i$.

Combining Equations (C.5.3) and (C.5.4) yields;

$$S_i = \sqrt{N_{3,i}/(N_{3,i} - N_{3,0}.\hat{c})}$$

$$= \delta z_i/z_i \qquad \text{(C.5.5)}$$

The same method of successive approximation will also be used in this case for the final determination of c.

The computer program for the calculations presented in this Appendix is similar to the program presented in Table C.4 (page 242). Only the computer statements for z and δz are different and have to be set according to Equations (C.5.2) and (C.5.3), respectively.

TABLE C1: COMPUTER PROGRAM FOR THE TRANSMISSION OF X-RAYS THROUGH ABSORBER

```
C
C TRANSMISSION OF L X-RAYS THROUGH ABSORBER
C
C CALCULATION OF BEST K
C
C AUTHOR JOHN AUSTIN
C
      REAL*4 X(30),N(30),P(30),Z(30),Y(30)
      REAL*4 DELTAZ(30),SY(30),K
      REAL*4 XYOSI2,X2OSI2,A1
      REAL*4 SAISQ,CHISQ,OCHISQ
C
C SET UP TO TALK TO TERMINAL
C
      CALL CONSW(1)
C
      WRITE(5,10)
   10 FORMAT($,' HOW MANY SETS OF VALUES?')
      READ(7,60)M
   60 FORMAT(I3)
      DO 90 I=1,M
         WRITE(5,20)
   20    FORMAT($,' WHAT IS YOUR VALUE OF X?')
         READ(7,70)X(I)
   70    FORMAT(F8.2)
         WRITE(5,30)
```

TABLE C1 (CONTD)

```
 30     FORMAT($,' WHAT IS YOUR VALUE OF N?')
        READ(7,70)N(I)
        WRITE(5,40)
 40     FORMAT($,' WHAT IS YOUR VALUE OF P?')
        READ(7,70)P(I)
 90 CONTINUE
C
      WRITE(5,100)
100 FORMAT($,' WHAT IS YOUR VALUE OF K?')
      READ(7,200)K
200 FORMAT(F6.3)
1000 CONTINUE
      OCHISQ=100
2000 CONTINUE
      XYOSI2=0
      X2OSI2=0
      DO 3000 I=1,M
         Z(I)=(N(I)-K*P(I))/(N(1)-K*P(1))
         Y(I)=ALOG(Z(I))
         DELTAZ(I)=SQRT(N(I)+K*K*P(I))/(N(1)-K*P(1))
         SY(I)=DELTAZ(I)/Z(I)
         XYOSI2=XYOSI2+X(I)*Y(I)/SY(I)**2
         X2OSI2=X2OSI2+(X(I)/SY(I))**2
3000 CONTINUE
      A1=XYOSI2/X2OSI2
      SAISQ=1/X2OSI2
      SA1=SQRT(SAISQ))
      CHISQ=0
```

TABLE C1 (CONTD)

```
      DO 4000 I=1,M
         CHISQ=CHISQ+((Y(I)-(A1*X(I)))/SY(I)**2
 4000 CONTINUE
      IF((OCHISQ-CHISQ) .GT. 0) GOTO 4050
      IF((OCHISQ-CHISQ) .LE. 0) GOTO 4100
 4050 K=K+0.01
      OCHISQ=CHISQ
      GOTO 2000
 4100 CHISQ=OCHISQ
      K=K-0.01
      WRITE(6,500)
  500 FORMAT(7X,'X',9X,'N',9X,'P',8X,'Z',8X,'SY'/
     1       6X,'===',7X,'===',7X,'===',6X,'===',7X,'===')
      DO 5000 I=1,M
 5000     WRITE(6,600)X(I),N(I),P(I),Z(I),SY(I)
  600     FORMAT(/,2X,F8.2,2X,F8.2,2X,F8.2,2X,F8.3,2X,F8.3)
 6000 CONTINUE
      WRITE(6,700)K
  700 FORMAT(/,10X,'K=:'F6.2)
      WRITE(6,800)A1
  800 FORMAT(/,9X,'A1=:'F6.3)
      WRITE(6,900)SA1
  900 FORMAT(/,8X,'SA1=:'F6.3)
C
      CALL CONSW(0)
      END
```

TABLE C2: COMPUTER PROGRAM FOR TRANSMISSION OF 60 keV PHOTONS VERSUS SCATTER-TO-PHOTOPEAK RATIOS.

```
C
C COMPUTER PROGRAM FOR TRANSMISSION OF
C 60 KEV PHOTONS VERSUS SCATTER-TO-
C PHOTOPEAK RATIOS.
C
C AUTHOR JOHN AUSTIN
C
      REAL*4 N3(30),N4(30),X(30),Y(30)
      REAL*4 DELTAZ(30),Z(30),SY(30)
      REAL*4 SX(30),S(30),SISQ(30)
      REAL*4 AHAT,TOP,BOT,EPS
      REAL*4 SUM1,SUM2,SUM3,SUM4
      REAL*4 TEMP1,TEMP2
      REAL*4 SAISQ,SA1,A1
C
C SET UP TO TALK TO TERMINAL
      CALL CONSW(1)
C
      WRITE(5,10)
   10 FORMAT($,' HOW MANY SETS OF VALUES?')
      READ(7,110)M
  110 FORMAT(I3)
      DO 1000 I=1,M
         WRITE(5,20)
   20    FORMAT($,' WHAT IS YOUR VALUE OF N3?')
```

TABLE C2 (CONTD)

```
        READ(7,120)N3(I)
 120    FORMAT(F8.2)
        WRITE(5,30)
  3     FORMAT($,' WHAT IS YOUR VALUE OF N4?')
        READ(7,120)N4(I)
1000 CONTINUE
     DO 2000 I=1,M
        Z(I)=N3(I)/N3(1)
        DELTAZ(I)=SQRT(N3(I))N3(1)
        SY(I)=DELTAZ(I)/Z(I)
        Y(I)=ALOG(Z(I))
        X(I)=N4(I)/N4(1)/Z(I)
        SX(I)=X(I)*SQRT(1/N4(I)+1/N3(I))
2000 CONTINUE
     AHAT=ALOG(Z(10))/X(10)-1.0)
3000 TOP=0.0
     BOT=0.0
     EPS=0.01
     DO 4000 I=1,M
        SISQ(I)=SY(I)**2+(AHAT*SX(I))**2
        S(I)=SQRT(SISQ(I))
        TOP=TOP+Y(I)*(1-X(I))/SISQ(I)
        BOT=BOT-(X(I)-1)**2/SISQ(I))
4000 CONTINUE
     A1=TOP/BOT
     IF(ABS(A1-AHAT) .LE. EPS) GOTO 5000
     IF(ABS(A1-AHAT) .GT. EPS) GOTO 5000
4500 AHAT=A1
```

TABLE C2 (CONTD)

```
      GOTO 3000
5000  SUM1=0.0
      SUM2=0.0
      SUM3=0.0
      SUM4=0.0
      WRITE(6,200)
 200  FORMAT(7X,'N3',7X,'N4',7X,'X',7X,'Z',7X,'S')
      DO 6000 I=1,M
         TEMP1=(1-X(I))/SISQ(I)
         TEMP2=Y(I)/SISQ(I)
         SUM1=SUM1+(TEMP1*SY(I))**2
         SUM2=SUM2+(TEMP2*SX(I))**2
         SUM3=SUM3+TEMP1*TEMP2*(SX(I)**2)
         SUM4=(TEMP1*SX(I))**2
6000  CONTINUE
      DO 7000 I=1,M
         WRITE(6,300)N3(I),N4(I),X(I),Z(I),S(I)
 300     FORMAT(/,2X,F8.2,2X,F8.2,2X,F8.2,2X,F6.3,2X,F6.3)
7000  CONTINUE
      SAISQ=(SUM1+SUM2+4.0*A1*(SUM3+A1*SUM4))/BOT**2
      SA1=SQRT(SAISQ)
      WRITE(6,400)A1
 400  FORMAT(/,10X,'A1=:'F6.3)
      WRITE(6,500)SA1
 500  FORMAT(/,9X,'SA1=:'F6.3)
      CALL CONSW(0)
      END
```

TABLE C3: COMPUTER PROGRAM FOR THE RATIOS OF THE 27 keV PEAK TO THE 31 keV PEAK VERSUS SCATTER TO PHOTOPEAK RATIOS OF 60 keV PHOTONS

```
C
C PROGRAM FOR THE RATIOS OF 27 KEV PEAK
C TO 31 KEV PEAK VERSUS SCATTER
C TO PHOTOPEAK RATIOS OF 60 KEV PHOTONS.
C
C AUTHOR JOHN AUSTIN
C
      REAL*4 N3(30),N4(30),N5(30),N6(30)
      REAL*4 X(30),Y(30),SX(30),SY(30)
      REAL*4 S(30),SISQ(30),TOP,BOT,EPS
      REAL*4 SUM1,SUM2,SUM3,SUM4
      REAL*4 TEMP1,TEMP2
C
      CALL CONSW(1)
C
      WRITE(5,10)
   10 FORMAT($,' HOW MANY SETS OF VALUES?')
      READ(7,60)M
   60 FORMAT(I3)
      DO 90 I=1,M
         WRITE(5,20)
   20    FORMAT($,' WHAT IS YOUR VALUE OF N3?')
         READ(7,70)N3(I)
   70    FORMAT(F8.2)
         WRITE(5,30)
```

TABLE C3 (CONTD)

```
 30     FORMAT($,' WHAT IS YOUR VALUE OF N4?')
        READ(7,70)N4(I)
        WRITE(5,40)
 40     FORMAT($,' WHAT IS YOUR VALUE OF N5?')
        READ(7,70)N5(I)
        WRITE(5,50)
 50     FORMAT($,' WHAT IS YOUR VALUE OF N6?')
        READ(7,70)N6(I)
 90 CONTINUE
    DO 1000 I=1,M
        X(I)=N4(I)/N3(I)/N4(1)*N3(1)
        Y(I)=N6(I)/N5(I)/N6(1)*N5(1)
        SX(I)=X(I)*SQRT(1/N3(I)+1/N4(I))
        SY(I)=Y(I)*SQRT(1/N6(I)+1/N5(I))
1000 CONTINUE
    AHAT=(1.0-Y(10))/(1.0-X(10))
2000 TOP=0.0
    BOT=0.0
    DO 3000 I=1,M
        SISQ(I)=SY(I)**2+(AHAT*SX(I))**2
        TOP=TOP-(Y(I)-1.0)*(X(I)-1.0)/SISQ(I)
        BOT=BOT-(X(I)-1.0)**2/SISQ(I)
        S(I)=SQRT(SISQ(I))
3000 CONTINUE
    A1=TOP/BOT
    IF(ABS(A1-AHAT) .LE. EPS) GOTO 4000
    IF(ABS(A1-AHAT) .GT. EPS) GOTO 3500
3500 AHAT=A1
```

TABLE C3 (CONTD)

```
      GOTO 2000
4000  SUM1=0.0
      SUM2=0.0
      SUM3=0.0
      SUM4=0.0
      WRITE(6,500)
 500  FORMAT(7X,'N3',7X,'N4',7X,'N5',7X,'N6',7X,'X',7X,'Y',7X,'S')
      DO 5000 I=1,M
         TEMP2=(1-Y(I))/SISQ(I)
         TEMP1=(1-X(I))/SISQ(I)
         SUM1=SUM1+(TEMP1*SY(I))**2
         SUM2=SUM2+(TEMP2*SX(I))**2
         SUM3=SUM3+TEMP1*TEMP2*SX(I)**2
         SUM4=SUM4+(TEMP1*SX(I))**2
5000     WRITE(6,600)N3(I),N4(I),N5(I),N6(I),X(I),Y(I),S(I)
 600  FORMAT(2X,F8.2,2X,F8.2,2X,F8.2,2X,F8.2,2X,F8.2/
     1       2X,F8.2,2X,F8.2)
6000  CONTINUE
      SAISQ=(SUM1+SUM2-A1*4.0*(SUM3-A1*SUM4))/BOT**2
      SA1=SQRT(SAISQ)
      WRITE(6,700)A1
 700  FORMAT(/,10X,'A1=:'F6.2)
      WRITE(6,800)SA1
 800  FORMAT(/,9X,'SA1=:'F5.3)
      CALL CONSW(0)
      END
```

TABLE C4: COMPUTER PROGRAM FOR GEOMETRY FACTOR VERSUS SOURCE TO DETECTOR DISTANCE

```
C
C COMPUTER PROGRAMME FOR 'GEOMETRY
C FACTOR' VERSUS SOURCE-TO-DETECTOR DISTANCE.
C
C AUTHOR JOHN AUSTIN
C
      REAL*4 X(30),N3(30),EM(30),GALPHA(30),Z(30)
      REAL*4 Y(30),DELTAZ(30),SY(30),A1,SA1
      REAL*4 CHAT,SIINV2,XOSI2,XOSI2,YOSI2,X2OSI2
      REAL*4 TEMPXY,TEMPX2,TEMPYO,TEMPXO,TEMPSI
      REAL*4,TEMPA1,C,CPRIME
C
C SETUP TO TALK TO TERMINAL
C
      CALL CONSW(1)
C
      WRITE(5,10)
   10 FORMAT($,' HOW MANY SETS OF VALUES?')
      READ(7,60)M
   60 FORMAT(I3)
      DO 90 I=1,M
      WRITE(5,20)
   20 FORMAT($,' WHAT IS YOUR VALUE OF X?')
      READ(7,70)X(I)
   70 FORMAT(F8.2)
```

TABLE C4 (CONTD)

```
      WRITE(5,30)
   30 FORMAT($,' WAHT IS YOUR VALUE OF N3?')
      READ(7,70)N3(I)
      WRITE(5,40)
   40 FORMAT($,' WHATIS YOUR VALUE OF EM?')
      READ(7,70)EM(I)
C
   90 CONTINUE
      WRITE(5,100)
  100 FORMAT($,' WHAT IS YOUR EYEBALL VALUE OF C?')
      READ(7,110)CHAT
  110 FORMAT(F6.3)
 1000 CONTINUE
      DO 2000 I=1,M
      GALPHA(I)=N3(I)/N3(1)/EM(I)*EM(1)
      DELTAZ(I)=GALPHA(I)*SQRT(1/N3(I)+EM(I))
 2000 CONTINUE
      SIINV2=0.0
      XOSI2=0.0
      YOSI2=0.0
      XYOSI2=0.0
      X2OSI2=0.0
      EPS=0.001
      DO 3000 I=1,M
      Z(I)=GALPHA(I)-CHAT
      IF(Z(I)) 2100,2100,2200
 2100 C=CPRIME
      XYOSI2=TEMPXY
```

TABLE C4 (CONTD)

```
      X2OSI2=TEMPX2
      YOSI2=TEMPYO
      XOSI2=TEMPXO
      SIINV2=TEMPSI
      A1=TEMPA1
      GOTO 4000
 2200 Y(I)=ALOG(Z(I))
      SY(I)=DELTAZ(I)/Z(I)
      SIINV2=SIINV2+(1/SY(I))**2
      XYOSI2=XYOSI2+X(I)*Y(I)/SY(I)**2
 3000 CONTINUE
      TEMPA1=A1
      A1=(XYOSI2*SIINV2-XOSI2*YOSI2)/(SIINV2*X2OSI2-XOSI2**2)
```

APPENDIX D: COMPUTER PROGRAM FOR PLUTONIUM & AMERICIUM MEASUREMENTS IN WOUNDS BY X- AND GAMMA-RAY SPECTRAL ANALYSIS

```
C COMPUTER PROGRAMME FOR "PLUTONIUM &
C AMERICIUM MEASUREMENTS IN WOUNDS BY
C X- AND GAMMA-RAY SPECTRAL ANALYSIS"
C
C AUTHOR JOHN AUSTIN
C
C
      REAL*4 N1,N4,N5,N7,N8,R1,R2,R3
      REAL*4 SR1(2),SR2(2),SR3(2),SAQ(2)
      REAL*4 SAL(2),SZ(2),SB(2),SQ(2)
      REAL*4 SL(2),SGL(2),RGLSQ(2),SN10(2),SN20,SN80
      REAL*4 SN20(2),SN80(2),SN30(2),SPUAMR(2)
      REAL*4 SN20PU(2),R1,R2,R3,C1,C2,AQ,SAQ(2)
      REAL*4 K1,K2,K8,H1,H2,F1,F2,F3,F8,
      REAL*4 N3,N2,N6,RHO
C
C
C SETUP TO TALK TO TERMINAL
C
      CALL CONSW(1)
C
      WRITE(5,10)
   10 FORMAT($,' WHAT IS THIS SCAN NO?')
      READ(7,60)M
   60 FORMAT(I3)
      WRITE(6,11)M
   11 FORMAT (/,'SCAN NO =:'I3)
      WRITE(5,15)
   15 FORMAT($,' WHAT IS YOUR VALUE OF N1?')
      READ(7,70)N1
   70 FORMAT(F8.2)
      WRITE(5,20)
   20 FORMAT($,' WHAT IS YOUR VALUE OF N2?')
      READ(7,70)N2
      WRITE(5,25)
   25 FORMAT($,' WHAT IS YOUR VALUE OF N4?')
      READ(7,70)N4
      WRITE(5,30)
   30 FORMAT($,' WHAT IS YOUR VALUE OF N5?')
      READ(7,70)N5
      WRITE(5,35)
   35 FORMAT($,' WHAT IS YOUR VALUE OF N6?')
      READ(7,70)N6
      WRITE(5,40)
   40 FORMAT($,' WHAT IS YOUR VALUE OF N7?')
      READ(7,70)N7
      WRITE(5,45)
   45 FORMAT($,' WHAT IS YOUR VALUE OF N8?')
      READ(7,70)N8
C
   90 CONTINUE
      R1 = -3.64
      R2 =  3.81
      R3 =  4.42
      SR1 = 0.0
```

APPENDIX D (CONTD)

```
      SR1(1) = 0.215
      SR2 = 0.0
      SR2(1) = 0.442
      SR3 = 0.0
      SR3(1) = 0.921
      C1 = 0.14
      RHO = 1.1
      T = 10.0
      AQ = -0.58
      SAQ = 0.0
      SAQ(1) = 0.0015
      C2 = 0.36
      AL = -0.54
      SAL = 0.0
      SAL(1) = 0.003
      K1 = 2.2
      K2 = 2.3
      K8 = 2.5
      H1 = 1.87
      H2 = 0.63
      F1 = 0.25
      F2 = 0.19
      F8 = 0.14
      F3 = 0.14
      IF (N4-N5) 100,100,120
100   WRITE(6,110)
110   FORMAT(/,10X,'LESS THAN TWO PERCENT AMERICIUM')
120   CONTINUE
      N3 = N7 + N5
      WRITE (6,130)N3
130   FORMAT(/,10X,'N3 = :'F8.2)
131   CONTINUE
      X = N4/N3/RN4N30
      WRITE (6,132)X
132   FORMAT(/,10X,'X = :'F8.2)
      IF ((N8-N2) .GT. 0) GOTO 140
140   WRITE (6,141)
141   FORMAT (/,10X,' N8 IS GREATER THAN N2)
      CONTINUE
      IF ((N8-(1.7*N1))) .GT. 0) GOTO 145
145   WRITE (6,146)
146   FORMAT (/,10X,' N8 IS GREATER THAN 1.7*N1)
      CONTINUE
      Y = N6/N5/RN6N50
      WRITE (6,147)Y
147   FORMAT (/,10X,'Y = :'F8.2)
      A = (1-Y)/(1-X)
      WRITE (6,148)A
148   FORMAT (/,10X,'A = :'F8.2)
      CONTINUE
      B = R1 + (A*R2) + (A*A*R3)
      WRITE (6,149)B
149   FORMAT (/,10X,'B = :'F8.2)
      CONTINUE
      Z = EXP(B*(X-1))
      N3P = N3/Z
```

APPENDIX D (CONTD)

```
      WRITE (6,150)Z
150   FORMAT (/,10X,'Z = :'F8.2)
      CONTINUE
      N30 = N3P/F3
      WRITE (6,151)N30
151   FORMAT (/,10X,'N30 = :'F8.2)
      CONTINUE
      BQAM = N30/60/T/0.359
      WRITE(6,152)BQAM
152   FORMAT(/,10X,'BQAM = :'F4.2)
      CONTINUE
      N10AM = 0.376*N30
      WRITE(6,153)N10AM
153   FORMAT (/,10X,'N10AM = :'F8.2)
      CONTINUE
      N80AM = 0.139*N30
      WRITE(6,154)N80AM
154   FORMAT (/,10X,'N80AM = :'F8.2)
      CONTINUE
      N20AM = 0.512*N30
      WRITE(6,155)N20AM
155   FORMAT (/,10X,'N20AM = :'F8.2)
      CONTINUE
      N1NET = N1 - (K1*P1)
      WRITE(6,156)N1NET
156   FORMAT (/,10X,'N1NET = :'F8.2)
      CONTINUE
      N2NET = N2 - (K2*P2)
      WRITE(6,157)N2NET
157   FORMAT (/,10X,'N2NET = :'F8.2)
      CONTINUE
      N3NET = N8 - (K8*P8)
      WRITE(6,158)N3NET
158   FORMAT (/,10X,'N3NET = :'F8.2)
      IF (N2NET)160,160,162
160   WRITE(6,161)
161   FORMAT(/,10X,'EVALUATION IMPOSSIBLE. ALL L BETA X-RAYS ABSORBED)
      GOTO 2000
162   Q = ALOG((Z-C1)/(1-C1)/AQ
      WRITE(6,163)Q
163   FORMAT (/,10X,'Q (g/sq.cm) = :'F8.2)
      CONTINUE
      L = Q/RHO
      WRITE(6,164)L
164   FORMAT (/,10X,'L (source to detector distance,cm) = :'F8.2)
      CONTINUE
      GL =  (1-C2)*FXP(AL*L) + C2
      SXSQ = X*X*(1/N4 +1/N3)
      SX = SQRT(SXSQ)
      WRITE(6,165)SX
165   FORMAT (/,10X,'SX = :'F8.2)
      CONTINUE
      SYSQ = Y*Y*(1/N6 + 1/N5)
      SY = SQRT(SYSQ)
      WRITE(6,166)SY
166   FORMAT (/,10X,'SY = :'F8.2)
```

APPENDIX D (CONTD)

```
      CONTINUE
      SASQ = (A*A*SXSQ + SYSQ)/(1-X)**2
      SA = SQRT(SASQ)
      WRITE(6,167)SA
 167  FORMAT (/,10X,'SA = :'F8.2)
      CONTINUE
      DO 1000 I = 0,1
      IF (I) 170,170,175
 170  SB(1) = 0.06
      GOTO 175
 175  SB(I) = SQRT(SR1(I)**2 + (A*SR2(I))**2 +
     1 (R2 + (2.0*A*R3))**2)*SASQ + (A*A*SR3(I))**2)
      END IF
      SZ(I) = Z*SQRT(B*B*SXSQ + ((X-1)*SB))**2)
      SN30(I) = SQRT(N3 + (N3P*SZ(I))**2)/Z/F3
      WRITE(6,176)SN30
 176  FORMAT (/,10X,'SN30 = :'F8.2)
      CONTINUE
      SQ(I) = SQRT((Q*SAQ(I))**2 + (SZ(I)/(Z-C1))**2)/AQ
      WRITE(6,177)SQ(I)
 177  FORMAT (/,10X,'SQ(I) = :'F8.2)
      CONTINUE
      SL(I) = SQ(I)/RHO
      WRITE(6,178)SL(I)
 178  FORMAT (/,10X,'SL(I) = :'F8.2)
      CONTINUE
      SGL(I) = (GL - C2)*SQRT((AL*SL(I))**2 + (L*SAL(I))**2)
      WRITE(6,179)SGL(I)
 179  FORMAT (/,10X,'SGL(I) = :'F8.2)
1000  CONTINUE
      A0 = 0.667
 190  MU2X = ALOG (N1NET/N2NET/A0*F2/F1)/(1-H1)
      MU1X = MU2X*H1
      N10 = N1NET*EXP(MU1X)/F1/GL
      N20 = N2NET*EXP(MU2X)/F2/GL
      N10PU = N10 - N10AM
      N20PU = N20 - N20AM
      IF (N10PU) 200,200,210
      IF (N20PU) 200,200,210
 200  WRITE(6,201)
 201  FORMAT($,'NO PLUTONIUM DETECTED')
      CONTINUE
      IF (N10PU) 202,202,210
      IF (N20PU) 202,202,210
 202  A0 = 0.734
      GOTO 190
 210  AN = 0.667*N20PU/N20 + 0.734*N20AM/N20
      IF(ABS(AN - A0) .GT. 0.001) GOTO 220
      IF(ABS(AN - A0) .LE. 0.001) GOTO 230
 220  A0 = AN
      GOTO 190
 230  CONTINUE
      B0 = 0.20
 300  MU2X = ALOG(N8NET/N2NET/B0*F2/F8)/(1-H2)
      MU8X = H2*MU2X
```

APPENDIX D (CONTD)

```
      N80 = N8NET*EXP(MU8X)/F8/GL
      N20 = N2NET*EXP(MU2X)F2/GL
      N80PU = N80 - N80AM
      N20PU = N20 - N80AM
      IF (N20PU .LE. 0) GOTO 310
      IF (N80PU .LE. 0) GOTO 310
      IF (N20PU AND N80PU .GT. 0) GOTO 320
310   B0 = 0.272
      GOTO 300
320   CONTINUE
      BN = 0.20*N20PU/N20 + 0.272*N20AM/N20
      IF(ABS(B0 - BN) .GT. 0.001) GOTO 311
      IF(ABS(B0 - BN) .LE. 0.001) GOTO 312
311   B0 = BN
      GOTO 300
312   BQPU = N20PU/60/T/0.021
      WRITE(6,320)BQPU
320   FORMAT(/,10X,'BQPU = :'F4.2)
      CONTINUE
      PUAMR = N20PU/N20AM*8.60
      WRITE(6,330)PUAMR
330   FORMAT(/,10X,'PU/AM RATIO = :'F4.2)
      CONTINUE
      SN1N2 = N1 + K1*K1*P1
      SN2N2 = N2 + K2*K2*P2
      SN8N2 = N8 + K8*K8*P8
      SN1NET = SQRT(SN1N2)
      SN2NET = SQRT(SN1N2)
      SN8NET = SQRT(SN8N2)
      WRITE(6,331)SN1NET
331   FORMAT(/,10X,'SN1NET = :'F4.2)
      CONTINUE
      WRITE(6,332)SN2NET
332   FORMAT(/,10X,'SN2NET = :'F4.2)
      CONTINUE
      WRITE(6,333)SN8NET
333   FORMAT(/,10X,'SN8NET = :'F4.2)
      RSN1 = SN1N2/N1NET**2
      RSN2 = SN2N2/N2NET**2
      RSN8 = SN8N2/N8NET**2
      SMU2X = SQRT(RSN1 + RSN2)/(1 - H1)
      SMU1X = H1*SMU2X
      WRITE(6,334)SMU2X,SMU1X
334   FORMAT(/,10X,'SMU2X = :'F4.2,10X,'SMU1X = :'F4.2)
      SMU2X = SQRT(RSN8 +RSN2)/(1 - H1)
      SMU8X = H2*SMU2X
      WRITE(6,335)SMU8X,SMU2X
335   FORMAT(/,10X,'SMU8X = :'F4.2,10X,'SMU2X = :'F4.2)
      DO 2000 I = 0,1
      RGLSQ(I) = (SGL(I)/GL)**2
      SN20(I) = N20*SQRT(RSN2 + SMU2X**2 + RGLSQ(I))
      SN80(I) = N80*SQRT(RSN8 + SMU8X**2 + RGLSQ(I))
      SN10(I) = N10*SQRT(RSN1 + SMU1X**2 + RGLSQ(I))
      WRITE(6,336)SN80(I),SN20(I),SN10(I)
336   FORMAT(/,10X,'SN80(I) = :'F4.2,10X,'SN20(I) = :'F4.2,10X,/
```

APPENDIX D (CONTD)

```
     1 SN10(I) = :'F4.2
       CONTINUE
       SN20PU(I) = SQRT(SN20(I)**2 + (0.512*SN30(I))**2)
       WRITE(6,337)SN20PU(I)
       SPUAMR(I) = 16.78/N30*SQRT(SN20PU(I)**2 +/
     1 (N20PU/N30*SN30(I))**2)
       WRITE(6,338)SPUAMR(I)
 338   FORMAT(/,10X,'SPUAMR(I) = :'F4.2)
2000   CONTINUE
       CALL CONSW(0)
       END
```

APPENDIX E THOUGHTS ON DOSE AND DOSE LIMITS

Regulation 7 of the Ionising Radiations Regulations 1985 (HSE, 1985) gives the following definition of committed dose: the words 'committed dose equivalent' refer to the dose equivalent accruing over the period of 50 years following the intake of radioactive material. Once the committed dose or committed effective dose equivalent has been assessed for a particular dosimetric purpose it is attributed to that period for the purpose of compliance with the dose limits. Thus, the only effective method of controlling and limiting the controlled dose quantity is by controlling and limiting the intake.

Doses to organs and tissues should normally be averaged over their volume, with the exception of skin which is specifically covered in Part II of Schedule 1 of the Regulations. In assessing dose equivalent to any part of the body from narrow beams of external radiation or from any small spots of contamination, it would be inappropriate to arrange the dose over an area of more than 1 cm^2 for the purpose of comparison with dose limits unless the radiation protection advisor or approved dosimetry service had sound evidence to average over a larger area.

It should be noted that averaging activity for the purpose of dose assessment under Regulation 13 should be made over an appropriate area which should not exceed 100

cm^2.

It should also be noted that for weakly penetrating radiation, measurements under the equivalent of 0.07 mm for tissue would be used to represent the dose equivalent to the skin.

SKIN

Part II of Schedule 1 states that "Without prejudice to Part 1 of this Schedule, the dose limit for individual organs or tissues, being the sum of the following dose quantities resulting from exposure to ionising radiation, namely the dose equivalent from external radiation, the dose equivalent from contamination and the committed dose equivalent from that years intake of radionuclides averaged throughout any individual organ or tissue (other than the lens of the eye) or any body extremity or over any area of skin shall in any calendar year be:-

a.	for employees aged 18 year or over	500 mSv
b.	for trainees aged under 18 year	150 mSv
c.	for any other person	50 mSv

In assessing the dose quantity to skin whether from contamination or external radiation, the area of skin over which the dose quantity is averaged should be appropriated to the circumstances but in the event shall

not exceed 100 cm^2.

PROBLEMS ASSOCIATED WITH LOCALISED SKIN EXPOSURES

The International Commission on Radiological Protection (ICRP) have stated that 'the aim of radiation protection should be to prevent detrimental non-stochastic effects and to limit the probability of stochastic effects to levels deemed to be acceptable' (ICRP 1977). However, for reasons explained elsewhere (ICRP 1984), ICRP state that 'it is not feasible at present to quantify the detriment from non-stochastic effects. Nevertheless, the risk of clinical detrimental non-stochastic effects can be restricted to zero merely by keeping the cumulative dose-equivalent limits for such effects below the respective threshold values'. Unfortunately, such statements still leave considerable uncertainty as to what constitutes a 'detrimental' or even 'clinical detrimental' effect in skin. For example, one can envisage blood vessel damage in limbs which in itself may not be clinically detrimental, but which may lead to reduced peripheral circulation and the premature appearance of associated sequelae. For highly non-uniform exposures, the identification of detrimental non-stochastic effects is even more crucial as ICRP did not give a specific dose-limit (ICRP 1977). The only recommendation for limiting dose in such cases is that detrimental effects should be prevented.

For routine purposes, ICRP now recommend that skin dose from contaminants should be averaged over 1 cm^2 regardless of the area exposed and the limit (0.5 Sv a^{-1}) applied to this measurement (ICRP, 1990). In accidents, an estimate should be made of the average dose equivalent over 1 cm^2 in the region of the highest dose equivalent. This dose equivalent should then be compared with the dose equivalent limit. No recommendation is made as to the area over which dose might be averaged for highly non-uniform exposures.

ICRP state that 'a range of 50 - 100 μm is appropriate for specifying the depth of the sensitive layer of most parts of the skin' and that 'the use of a depth of 70 μm is a reasonable mean value', (ie, skin dose should be measured at a depth of 70 μm). The depth may be appropriate for limiting stochastic effects which arise from damage for the basal layer. however, it is inappropriate in relation to non-stochastic effects to two reasons. Firstly, not all non-stochastic effects are as a result of damage to the epidermis (eg blood vessel damage/dermal atrophy) and, secondly, the basal layer can be considerably nearer to the skin surface than 70 μm (20 μm) (Whitton, 1973; Konishi and Yoshizawa 1985). Therefore, with poorly-penetrating radiations, non-stochastic effects may be prevented by limiting the dose at 70 μm for some body sites, but for other sites, the basal layer could still receive doses many times higher than the recommended limit. Consequently, minimum values

of epidermal thickness are more appropriate when one is considering prevention, rather than limitation, of a given effect.

Epidemiologically-derived overestimates of stochastic risks can also result if dose is only measured at 70 μm. This is particularly true for alpha-irradiation of the skin where the dose at 70 μm can be negligible but the dose at 40 μm can be considerable (Harvey, 1971) thus giving rise to a high probability of tumour formulation for a minimal officially-recorded dose. Konishi and Yoshizawa (1985) have recommended that 'The current value of 70 μm, which is in general use in radiation practice, should be replaced by a value of 40 μm'.

We are therefore left with four main uncertainties:

(1) What effect do we wish to limit or prevent?
(2) What dose limits are appropriate for these effects?
(3) Over what area should dose be measured?
(4) At what depth should dose be measured?

DOSE MEASUREMENT AND DEPTH

It has already been indicated that 70 μm is not necessarily the most appropriate depth for measuring skin dose and it represents effectively a compromise figure for limiting, or preventing, different types of damage

with due regard to the capabilities of the personal dosimetric techniques available.

However, as highly localised exposures appear to represent no more of a risk than the same doses delivered uniformly, the incidence of non-stochastic effects (by ICRP's own definition of aims of radiological protection) must be considered as the dose-limiting criteria when small areas of the total body skin are involved.

Therefore, the appropriate depth at which to measure dose for highly localised exposures can only be decided upon once the effects which is to be presented have been ascertained. A cycle point depth dose in skin, however, has little meaning in respect of the biological consequences. Therefore, area must be taken into account when dosimetry is considered as well as depth.

DOSE MEASUREMENT AND AREA

Krebs (1967), as part of a study of the response of mammalian skin to irradiation with particles of irradiated nuclear fuel, gave the first guidelines as to the effects of radioactive particulates on skin with regard to both depth and area of dose measurement.

In a preliminary study to verify the usefulness of Krebs's criteria, Forbes (1975) evaluated the effects of

irradiated uranium fuel microspheres on the skin of mice and pigs. The microspheres varied in size but could be categorised as being either small (138 - 154 μm) or large (277 - 328 μm), the outermost part being a shell of graphite 23 - 24 μm thickness.

The 'point depth dose' (ie, dose 100 μm directly below the particle) and the 'Krebs dose' (dose at the margin of a circular field of 4 mm radius at a depth of 100 μm below the surface of the skin) were both found to correlate well with the area of damage (desquamation, ulceration, etc) in pig skin and with the area of hair growth inhibition in mouse skin. However, both ulceration and desquamation occurred in pig skin, for a Krebs dose of less than 15 Gy in disagreement with Krebs's first criterion. The minimum Krebs dose required to produce a small but recognisable ulcer in pig skin was below 4 Gy, however, extrapolation of the data to derive threshold doses is difficult since no sub-threshold data were generated.

LIMITATION ON DOSE

As mentioned previously, it is the dose under the equivalent of 0.07 mm for tissue which would be used to express the dose equivalent to the skin. This dose, however, may not bear any relation to the dose to the basal layer, which in some situations may be between 20 -

70 μm. It cannot be stated unreservedly, therefore, that non-stochastic effects will be prevented by applying the dose limit at 0.07 mm (70 μm) in either the case of uniform or non-uniform exposures. If skin dose measurements are to be made of 70 μm, it has to be accepted that the effective policy is to <u>limit</u> rather than <u>prevent</u> non-stochastic effects.